Fermi National Accelerator Laboratory

FERMILAB-Pub-75/90-EXP
7100.063

(Submitted to Phys. Rev.)

AN ANALYSIS OF RADIAL SCALING IN SINGLE PARTICLE INCLUSIVE REACTIONS

F. E. Taylor
Northern Illinois University, DeKalb, Illinois 60115

and

D. C. Carey, J. R. Johnson, R. Kammerud,
D. J. Ritchie, A. Roberts, J. R. Sauer,
R. Shafer, D. Theriot, and J. K. Walker
Fermi National Accelerator Laboratory, Batavia, Illinois 60510

December 1975

AN ANALYSIS OF RADIAL SCALING IN SINGLE PARTICLE INCLUSIVE REACTIONS

F. E. Taylor
Northern Illinois University, DeKalb, Illinois 60115

and

D. C. Carey, J. R. Johnson,* R. Kammerud,
D. J. Ritchie, A. Roberts, J. R. Sauer,†
R. Shafer, D. Theriot, and J. K. Walker
Fermi National Accelerator Laboratory, Batavia, Illinois 60510

ABSTRACT

An analysis of an extensive sample of the world's data has been performed to test the hypothesis of radial scaling. We have studied the inclusive reactions:

$$p + p \rightarrow \begin{matrix} \pi^{\pm,0} \\ K^{\pm} \\ p^{\pm} \end{matrix} + \text{anything}$$

to determine the behavior of the invariant cross section as a function of $p_\perp$, $x_R = E^*/E^*_{max}$, the radial scaling variable, and s. The data cover a range in $p_\perp$ from 0.25 to ~6.0 GeV/c and a range in $\sqrt{s}$ from 3.0 GeV to 63 GeV.

1) For small x_R and all available $p_\perp$ the single particle inclusive cross sections for the reactions:

$$p + p \rightarrow \begin{matrix} \pi^{\pm,0} \\ K^{\pm} \\ p^{\pm} \end{matrix} + \text{anything}$$

to a good approximation scale for all $\sqrt{s}$, even down to the kinematic threshold.

2) For large x_R, the single particle inclusive cross sections for increasing $\sqrt{s}$ show a rapid approach to the scaling limit from above. In

these cases the scaling limit is always approached by $\sqrt{s}$ = 10 GeV. Thus data for all particles to a good approximation exhibit radial scaling at all available $p_\perp$ and x_R over ISR energy range.

A comparison of radial scaling with Feynman scaling is given. It is shown that in the Feynman case the cross sections for small $x_\parallel$ ($x_\parallel = p_\parallel^*/p_{max}^*$) approach their scaling limit from below, and that the approach to the scaling limit is slower than is exhibited for the case of small x_R.

The systematic differences among the inclusive cross sections of various particles are discussed in the range of $\sqrt{s}$ where radial scaling has been shown to be valid. In particular, the $p_\perp$ and x_R distributions of $E\, d\sigma/dp^3$ are examined.

I. INTRODUCTION

In a separate paper we have presented data on inclusive π^o production from pp collisions at the Fermi National Accelerator Laboratory.[1] Here we present an analysis and interpretation of these π^o data. In addition we examine other single particle inclusive cross sections to search for systematics in their behavior.

To study the single particle inclusive experiments, a set of variables should be chosen such that the single particle inclusive cross section displays the simplest behavior with respect to energy, $p_\perp$, center of momentum frame angle, etc. It is natural to choose a parameterization of the inclusive cross section which is meaningful in the exclusive limit.[2] We therefore define the scaling variable:

$$x_R = \left(\frac{E^*}{E^*_{max}} \right), \qquad (1)$$

where E^* = the energy of the detected particle in the center of momentum frame, and E^*_{max} = the maximum energy kinematically available to the detected particle in the c.o.m. frame. The range of x_R is $0 < x_R \leq 1$ for all $p_\perp$, and the case $x_R = 1$ corresponds to the exclusive limit. Since this variable is independent of the center of momentum angle and depends on only the radial distance from the kinematic boundary, we have called it the "radial" scaling variable.

Using this variable x_R, the proton-proton single particle inclusive cross section can be expressed as a function of three

variables s, $p_\perp$ and x_R:

$$E \frac{d\sigma}{dp^3} = f(s, p_\perp, x_R) \qquad (2)$$

where s is the square of the total c.o.m. energy. In this work we study whether the invariant cross section at sufficiently high energy scales, that is, becomes independent of s. It is shown that this scaling is reached at a lower s than obtained with the use of the Feynman variable $x_{||}$.

In an analysis of a single π^o inclusive experiment in p-p collisions[3] it has been shown that for sufficiently high $\sqrt{s}$ ($\sqrt{s} \gtrsim 10$ GeV) there is radial scaling:

$$E \frac{d\sigma}{dp^3} = f(p_\perp, x_R). \qquad (3)$$

This scaling is observed for 0.3 GeV/c $\leq p_\perp \leq$ 3.0 GeV/c and for 10 GeV $\leq \sqrt{s} \leq$ 27 GeV and for center of mass angle $20^o \leq \theta^* \leq 150^o$. It is therefore interesting to test this new form of scaling over as wide a kinematic range as possible for other particles produced in p-p collisions. We shall discuss the reactions:

$$p + p \rightarrow \begin{matrix} \pi^{\pm o} \\ K^{\pm} \\ p^{-} \end{matrix} + \text{anything}.$$

In Section II, the variable x_R is discussed and it is compared with the Feynman scaling variable $x_{||}$. Section III is a discussion of the method of data analysis. A comparison of radial scaling with Feynman scaling is given in Section IV. Section V is a presentation of the various systematic differences among single particle inclusive cross sections for various particles in p-p

collisions in the radial scaling region. A summary is given in Section VI.

II. THE x_R VARIABLE

In an analysis of single π^o inclusive production,[3] it has been shown that the s-dependence and the laboratory angular dependence of the invariant cross section could be succinctly described by writing the invariant cross section in terms of the transverse momentum $p_\perp$ and the variable x_R. This variable may be written in Lorentz invariant form as:

$$x_R = \frac{E^*}{E^*_{max}} = \frac{1 - \frac{M_x^2}{s} + \frac{M_c^2}{s}}{1 - \frac{\bar{M}_x^2}{s} + \frac{M_c^2}{s}}, \qquad (4)$$

where M_x = the invariant mass of the unspecified particle(s) (undetected), $\bar{M}_x$ = the minimum possible M_x value, M_c = the rest mass of the detected particle and s = the square of the total energy in the center of momentum frame. The variable x_R has been used by several authors and was probably first used by Kinoshita and Noda[4] in 1971 although apparently it had been discussed by Feynman[5] in 1969.

The maximum energy (E^*_{max}) kinematically available to the detected particle c in the inclusive reaction:

$$p + p \rightarrow c + \text{anything}$$

is determined by s, the square of the total energy in the c.o.m. frame, by the mass M_c of the detected particle c, and by $\bar{M}_x$, the minimum mass of the undetected particle system consistent with quantum number conservation (charge, strangeness, baryon number, etc.). For a single particle inclusive reaction this minimum value of M_x corresponds to the exclusive limit. A compilation of the minimum value of M_x and the exclusive limit reactions is given in Table I. We can express E^*_{max} as:

$$E^*_{max} = \frac{s - \bar{M}_x^2 + M_c^2}{2\sqrt{s}} . \qquad (5)$$

Since x_R is a ratio of total energies, the value of x_R at the particle c production threshold is 1, and for fixed, finite E^*, $x_R = 0$ only at infinite s.

The radial scaling variable x_R is distinguished from the Feynman[6] variable $x_{\parallel} = P_{\parallel}^*/P^*_{max} = 2p_{\parallel}^*/\sqrt{s}$ in that the detected

TABLE I

Inclusive Reaction	Exclusive Reaction	$\bar{M}_x$
$p + p \to \pi^+ +$ anything	$p + p \to p + n + \pi^+$	1.88 GeV/c^2
$p + p \to \pi^- +$ anything	$p + p \to p + \bar{p} + \pi^+ + \pi^-$	2.02 GeV/c^2
$p + p \to \pi^0 +$ anything	$p + p \to p + p + \pi^0$	1.88 GeV/c^2
$p + p \to K^+ +$ anything	$p + p \to \Lambda^0 + p + K^+$	2.05 GeV/c^2
$p + p \to K^- +$ anything	$p + p \to p + p + K^+ + K^-$	2.37 GeV/c^2
$p + p \to p +$ anything	$p + p \to p + p$	0.94 GeV/c^2
$p + p \to \bar{p} +$ anything	$p + p \to p + p + p + \bar{p}$	2.81 GeV/c^2

particle's total energy is scaled by its maximum value, rather than its longitudinal momentum by the maximum momentum. The use of only the longitudinal momentum component means that the variable $x_{\parallel}$ is not related to the location of the kinematic boundary at finite $p_{\perp}$. One might, therefore, expect the invariant cross section to have an s-dependence for fixed $p_{\perp}$ due entirely to kinematic effects. In particular one would expect $E\, d\sigma/dp^3$ for fixed $p_{\perp}$ and $x_{\parallel} = 0$ to rise with increasing $\sqrt{s}$ as the point in the $x_{\parallel}$, $x_{\perp}$ plane at which the measurement is being made moves further from the kinematic boundary. Therefore, in the region of center of mass angle $\theta^* = \pi/2$, $x_{\parallel}$ is clearly not the best variable for studying scaling and the systematics of single particle inclusive production. Other frequently used variables such as rapidity:

$$y^* = 1/2 \ln\left(\frac{E^* + p_{\parallel}^*}{E^* - p_{\parallel}^*}\right), \qquad (6)$$

and $x_{\perp}$:

$$x_{\perp} = \frac{2p_{\perp}}{\sqrt{s}}, \qquad (7)$$

also and not related to the location of the kinematic boundary, and suffer the same defects. On the other hand the expression of the invariant cross section in terms of the variables x_R and $p_{\perp}$ allows the s-dependence of the cross section to be studied at a fixed distance from the kinematic boundary.

It is instructive to contrast radial scaling with Feynman scaling by examining the methods by which single particle inclusive measurements are made. In both cases, consider the invariant cross

section at a fixed $p_\perp$ and compare, for example, $x_{\parallel} = 0.3$ to $x_R = 0.3$. Figure 1 shows the curves as a function of s along which these measurements are made in both cases. This plot is made in the $x_\perp = 2p_\perp/\sqrt{s}$ and $x_{\parallel} = 2\ p_{\parallel}^{*}/\sqrt{s}$ plane. In the limit of $s \to \infty$ we see that radial scaling and Feynman scaling are identical hypotheses:

$$E\frac{d\sigma}{dp^3} \overset{?}{=} f(p_\perp, x_R) = f(p_\perp, x_{\parallel}) \qquad (8)$$

However, the finite s behavior is quite different in the two cases. In the case of Feynman scaling the point at which the measurement is made moves away from the kinematic boundary. A large s-dependent increase in the cross section due to increasing phase space is thereby introduced. On the other hand measurements at fixed x_R require that the fractional distance to the kinematic boundary remain constant. In this way, it appears that the s-dependence of the dynamics may be more directly probed.

Another property of the variable x_R which distinguishes it from the Feynman variable $x_{\parallel}$ is its totally different s-threshold behavior. The s-threshold for a given value of $p_\perp$ is defined as the minimum value of s which can have the specified value of x_R or $x_{\parallel}$. For the x_R variable, this threshold is given by:

$$s_T = 2T + \bar{M}_x^2 - M_c^2 + 2[T^2 + T(\bar{M}_x^2 - M_c^2)]^{\frac{1}{2}} \qquad (9)$$

where: $T = \dfrac{p_\perp^2 + M_c^2}{x_R^2}$.

Hence for the limit $x_R = 0$, the s-threshold s_T is $= \infty$, for a fixed value of $p_\perp$. The limit $x_R = 1$ (the exclusive limit) corresponds

to a finite s_T for finite $p_\perp$. Comparing the s-threshold values at these two extreme values of $x_R = 0$ and $x_R = 1$ with the corresponding s-thresholds for the same extremes for $x_{||}$, there are very great differences. The s-threshold for the Feynman variable $x_{||}$ is determined by the kinematic boundary, so letting p^*_{max} be the maximum possible momentum of the particle in the c.o.m. then,

$$p^*_{max} = \frac{p_\perp}{\sqrt{1 - x_{||}^2}} = \frac{\sqrt{s_T}}{2} \qquad (10)$$

Hence in the limit $x_{||} = 0$, and $p_\perp$ fixed,

$$\sqrt{s_T} = 2p_\perp \qquad (11)$$

The limit $x_{||} = 1$ corresponds to $\sqrt{s} = \infty$ for fixed $p_\perp$. Thus for a given $x_{||}$ or x_R and fixed $p_\perp$ the threshold energy in the two cases is quite different.

We wish to compare the s-dependence of the invariant cross section for fixed x_R, $p_\perp$ with the invariant cross section for the <u>same numerical value</u> of $x_{||}$ at the same value of $p_\perp$. In this way the two cross sections will approach the same asymptotic limit. We are interested in this approach to the asymptotic limit. There is clearly some point at which the thresholds occur at the same energy $\sqrt{s_T}$. This happens for: (using high energy approximations)

$$\frac{2p_\perp}{x_R} = \frac{2p_\perp}{\sqrt{1 - x_{||}^2}} \qquad (12)$$

i.e., $x = x_R = x_{\parallel} = \frac{1}{\sqrt{2}}$.

Hence for $x_R = x_{\parallel} < \frac{1}{\sqrt{2}}$, the threshold for the radial variable x_R lies at a higher $\sqrt{s}$ than the threshold for the Feynman variable $x_{\parallel}$, whereas the opposite is true for $x_R = x_{\parallel} > \frac{1}{\sqrt{2}}$.

Finally it should be emphasized that $E\, d\sigma/dp^3$ is always finite at the s-threshold for fixed x_R and $p_\perp$, but is zero (excluding p-p elastic scattering) at the s-threshold for fixed $x_{\parallel}$ and $p_\perp$. This means that the cross section for fixed $x_{\parallel}$, $p_\perp$ must rise over some range in $\sqrt{s}$ due to purely kinematic effects. This s-dependence seems to be a major cause for the observed fixed $x_{\parallel}$, $p_\perp$ behavior of inclusive cross sections.

III. THE DATA ANALYSIS

A. The Object of the Data Analysis:

The object of the data analysis is to convert the data from each experiment into a table of invariant cross sections as a function of $\sqrt{s}$ for given values of $p_\perp$ and x_R or $p_\perp$ and $x_{\parallel}$. We divided the range of x_R into 10 bins of 0.1 units, ranging from 0.0 to 1.0 and the $p_\perp$ range from 0.125 GeV/c to 10.125 GeV/c was divided into 40 bins of 0.25 GeV/c. The variable $\sqrt{s}$ was not binned, and therefore each value of $\sqrt{s}$ of a given experiment provided a unique entry into the compilation.

Since a given datum generally did not fall at exactly the middle of the $p_\perp$, x_R or $x_{\parallel}$ bin, a small adjustment was performed

to move it to the center of the bin. This procedure is described in more detail later. Only statistical errors were used to denote the experimental uncertainty of each data point. The experiment-to-experiment systematic errors were estimated from the consistency of the data set to be $\tilde{\sim}$ ± 15%, but in many cases they could not be reliably determined, and were therefore not included.

B. Criteria for Choice of Data:

The requirement for including data in the compilation was the existence of a published table of cross sections for the production process $p + p \rightarrow c +$ anything, $c = \pi^{\pm,0}$, $K^{\pm}$, or $p^{\pm}$. In only a few instances were fits to the data used to generate values of $E\, d\sigma/dp^3$. These exceptions were made when there were no other data in the same kinematic range. A list of the data used is given in Table II.

C. The Finite Binning Corrections:

Each set of data was binned in 0.25 GeV/c units of $p_\perp$ and in 0.1 units of x_R or $x_{//}$ and it was found that the variation of $E \frac{d\sigma}{dp^3}$ even for these small bins was sizable. Therefore, it was necessary to adjust the data to the center of each bin, both in $p_\perp$, and in x_R or $x_{//}$. The value of the invariant cross section for a given experiment entered into the compilation for a fixed $p_\perp$ and x_R was computed by an expression of the form:

$$E\frac{d\sigma}{dp^3}(p_\perp^o, x_R^o, s) = \overline{E\frac{d\sigma}{dp^3}}(\hat{p}_\perp, \hat{x}_R, s)\, g(\hat{p}_\perp, p_\perp^o)\, f(\hat{x}_R, x_R^o) \quad (13)$$

where: $p_\perp^o$, x_R^o are the central values of the $p_\perp$ and x_R bins; $\overline{E\frac{d\sigma}{dp^3}}(\hat{p}_\perp, \hat{x}_R, s)$ is the cross section averaged over the $p_\perp$, x_R bins weighted by its statistical error. The functions $f(\hat{x}_R, x_R^o)$ and $g(\hat{p}_\perp, p_\perp^o)$ are the finite binning corrections in x_R and $p_\perp$ respectively. They shift the data average from the statistical mean values $\hat{x}_R$ and $\hat{p}_\perp$ to the centers of the x_R and $p_\perp$ bins (to x_R^o, $p_\perp^o$). The functions f and g depend on the particle type, and $g(\hat{p}_\perp, p_\perp^o)$ was also allowed to depend on x_R. The explicit functional forms of $f(\hat{x}_R, x_R^o)$ and $g(\hat{p}_\perp, p_\perp^o)$ were determined by performing a rough fit to the binned, uncorrected data. Since these corrections are typically $\lesssim$ 30%, a rough determination of these functional forms was adequate to describe the data over one bin width.

The form adapted for the $f(\hat{x}_R, x_R^o)$ correcting function is given by:

$$f(\hat{x}_R, x_R^o) = \frac{(1 - x_R^o)^n}{(1 - \hat{x}_R)^n} \quad (14)$$

where the exponent n is a function of the detected particle type.

The function $g(\hat{p}_\perp, p_\perp^o)$ used is given by:

$$g(\hat{p}_\perp, p_\perp^o) = \frac{(\hat{p}_\perp^2 + m^2)^q}{(p_\perp^{o2} + m^2)^q} \quad (15)$$

where the power q and the parameter m^2 showed a slight dependence on x_R but was roughly independent of particle species.

Although the explicit determination of the various parameters n, m^2, q was approximate, the resulting error in these corrections was small. It is estimated that the error in the parameter n is ± 1, the error in q is ± 1 and the error in m^2 is ± 0.1 GeV^2 giving rise to an error in the x_R correcting function of:

$$\frac{\Delta f}{f} \leq \pm 5\%$$

and in the $p_\perp$ correcting function of

$$\frac{\Delta g}{g} \simeq \pm 6\%.$$

D. The Rebinning in $x_{\parallel}$:

The final stage of the data analysis was to compute the invariant cross section for fixed $\sqrt{s}$, $p_\perp$, with $x_{\parallel}$ replacing x_R. This was performed on the compiled data for fixed x_R, $p_\perp$, by calculating for each table entry the corresponding value of $x_{\parallel}$ and using a small correction to shift the $x_{\parallel}$ binned data to the middle of the $x_{\parallel}$ bin. This small correction ($\lesssim$ 30%) was performed by using the x_R dependence of $E\, d\sigma/dp^3$ to shift to the appropriate x_R value corresponding to the middle of the $x_{\parallel}$ bin.

IV. COMPARISON OF RADIAL SCALING WITH FEYNMAN SCALING

The invariant cross section for $\pi^{\pm}$, $K^{\pm}$, and $p^{\pm}$ are presented in figures 2 through 8 for constant $p_\perp$, x_R and constant $p_\perp$, $x_{\parallel}$ versus $\sqrt{s}$. These graphs cover roughly 25% of the data compilation. The

qualitative features of this comparison between the radial scaling hypothesis and the Feynman scaling hypothesis for these single particle inclusive cross sections are given below.

1) In the low x region ($x \leq 0.2$) radial scaling is good to within the estimated ± 15%, experiment to experiment systematic errors, from the s-threshold to the highest energy available at the ISR. On the other hand, above the corresponding $x_{\parallel}$ energy threshold, there is a very large energy dependence of the cross sections. In this low $x_{\parallel}$ region, the approach to the Feynman scaling limit is from below, and in the case of large $p_{\perp} \sim 3.0$ GeV/c the Feynman scaling limit is not obtained even in the ISR energy range.[7,8] If one restricts the comparison of these two types of scaling to the $\sqrt{s}$ region above the radial variable s-threshold, one observes less difference. In the same range of $\sqrt{s}$, the s-dependence of $E\, d\sigma/dp^3$ for fixed $x_{\parallel}$ is slightly greater than that for fixed x_R, and the cross section appears to rise to its asympotic limit at large $\sqrt{s}$. Therefore in the low x (x_R or $x_{\parallel}$) region, the primary breakdown in Feynman scaling is below the radial variable s-threshold.

2) For $x_R > 0.20$ there is a rapid approach to a radial scaling after $\sqrt{s}$ passes above the x_R threshold. Furthermore for $\sqrt{s} \overset{>}{\sim} 10$ GeV radial scaling appears to be achieved for all $p_{\perp}$.[9] The deviation from radial scaling at low $\sqrt{s}$ is greater for larger values of x_R. In all cases the radial scaling limit is approached from above for increasing $\sqrt{s}$.

For $x_{\parallel} > 0.2$, the approach to the Feynman scaling limit is also from above. This is in contrast to the situation at low $x_{\parallel}$ where the approach to the scaling limit is from below. Since for

a given point on the Peyrou plot $x_{\parallel} \leq x_R$, large $x_{\parallel}$ implies $x_{\parallel} = x_R$ and therefore in this limit x_R and $x_{\parallel}$ scaling are the same. Because of this transition from an approach to scaling from below at small $x_{\parallel}$ to an approach from above at larger $x_{\parallel}$, there are values of $x_{\parallel}$ and $p_\perp$ where Feynman scaling is good at very low $\sqrt{s}$ ($\sim$ 5.0 GeV). For example Feynman scaling for π^+, $x_{\parallel} = 0.25$ and $p_\perp = 0.75$ GeV/c is good to within experimental systematic errors from $\sqrt{s} = 5$ GeV up to $\sqrt{s} = 53$ GeV. It appears that a kinematic threshold effect is superimposed on a dynamically induced decreasing cross section. Thus the s-dependence of the cross sections, for fixed $x_{\parallel}$, $p_\perp$ and for fixed x_R, $p_\perp$, as they fall to their scaling limit are different. In the former case, kinematic boundary effects distort the behavior. A discussion of the various inclusive cross sections will now be given. Referring to figures 2 through 8 we see:

A) $\pi^{\pm}$: (Figures 2 and 3) For $x_R = 0.05$, radial scaling is good down to the radial scaling threshold as is evident from Figure 2a and 3a. Feynman scaling for $x_{\parallel} = 0.05$ is evidently violated even for small $p_\perp$ and the invariant cross section for fixed $x_{\parallel}$ and $p_\perp$ is rising with increasing $\sqrt{s}$. For $x_R \geq 0.20$ the radial scaling limit is always approached from above for increasing $\sqrt{s}$ and by roughly $\sqrt{s} \gtrsim 10$ GeV the scaling limit has been attained for all $p_\perp$. The approach to the Feynman scaling limit for $x_{\parallel} > 0.2$ shows a turn over. For small $p_\perp$ ($\lesssim$ 1 GeV/c) the approach to the scaling limit is from above with increasing $\sqrt{s}$, but for larger $p_\perp$ ($\gtrsim$ 1.25 GeV/c) the approach to the scaling limit is from below. In all cases radial scaling appears to be good for

$\sqrt{s} \gtrsim 10$ GeV, whereas Feynman scaling may be violated by a factor of ten from $\sqrt{s} \sim 27$ to 53 GeV.

B) $\underline{\pi^o}$: (Figure 4) For $x_R = 0.05 \pm 0.05$, there is good evidence for radial scaling down to the radial scaling threshold. Feynman scaling for $x_{||}$ in the same range is again violated and the invariant cross section rises from below for increasing $\sqrt{s}$. For $x_R = 0.25 \pm .05$ radial scaling is good down to $\sqrt{s} \approx 10$ GeV for all $p_\perp$. For $x_{||} = 0.25 \pm .05$ Feynman scaling over the same $\sqrt{s}$ region is violated by approximately a factor of 2 for $p_\perp = 1.25$ GeV/c and by a factor of 4 for $p_\perp = 2.25$ GeV/c. Feynman scaling appears to hold for $p_\perp \lesssim 0.75$ GeV/c. For $x_R \geq 0.35$ radial scaling is good to within experimental errors for $\sqrt{s} > 10$ GeV, whereas for $x_{||} \geq 0.35$ Feynman scaling is obeyed for only low $p_\perp$.

C) $\underline{K^\pm}$: (Figure 5 and 6) The $K^\pm$ data show the same qualitative features as the $\pi^{\pm,o}$ data. There is however a difference between K^+ and K^-. The K^+ data for fixed $p_\perp$, $x_{||}$ appear to have somewhat less s-dependence than the corresponding K^- data. A comparison of the two scaling hypotheses in the same range of $\sqrt{s}$ for $K^\pm$ shows a systematic s-dependence for fixed $p_\perp$, $x_{||}$ (especially for K^-), which is absent in the data for fixed x_R.

D) $\underline{p^+}$: (Figure 7) The data at $x_R = 0.05 \pm 0.05$ exhibits good radial scaling down to the radial scaling s-threshold, but for large $p_\perp \approx 3.75$ GeV/c the Feynman scaling hypothesis for $x_{||} = 0.05$ is violated by almost an order of magnitude over the ISR energy range, and appears to be approaching the scaling limit from below. For small $p_\perp$ ($\lesssim 0.75$ GeV/c) Feynman scaling is approached from above. In general the violations of Feynman

scaling are less severe for protons than for any other particle. At low $p_\perp$, high x_R ($\gtrsim$ 0.65) the radial scaling limit is approached from above, and as for the other particles, this approach to radial scaling is more pronounced for large rather than small x_R.

E) $\bar{p}$: (Figure 8) Radial scaling for small $x_R \lesssim 0.2$ appears to be satisfied for anti-protons down to the radial scaling s-threshold. For larger x_R there are indications that the radial scaling limit is approached from above, although the data are incomplete. Feynman scaling is badly violated for anti-protons even at very high energies. For example at $p_\perp$ = 1.25 GeV/c, $x_{||}$ = 0.05, the anti-proton invariant cross section rises by roughly a factor of 2 for the $\sqrt{s}$ range from 30 GeV to 60 GeV.

In conclusion, for single particle inclusive reactions use of the radial scaling variable x_R leads to an earlier scaling of the invariant cross sections than use of the $x_{||}$ variable. Unlike the Feynman scaling limit, the radial scaling limit is always approached from above for increasing s and is reached by $\sqrt{s} \cong$ 10 GeV. This is consistent with the s-dependence of the total proton-proton cross section at low $\sqrt{s}$ ($\sim$ 5 to 10 GeV). The Feynman scaling limit is approached either from below, from above, or is exact depending on the dominance of phase space effects, dynamic effects or the fortuitous cancellation of these two effects. At small $x_{||}$ ($\sim$0.05 to 0.20) there are large violations of Feynman scaling due to large changes in the phase space suppression, which for

large $p_\perp$ (especially for $\bar{p}$ and K^- data) remain even at ISR energies.

V. INCLUSIVE CROSS SECTIONS IN THE RADIAL SCALING REGION

Since all single particle inclusive cross sections for fixed x_R and $p_\perp$ appear to scale for energies $\sqrt{s} \gtrsim 10$ GeV, there are sufficient data to examine the systematic differences between particle species in this radial scaling region.

To illustrate the kinematic range in the radial scaling region, ($\sqrt{s} \gtrsim 10$ GeV) covered by the compilation, normalized Peyrou plots for each particle type are presented in Figure 9. In these plots, $x_{\parallel} = 2p_{\parallel}^*/\sqrt{s}$ is plotted against $x_\perp = 2p_\perp/\sqrt{s}$ for a given x_R value of a given particle. It is seen that only in the case of π^o mesons (Figure 9c) is a wide range in $x_{\parallel}$, $x_\perp$ for a given x_R covered.[1] For the other particles, most of the data for large x_R are concentrated either in the forward direction, or near 90^o.

It is of particular interest to compare the dependence of $E\, d\sigma/dp^3$ on $p_\perp$ for constant x_R and on x_R for constant $p_\perp$. We make this comparison for each detected particle in the single particle inclusive reactions: $p + p \to \pi^{\pm,o}, K^\pm, p^\pm$ + anything.

A) The $p_\perp$ dependence of $E\, d\sigma/dp^3$ for constant x_R is displayed in Figure 10 for each of the single particle inclusive reactions listed above. These graphs were generated by projecting on the $p_\perp$ axis all of the data in the particle compilation for a given constant value of x_R. A separate point is plotted for each $\sqrt{s}$ value in the table above 10 GeV. Referring to these figures, it is noticed that the invariant cross section for $p_\perp \gtrsim 1.5$ GeV/c

for all particles becomes steeper for increasing $p_\perp$ as x_R increases. Furthermore the slope of $E\, d\sigma/dp^3$ versus $p_\perp$ at low $p_\perp$ decreases for increasing x_R. This $p_\perp$ dependence of $E\, d\sigma/dp^3$ can be parameterized by the following universal form, applicable to all particles and at all x_R:

$$E \frac{d\sigma}{dp^3}\Bigg|_{x_R = \text{constant}} \approx \frac{A}{(1 + \frac{p_\perp^2}{m^2})^q} . \qquad (16)$$

A minimum χ^2 fit was performed on the data to determine the values of the parameters A (mb/GeV^2), m^2 (GeV^2), q for each particle in each slice in x_R. These parameters are presented in Table III. It is evident that for low x_R and small $p_\perp$ the largest invariant cross section is for π^+. Then π^-, π^o, K^+, K^-, p and $\bar{p}$ respectively follow in order of decreasing magnitude.[10] At large x_R, the proton inclusive cross section dominates because of leading particle effects.

The fit parameters m^2 and q for mesons display an interesting similarity. The evident general trend of the parameter m^2 is to grow from approximately 0.3 GeV^2/c^4 at $x_R \sim 0.05$ to roughly 1.5 GeV^2/c^4 at $x_R \approx 0.55$. This growth in m^2 with increasing x_R is an expression of the flattening at low $p_\perp$ of $E\, d\sigma/dp^3$ with increasing x_R. The fit parameter q shows the general trend of growing for increasing x_R from approximately 3 at small $x_R \approx 0.05$ to roughly 6 at $x_R \approx 0.55$. The m^2 and q parameters from the fits to the p and $\bar{p}$ invariant cross section show this same behavior with increasing x_R. However m^2 for protons and anti-protons grows

from $\sim$ 1.0 at $x_R \simeq 0.05$ to $\sim$ 2.0 at $x_R \simeq 0.55$ and is therefore generally larger than the value of m^2 for mesons. The parameter q for protons and anti-protons is also different from mesons: q increases from roughly 4 at $x_R \simeq 0.05$ to 8 at $x_R \simeq 0.55$ and is therefore systematically larger than the corresponding values for mesons.

A check was made to insure that this general behavior of the parameters m^2 and q is not a consequence of relative normalization errors among various experiments. A fit to only the π^o data of D. C. Carey et al.,[1] showed the same general behavior. To verify that the trend is not due to an increasing $p_\perp$ range with increasing x_R, additional fits were made with cuts in the $p_\perp$ range to constrain it between $0.5 \leq p_\perp \leq 2.25$ GeV/c for π^+ and for $p_\perp \leq 2.25$ GeV for π^o. The calculated parameters A, m^2 and q for this test were found to be consistent with the values from the unconstrained fits.

It is interesting to note that in the limit as $x_R \to 0$ (or equivalently, $p_\perp$ fixed as $\sqrt{s} \to \infty$) the extrapolated form of the invariant cross section for mesons is consistent with:

$$\lim_{x_R \to 0} E \frac{d\sigma}{dp^3} = \frac{\tilde{A}}{p_\perp^{5 \pm 1}} \qquad (17)$$

This observed $p_\perp$-dependence seems to exclude the constituent interchange model[11] which predicts a $1/p_\perp^8$ behavior, and is closer to the $1/p_\perp^4$ dependence postulated by Berman, Bjorken and Kogut.[12] Protons and anti-protons, however appear to be more consistent with the form:

$$\lim_{x_R \to 0} \left(E \frac{d\sigma}{dp^3} \right) \simeq \frac{A}{(1 + \frac{p_\perp^2}{1.0})^4} \quad , \qquad (18)$$

giving a $p_\perp$ dependence of $\sim 1/p_\perp^8$ at large $p_\perp$.

B) The x_R dependence of $E\, d\sigma/dp^3$ for constant $p_\perp$ for various particles in the radial scaling region of $\sqrt{s} \gtrsim 10$ GeV is shown in Figure 11. It is seen that the cross sections for all particles with the exception of protons at low $p_\perp$, fall as $x_R \to 1$ for all $p_\perp$. To parameterize this x_R dependence (for all particles except protons) we performed a minimum χ^2 fit of the invariant cross section to the theoretically motivated form:[4,11]

$$E \frac{d\sigma}{dp^3}\Big|_{\text{fixed } p_\perp} \simeq B(1 - x_R)^n \quad , \qquad (19)$$

where B and n are free parameters. Reasonable fits were obtained in all cases. The resulting values of B (mb/GeV^2) and n are tabulated in Table IV. The particles listed in rough order of increasing n, are (p), K^+, π^+, π^-, π^o, K^-, $\bar{p}$. To check that these fits were independent of the x_R interval, a cut in x_R was made for the π^o data constraining $0.15 \leq x_R \leq 0.35$, and a minimum χ^2 fit was again performed. Within errors, the fit parameters were the same.

The power of n for a fixed $p_\perp$, in the preceding parameterization of $E \frac{d\sigma}{dp^3}\Big|_{p_\perp}$, reflects perhaps, the quantum number conservation requirements (charge, baryon number, strangeness etc.) in the production of particle c.[11] These requirements may be calculated from the exclusive limit of the invariant cross section,

since the undetected particles in the inclusive experiment must contain the same quantum numbers as the exclusive limit.[2] It appears that the more a given single particle inclusive reaction is forbidden (i.e., more quantum numbers to balance in the production of particle c), the larger is the value of the exponent n.

VI. SUMMARY

We have parameterized the single particle inclusive production cross sections in terms of s, $p_\perp$ and the radial scaling variable x_R:

$$E \frac{d\sigma}{dp^3} = f(s, p_\perp, x_R) ,$$

where $x_R = E^*/E^*_{max}$.

We have found that above $\sqrt{s} \gtrsim 10$ GeV, all of the cross section data are consistent with radial scaling for all $p_\perp$:

$$E \frac{d\sigma}{dp^3} = f(p_\perp, x_R) ,$$

$$\sqrt{s} \gtrsim 10 \text{ GeV}.$$

Below $\sqrt{s} = 10$ GeV and for $x_R \gtrsim 0.2$, there is a rapid approach to the scaling limit from above. For $x_R \lesssim 0.20$, there is good radial scaling down to the threshold.

Feynman scaling is achieved at a larger value of $\sqrt{s}$ where the suppression due to the presence of the kinematic boundary is sufficiently small. In the cases of large $p_\perp$, (or even small $p_\perp$ for $\bar{p}$ and $\bar{K}$), this s-dependence is still present even in the ISR energy range.

Parameterizing the single particle inclusive cross sections in terms of $p_\perp$, x_R and $\sqrt{s}$, we find in the radial scaling region $\sqrt{s} \gtrsim 10$ GeV, that the shape of the $p_\perp$ dependence of $E\, d\sigma/dp^3$ for all particles for constant x_R as a function of x_R show the same general behavior. From the minimum χ^2 fits to the invariant cross section to the form:

$$E \frac{d\sigma}{dp^3}\Bigg|_{x_R \text{ fixed}} = \frac{A}{(1 + \frac{p_\perp^2}{m^2})^q}$$

we find:

1) The parameter m^2 grows with increasing x_R for all particles and is generally larger for protons and anti-protons than for mesons.

2) The parameter q grows with increasing x_R for all particles.

3) The parameter A, which reflects the overall magnitude of the invariant cross section, decreases for increasing x_R for π^+, π^-, π^o, K^+, K^-, $\bar{p}$. For protons, A increases with increasing x_R.

4) In the limit of $x_R \to 0$, the invariant cross section for meson production is consistent with:

$$\lim_{x_R \to 0} \left(E \frac{d\sigma}{dp^3}\right) \propto \frac{1}{p_\perp^5}$$

and for protons and anti-protons (although the errors in the $\bar{p}$ cross section are large) with the form:

$$\lim_{x_R \to 0} \left(E \frac{d\sigma}{dp^3} \right) \propto \frac{1}{p_\perp^8} \quad .$$

The shape as a function of x_R of the single particle inclusive cross section for constant $p_\perp$ shows a very strong dependence on the species of the detected particle. In particular, the more forbidden the production of the detected particle is, the steeper the slope of $E \frac{d\sigma}{dp^3}\Big|_{p_\perp \text{ fixed}}$ versus x_R. Parameterizing the invariant cross section for fixed $p_\perp$ in the form:

$$E \frac{d\sigma}{dp^3}\Big|_{p_\perp \text{ fixed}} = B(1 - x_R)^n \ ,$$

we find that:

the parameter n for the various particles is given by the following increasing order: p, K^+, π^+, π^o, π^-, K^-, $\bar{p}$. Only protons at low $p_\perp$ show an increasing $E\, d\sigma/dp^3$ versus increasing x_R for $p_\perp$ fixed.

In conclusion, the most important result of this investigation is that all data for long lived particle production in proton-proton collisions exhibit radial scaling at all $p_\perp$ for $\sqrt{s} \gtrsim$ 10 GeV.

Expressing single particle inclusive cross sections in terms of $p_\perp$ and x_R allows a simple and systematic behavior to be revealed for particle production.

Acknowledgements.

We would like to acknowledge the assistance given by Prof. M. Peters in the very early stages of this work.

REFERENCES

*Present address: Physics Department, Northeastern University, Boston, Massachusetts 02115.

†Present address: Physics Department, Indiana University, Bloomington, Indiana 47401.

[1]D. C. Carey et al., FERMILAB-Pub-75/75-EXP, submitted to Phys. Rev. D. Sept. 1975.

[2]J. D. Bjorken, J. Kogut, Phys. Rev. D 8, 1341 (1973).

[3]D. C. Carey et al., Phys. Rev. Lett. 33, 327 (1974); Phys. Rev. Lett. 33, 330 (1974); FERMILAB-Pub-75/20-EXP.

[4]K. Kinoshita and H. Noda, Prog. Theo. Phys. 6, 1639 (1971), ibid 49, 896 (1973); Memoirs of the Faculty of Science, Kyushu Univ., Ser. B, Vol. 4, No. 5, May 1973; Prog. Theo. Phys. 50, 915 (1973). A preliminary analysis of the proton-proton single particle inclusive data using the radial scaling variable was performed by E. Yen, Phys. Rev. D 10, 836 (1974).

[5]As far as we are aware the variable x_R was first suggested by R. P. Feynman 1969 (private communcation from N. Byers).

[6]R. P. Feynman, Phys. Rev. Lett. 23, 1415 (1969); J. Benecke, T. T. Chou, C. N. Yang, and E. Yen, Phys. Rev. 188, 2159 (1969).

[7]T. Ferbel, Phys. Rev. D 8, 2321 (1973).

[8]A. M. Rossi et al., Nuclear Physics B 84, 269 (1975).

[9]There is some evidence in unpublished data for a small rise in the single particle inclusive cross section for constant $p_\perp$, x_R with increasing $\sqrt{s}$ over the ISR energy range. This could be related to the rise in the total pp cross section. It is therefore

of interest to obtain high precision data in this energy range to study the onset of this radial scaling breakdown. It should be noted that the approach to a radial scaling limit is from above at low energies so that if the single particle cross sections at the ISR really begin to rise, it corresponds to a minimum having occurred in the cross sections--reminiscent of the total cross section behavior. The corresponding behavior of the single particle cross sections for fixed $x_{||}$ is much more complicated, and any subsequent rise over the ISR energy range produces a complex energy dependence arising from both kinematical and dynamical effects. In this case the cross sections approach their limit from below for $x_{||} < 0.2$ and any subsequent rise over the ISR range tends to be seen as a retarded approach to an ultimate scaling limit. For $x_{||} > 0.2$, the cross sections at low energy first rise rapidly from threshold, then turn around and approach their limits from above. Any subsequent rise over the ISR energy range then produces a very complex energy dependence.

[10] Typical π^o cross section measured at FNAL and ISR appear to be typically half of the average of the π^+, π^- production cross section. Of course, there is no reason in principle why this may not be the case. However, there are severe difficulties in absolute normalization of π^o cross sections. For this reason, quoted systematic errors in absolute normalization of π^o cross sections are large enough that no definitive conclusion can be made about the difference of π^o and $(\pi^+ + \pi^-)/2$ cross sections.

[11]Stanley J. Brodsky, Glennys R. Farrar, Phys. Rev. D 11, 3109 (1975); R. Blankenbecler and S. J. Brodsky, Phys. Rev. D 10, 2973 (1974); and J. Gunion, Phys. Rev. D 10, 242 (1974), J. Gunion, Particles and Fields, AIP Conference Proceedings No. 23, (American Institute of Physics, New York, 1975), edited by C. E. Carlson.

[12]S. M. Berman, J. D. Bjorken, J. B. Kogut, Phys. Rev. D 4, 3388 (1971).

TABLE II

Reference	$\sqrt{s}$ (GeV)	Particle
J. T. Reed et al., Phys. Rev. 168, 1495 (1968).	2.83 2.98	K^+
W. J. Hogan et al., Phys. Rev. 166, 1472 (1968).	2.88 2.99 3.03	K^+
A. C. Melissinos et al., Phys. Rev. 128, 2373 (1962).	2.98	π^+, π^-
E. R. Gellert (Thesis) LBL-749 (1972).	3.78	π^+, π^-
V. Blobel et al., DESY 73/36 (1973).	4.93 6.84	π^+, π^-
C. W. Akerlof et al., Phys. Rev. D 3, 645 (1971).	5.02	π^+, π^-, K^+, K^-, p, $\bar{p}$
D. Dekkers et al., Phys. Rev. 137, B962 (1965).	6.09 6.72	π^+, π^-, K^+, K^-, p, $\bar{p}$
A. N. Diddens et al., Nuovo Cimento 31, 961 (1964).	6.12 6.84	π^+, π^-, K^+, K^-, p, $\bar{p}$

TABLE II (cont'd)

Reference	$\sqrt{s}$ (GeV)	Particle
J. V. Allaby et al., CERN 70-12 (1970).	6.15	π^+, π^-, K^+, K^-, p, $\bar{p}$
W. H. Sims et al., Nucl. Phys. B41, 317 (1972).	7.43	π^+, π^-
D. C. Carey et al., Phys. Rev. Letters 33, 327 (1974) and submitted to Phys. Rev. Sept., 1975. FERMILAB-Pub-75/75-EXP. (The values of $\sqrt{s}$ from this reference were combined in this compilation to diminish the size of the data sample.)	10.2 11.1 12.3 13.4 14.6 15.7 16.9 18.2 19.5 20.7 21.8 23.1 24.6 25.7 27.0	π^0

TABLE II (cont'd)

Reference	$\sqrt{s}$ (GeV)	Particle
J. W. Cronin et al., Phys. Rev. D 11, 3105 (1975)	19.4 23.8 27.4	π^+, π^-, K^+, K^-, p, $\bar{p}$
P. Capiluppi et al., Nucl. Phys. B79, 189 (1974).	23.3 30.6 44.6 53.0 62.7	π^+, π^-, K^+, K^-, p, $\bar{p}$
B. Alper et al., Nucl. Phys. B87, 19 (1975).	23.4 30.6 44.6 52.8 63.0	π^+, π^-, K^+, K^-, p, $\bar{p}$
M. G. Albrow et al., Nucl. Phys. B73, 40 (1974).	31.0 45.0 53.2 62.6	π^+, K^+, p
M. G. Albrow et al., Nucl. Phys. B56, 333 (1973).	23.6 30.8 45.0 53.2 62.8	π^-, K^-, $\bar{p}$

TABLE II (cont'd)

Reference	$\sqrt{s}$ (GeV)	Particle
M. G. Albrow et al., Nucl. Phys. B54, 6 (1973).	31.0	p
M. Banner et al., Phys. Letters 41B, 547 (1972).	23.2 30.4 44.4 52.7	π^+, π^-, p, $\bar{p}$
F. W. Büsser et al., Phys. Letters 46B, 471 (1973); and F. W. Büsser et al., Phys. Letters 55B, 232 (1975).	23.5 30.6 44.8 52.7 62.4	π^0
K. Eggert et al., submitted to the Palermo International Conf. on HEP, Palermo, Italy, 23 June, 1975.	23.6 30.8 45.1 53.2 62.9	π^0

TABLE III

$A(mb/GeV^2)$, $m^2(GeV^2)$

x_R		π^+	π^-	π^o	K^+	K^-	p^+	p^-
0.05	A	51.460±2.90	45.220±2.10	19.210±0.060	4.820±1.630	2.180±0.43	2.95±0.220	0.960±0.080
	m^2	0.298±0.02	0.348±0.02	0.358±0.001	0.285±0.070	0.538±0.09	1.00±0.095	1.680±0.200
	q	3.390±0.07	3.450±0.06	3.230±0.005	2.717±0.140	3.210±0.16	4.25±0.190	4.840±0.300
0.15		25.150±2.24	14.170±0.50	5.330±0.030	2.139±0.320	1.080±0.09	3.62±0.130	0.547±0.030
		0.523±0.04	0.610±0.03	0.908±0.001	0.836±0.110	0.757±0.07	1.13±0.040	1.150±0.070
		4.010±0.09	4.080±0.07	4.357±0.004	4.020±0.180	3.890±0.12	4.85±0.070	4.490±0.110
0.25		10.660±1.15	7.910±0.29	2.070±0.006	0.791±0.150	0.535±0.07	5.84±0.300	0.165±0.006
		0.873±0.09	0.726±0.05	1.332±0.001	1.620±0.360	0.990±0.18	1.88±0.120	2.550±0.040
		5.060±0.17	4.650±0.15	4.953±0.002	5.610±0.460	4.780±0.31	7.06±0.200	7.180±0.060
0.35		5.970±0.53	2.740±0.09	0.993±0.005	0.536±0.080	0.135±0.02	8.45±0.430	0.038±0.002
		1.198±0.07	1.320±0.06	1.569±0.002	2.070±0.260	2.280±0.36	1.91±0.070	4.290±0.060
		5.840±0.10	5.740±0.09	5.231±0.004	6.350±0.260	6.750±0.37	7.59±0.110	9.040±0.070
0.45		3.100±0.36	1.790±0.11	0.770±0.020	0.365±0.033	0.070±0.01	9.18±0.550	0.015±0.004
		1.330±0.09	1.109±0.07	1.410±0.040	1.895±0.120	2.250±0.33	1.91±0.070	2.500±1.270
		6.070±0.12	5.640±0.10	5.200±0.020	6.340±0.130	6.890±0.32	7.81±0.110	7.080±1.510
0.55		1.427±0.14	2.490±0.38	0.420±0.040	0.319±0.070		13.05±0.400	
		1.460±0.11	0.590±0.05	1.730±0.120	1.630±0.280		2.02±0.010	
		6.390±0.19	5.220±0.07	5.860±0.170	6.390±0.310		8.48±0.040	
0.65		0.821±0.05		0.210±0.020	0.134±0.011		12.11±0.160	
		1.520±0.07		2.110±0.030	2.025±0.160		2.28±0.010	
		6.680±0.14		6.529±0.040	7.070±0.290		9.24±0.030	
0.75		C.210±0.03		0.279±0.100	0.052±0.012		10.47±0.170	
		3.010±0.94		1.600±0.500	3.390±1.250		2.55±0.014	
		10.700±2.39		6.200±0.700	10.900±2.900		10.13±0.040	
0.85		0.370±0.37					10.20±0.600	
		0.330±0.21					1.24±0.030	
		3.740±0.44					6.47±0.130	
0.95							18.30±0.600	
							2.59±0.030	
							13.10±0.100	

TABLE IV

B (mb/GeV^2)

$p_\perp$	π^+	π^-	π^o	K^+	K^-	$\bar{p}$
0.25 B	36.3±1.4	28.7±2.8	16.6±.4	4.0±.5	2.0±.2	1.7±.2
n	4.2±0.2	6.0±0.5	7.0±.3	4.9±.9	5.1±.4	8.5±.5
0.5	8.72±.28	7.7±.4	4.29±.07	1.06±.06	$(8.1\pm.9)\times10^{-1}$	$(8.0\pm.7)\times10^{-1}$
	3.52±.08	4.6±.1	4.60±.10	2.90±.10	5.6±.3	8.1±.3
0.75	2.01±.04	1.93±.05	1.09±.02	$(3.1\pm.1)\times10^{-1}$	$(3.5\pm.5)\times10^{-1}$	$(3.2\pm.2)\times10^{-1}$
	2.87±.04	4.07±.04	3.50±.10	2.5±.1	7.0±.4	7.2±.4
1.0	$(5.32\pm.14)\times10^{-1}$	$(5.28\pm.01)\times10^{-1}$	$(3.25\pm.08)\times10^{-1}$	$(7.3\pm.6)\times10^{-2}$		$(1.3\pm.7)\times10^{-1}$
	2.82±.06	3.94±.07	3.20±.10	2.1±.2		7.4±.5
1.25	$(1.79\pm.05)\times10^{-1}$	$(1.76\pm.07)\times10^{-1}$	$(1.14\pm.04)\times10^{-1}$	$(3.9\pm.2)\times10^{-2}$	$(3.8\pm.3)\times10^{-2}$	$(7.9\pm0.9)\times10^{-2}$
	3.24±.07	4.60±.30	3.30±.09	2.7±.2	6.1±.7	10.5±1.0
1.50	$(6.00\pm.2)\times10^{-2}$	$(6.03\pm.02)\times10^{-2}$	$(3.89\pm.13)\times10^{-2}$	$(1.80\pm.06)\times10^{-2}$	$(2.1\pm.7)\times10^{-2}$	$(4.7\pm0.7)\times10^{-2}$
	3.51±.09	4.90±.20	3.24±.09	3.20±.10	8.5±.4	15.7±1.3
1.75	$(2.33\pm.09)\times10^{-2}$	$(2.3\pm0.02)\times10^{-2}$	$(1.51\pm.05)\times10^{-2}$	$(7.6\pm.6)\times10^{-3}$	$(7.8\pm1.0)\times10^{-3}$	$(1.3\pm0.2)\times10^{-2}$
	3.90±.20	5.8±1.10	3.33±.09	3.7±.5	7.6±1.2	10.8±1.2
2.0	$(9.3\pm.7)\times10^{-3}$	$(9.3\pm1.5)\times10^{-3}$	$(6.28\pm.17)\times10^{-3}$	$(3.2\pm.4)\times10^{-3}$	$(3.3\pm0.6)\times10^{-3}$	$(3.9\pm0.8)\times10^{-3}$
	3.7±.4	5.2±1.3	3.38±.07	3.7±.8	7.4±1.6	10.1±1.7
2.25	$(4.8\pm.4)\times10^{-3}$	$(4.7\pm.4)\times10^{-3}$	$(2.88\pm.1)\times10^{-3}$	$(1.6\pm.2)\times10^{-3}$	$(1.7\pm.1)\times10^{-3}$	$(1.7\pm0.4)\times10^{-3}$
	5.7±.5	6.6±.6	3.70±.1	5.1±.7	8.8±.6	11.5±1.5
2.5	$(2.2\pm.3)\times10^{-3}$		$(1.29\pm.06)\times10^{-3}$	$(6.9\pm.9)\times10^{-4}$		
	4.6±.7		3.90±.10	2.6±.8		
2.75			$(6.84\pm.6)\times10^{-4}$			
			4.60±.2			
3.0	$(7.7\pm2.4)\times10^{-4}$	$(7.2\pm2.5)\times10^{-4}$	$(2.72\pm.2)\times10^{-4}$	$(3.7\pm1.6)\times10^{-4}$	$(3.0\pm0.9)\times10^{-4}$	$(4.8\pm0.2)\times10^{-4}$
	8.2±1.6	8.8±1.8	4.40±.2	8.8±2.2	10.7±1.4	16.7±2.0

Figure Captions

Fig. 1: The plot shows the lines in the center of momentum frame along which measurements are made to study scaling in the case of fixed Feynman (F) variable $x_{\parallel}$, and fixed radial (R) variable x_R.

Fig. 2: The π^+ invariant cross section $E\frac{d\sigma}{dp^3}$ for constant x_R or $x_{\parallel}$ and for various constant values of $p_\perp$ versus the center of momentum energy $\sqrt{s}$. The dotted line is to guide the eye through points of constant $x_{\parallel}$ and $p_\perp$. The smooth line is the average value of $E\frac{d\sigma}{dp^3}$ for constant x_R and $p_\perp$ for $\sqrt{s} \gtrsim 10$ GeV, and extends from the $\sqrt{s}$ threshold (calculated using Eq. 9, taking into account the finite bin widths in x_R and $p_\perp$) to $\sqrt{s} = 70$ GeV. The cases where there was only one high $p_\perp$ data point were not plotted.

a) x_R or $x_{\parallel} = 0.05 \pm 0.05$

b) x_R or $x_{\parallel} = 0.25 \pm 0.05$

c) x_R or $x_{\parallel} = 0.45 \pm 0.05$

d) x_R or $x_{\parallel} = 0.65 \pm 0.05$

e) x_R or $x_{\parallel} = 0.85 \pm 0.05$

Fig. 3: The π^- invariant cross section $E\frac{d\sigma}{dp^3}$ for constant x_R or $x_{\parallel}$ and constant values of $p_\perp$ versus $\sqrt{s}$.

a) x_R or $x_{\parallel} = 0.05 \pm 0.05$

b) x_R or $x_{\parallel} = 0.25 \pm 0.05$

c) x_R or $x_{\parallel} = 0.45 \pm 0.05$

d) x_R or $x_{\parallel} = 0.65 \pm 0.05$

Fig. 4: The π^o invariant cross section $E\frac{d\sigma}{dp^3}$ for constant x_R or $x_{\parallel}$ and constant values of $p_\perp$ versus $\sqrt{s}$.

a) x_R or $x_{\parallel} = 0.05 \pm 0.05$

b) x_R or $x_{\parallel} = 0.25 \pm 0.05$

c) x_R or $x_{\parallel} = 0.45 \pm 0.05$

d) x_R or $x_{\parallel} = 0.65 \pm 0.05$

Fig. 5: The K^+ invariant cross section $E \frac{d\sigma}{dp^3}$ for constant x_R or $x_{\parallel}$ and constant values of $p_\perp$ versus $\sqrt{s}$.

a) x_R or $x_{\parallel} = 0.05 \pm 0.05$

b) x_R or $x_{\parallel} = 0.25 \pm 0.05$

c) x_R or $x_{\parallel} = 0.45 \pm 0.05$

d) x_R or $x_{\parallel} = 0.65 \pm 0.05$

Fig. 6: The K^- invariant cross section $E \frac{d\sigma}{dp^3}$ for constant x_R or $x_{\parallel}$ and constant values of $p_\perp$ versus $\sqrt{s}$.

a) x_R or $x_{\parallel} = 0.05 \pm 0.05$

b) x_R or $x_{\parallel} = 0.25 \pm 0.05$

c) x_R or $x_{\parallel} = 0.45 \pm 0.05$

d) x_R or $x_{\parallel} = 0.65 \pm 0.05$

Fig. 7: The proton invariant cross section $E \frac{d\sigma}{dp^3}$ for constant x_R or $x_{\parallel}$ and constant values of $p_\perp$ versus $\sqrt{s}$.

a) x_R or $x_{\parallel} = 0.05 \pm 0.05$

b) x_R or $x_{\parallel} = 0.25 \pm 0.05$

c) x_R or $x_{\parallel} = 0.45 \pm 0.05$

d) x_R or $x_{\parallel} = 0.65 \pm 0.05$

e) x_R or $x_{\parallel} = 0.85 \pm 0.05$

Fig. 8: The anti-proton invariant cross section $E \frac{d\sigma}{dp^3}$ for constant x_R or $x_{\parallel}$ and constant values of $p_\perp$ versus $\sqrt{s}$.

a) x_R or $x_{\parallel} = 0.05 \pm 0.05$

b) x_R or $x_{\parallel} = 0.25 \pm 0.05$

c) x_R or $x_{\parallel} = 0.45 \pm 0.05$

d) x_R or $x_{\parallel} = 0.65 \pm 0.05$

Fig. 9: The normalized Peyrou plot showing the kinematic region covered for each particle species in the data compilation. The forward-backward symmetry of p-p collisions was used to map $-|x_{\parallel}|$ to $+|x_{\parallel}|$. The quarter circles are lines of various constant values x_R.

a) Normalized Peyrou plot for π^+

b) Normalized Peyrou plot for π^-

c) Normalized Peyrou plot for π^o

d) Normalized Peyrou plot for K^+

e) Normalized Peyrou plot for K^-

f) Normalized Peyrou plot for p

g) Normalized Peyrou plot for $\bar{p}$

Fig. 10: The transverse momentum dependence of the invariant cross section $E\frac{d\sigma}{dp^3}$ for various constant values of x_R in the radial scaling region: $\sqrt{s} \gtrsim 10$ GeV. The solid lines are the function $\frac{A}{(1 + \frac{p_\perp^2}{m^2})^q}$ where the values of A, m^2, q are given in Table III.

a) π^+ invariant cross section: $E\frac{d\sigma}{dp^3}\Big|_{<x_R>}$

b) π^- invariant cross section: $E\frac{d\sigma}{dp^3}\Big|_{<x_R>}$

c) π^o invariant cross section: $E\frac{d\sigma}{dp^3}\Big|_{<x_R>}$

d) K^+ invariant cross section: $E\frac{d\sigma}{dp^3}\Big|_{<x_R>}$

e) K^- invariant cross section: $E\frac{d\sigma}{dp^3}\Big|_{<x_R>}$

f) p invariant cross section: $E\frac{d\sigma}{dp^3}\Big|_{<x_R>}$

g) $\bar{p}$ invariant cross section: $E \frac{d\sigma}{dp^3}\Big|_{<x_R>}$

Fig. 11: The x_R dependence of the invariant cross section $E \frac{d\sigma}{dp^3}$ for various constant values of $p_\perp$ in the radial scaling region: $\sqrt{s} \gtrsim 10$ GeV. The solid lines are the function $B(1 - x_R)^n$ where B and n are determined from the minimum χ^2 fit to $E \frac{d\sigma}{dp^3}\Big|_{<p_\perp>}$, and are given in Table IV.

a) π^+ invariant cross section: $E \frac{d\sigma}{dp^3}\Big|_{<p_\perp>}$

b) π^- invariant cross section: $E \frac{d\sigma}{dp^3}\Big|_{<p_\perp>}$

c) π^o invariant cross section: $E \frac{d\sigma}{dp^3}\Big|_{<p_\perp>}$

d) K^+ invariant cross section: $E \frac{d\sigma}{dp^3}\Big|_{<p_\perp>}$

e) K^- invariant cross section: $E \frac{d\sigma}{dp^3}\Big|_{<p_\perp>}$

f) p invariant cross section: $E \frac{d\sigma}{dp^3}\Big|_{<p_\perp>}$

The dotted line is to guide the eye, since no fit of the form $B(1 - x_R)^n$ was performed.

g) $\bar{p}$ invariant cross section: $E \frac{d\sigma}{dp^3}\Big|_{<p_\perp>}$

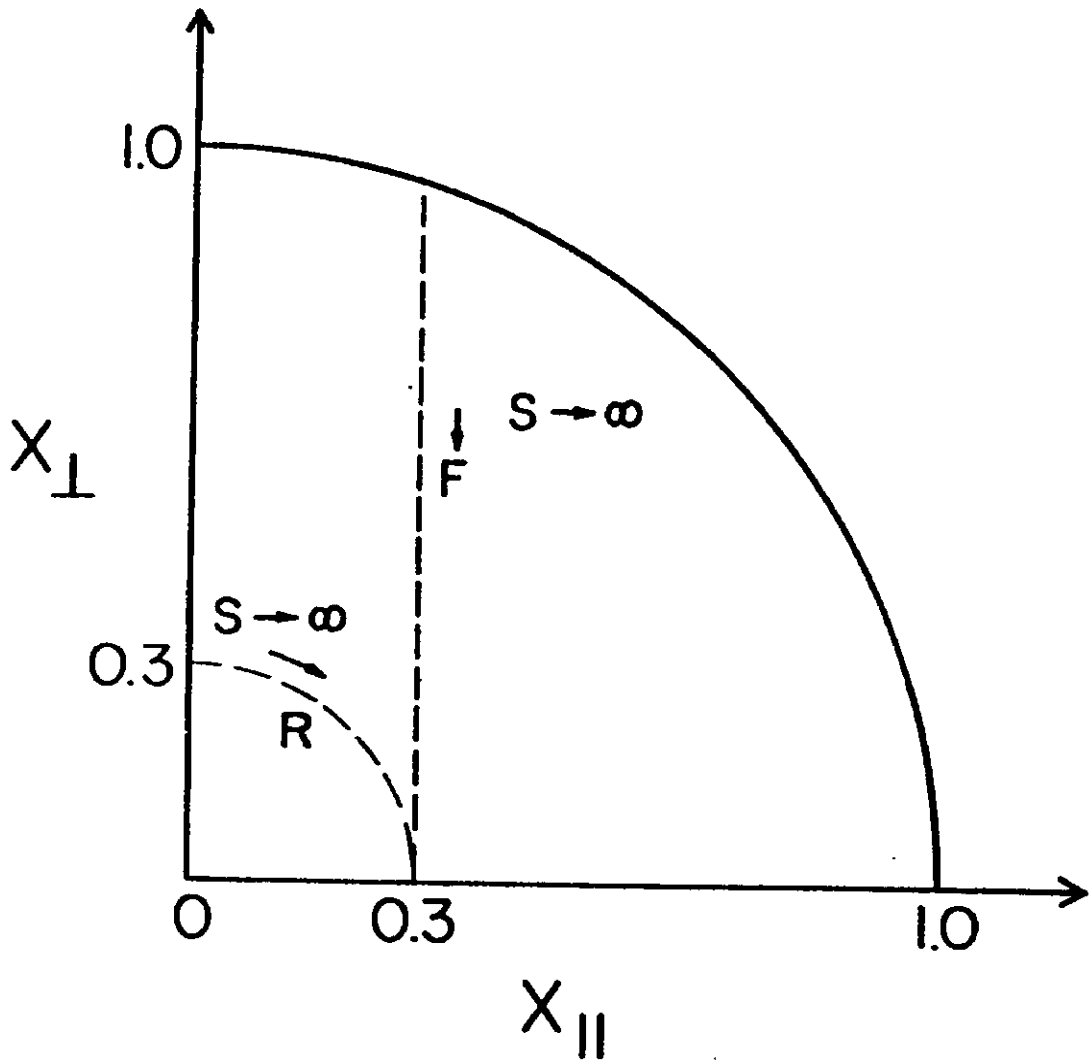

Fig. 1

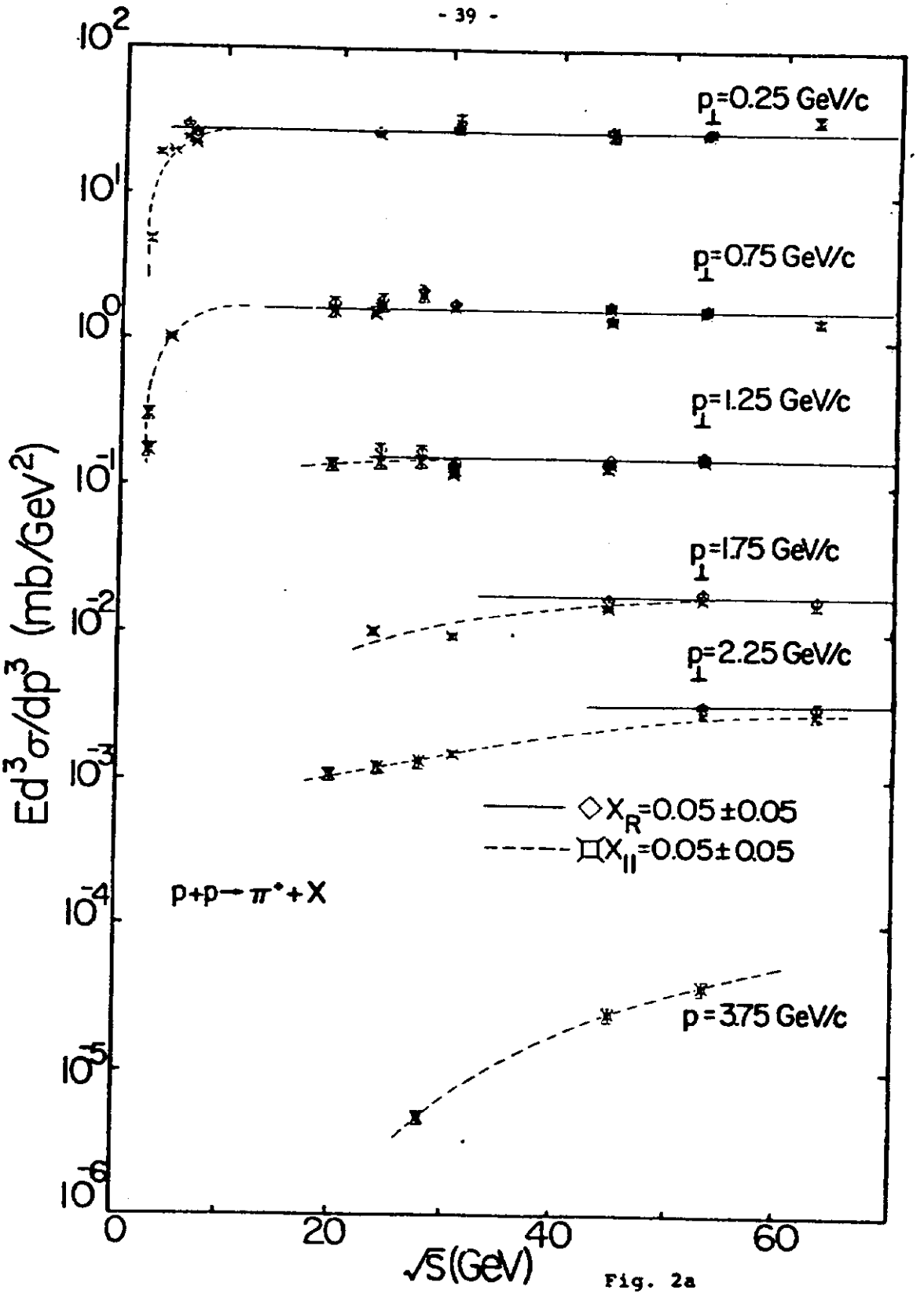
10^2
10^1
10^0
10^{-1}
10^{-2}
10^{-3}
10^{-4}
10^{-5}
10^{-6}
$Ed^3\sigma/dp^3$ (mb/GeV^2)
$p_\perp$=0.25 GeV/c
$p_\perp$=0.75 GeV/c
$p_\perp$=1.25 GeV/c
$p_\perp$=1.75 GeV/c
$p_\perp$=2.25 GeV/c
p = 3.75 GeV/c
$\diamond X_R$=0.05 ±0.05
$\square X_{||}$=0.05± 0.05
p+p→ π° + X
0
20
40
60
√S(GeV)

Fig. 2a

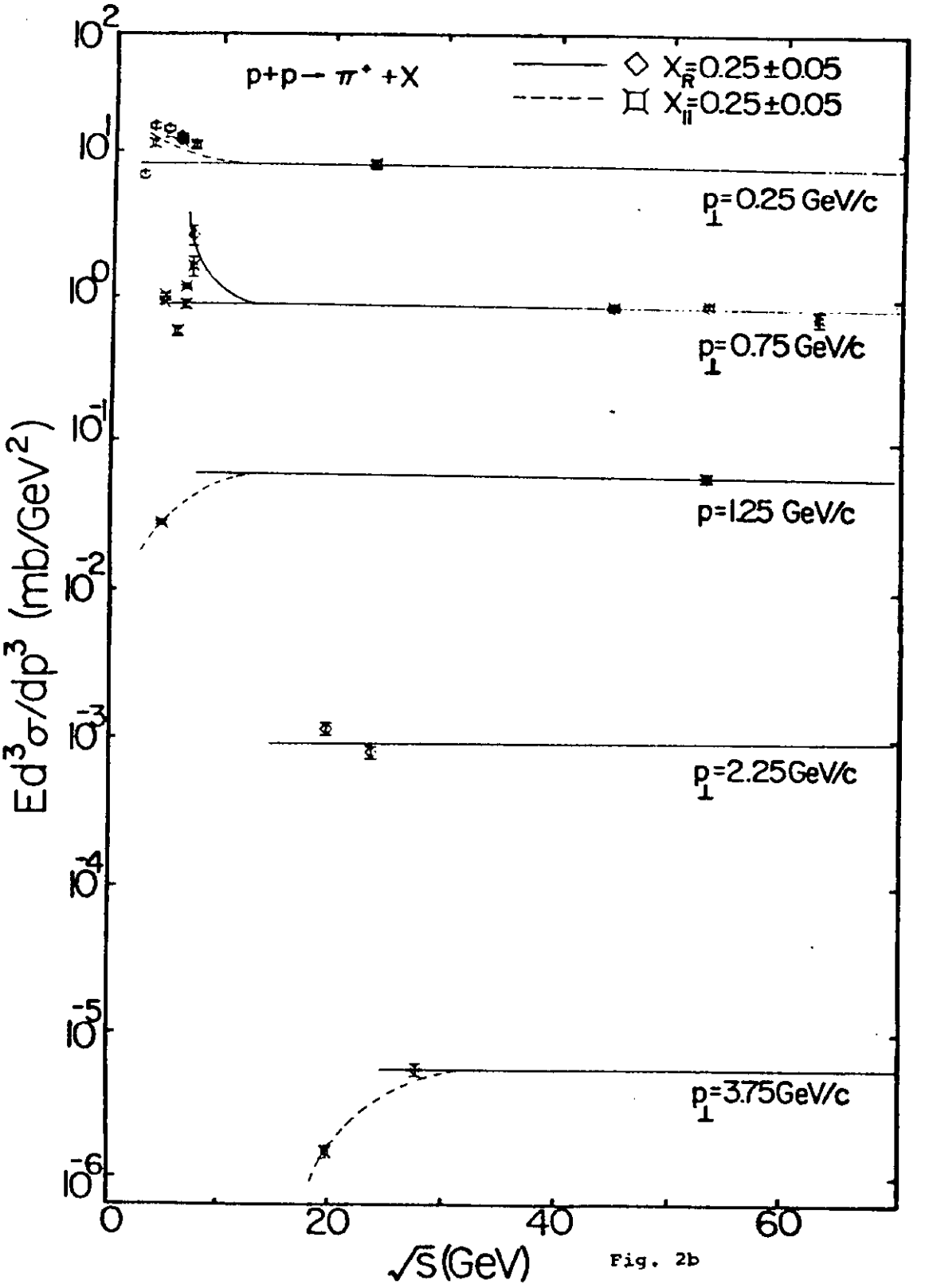
p+p→π⁺+X
X_R=0.25±0.05
X_II=0.25±0.05
p_⊥=0.25 GeV/c
p_⊥=0.75 GeV/c
p=1.25 GeV/c
p_⊥=2.25GeV/c
p_⊥=3.75GeV/c
Ed³σ/dp³ (mb/GeV²)
√s(GeV)
0
20
40
60

Fig. 2b

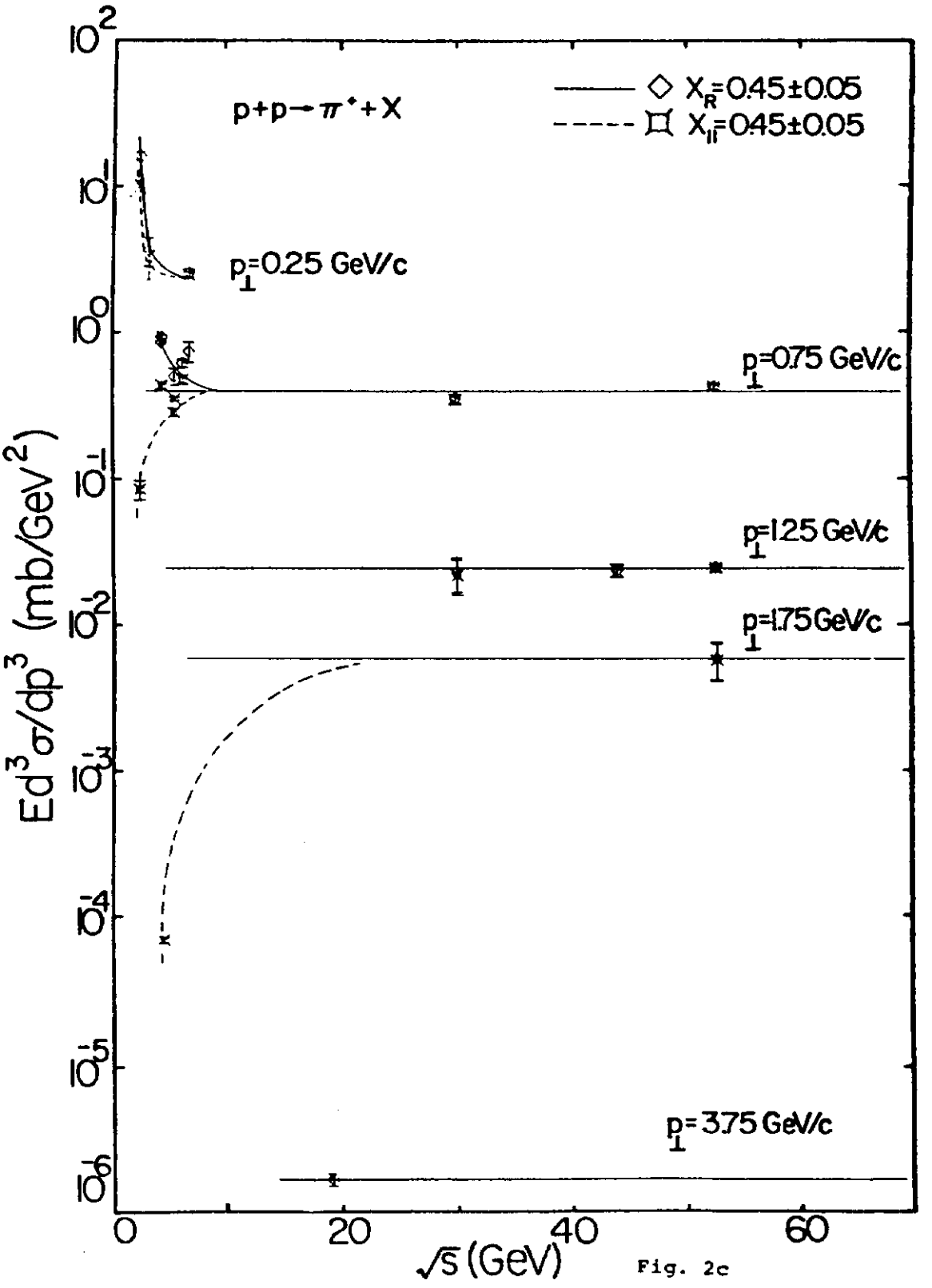
p+p→π°+X
X_R=0.45±0.05
X_II=0.45±0.05
p_⊥=0.25 GeV/c
p_⊥=0.75 GeV/c
p_⊥=1.25 GeV/c
p_⊥=1.75 GeV/c
p_⊥=3.75 GeV/c
Ed³σ/dp³ (mb/GeV²)
√s (GeV)
0
20
40
60

Fig. 2c

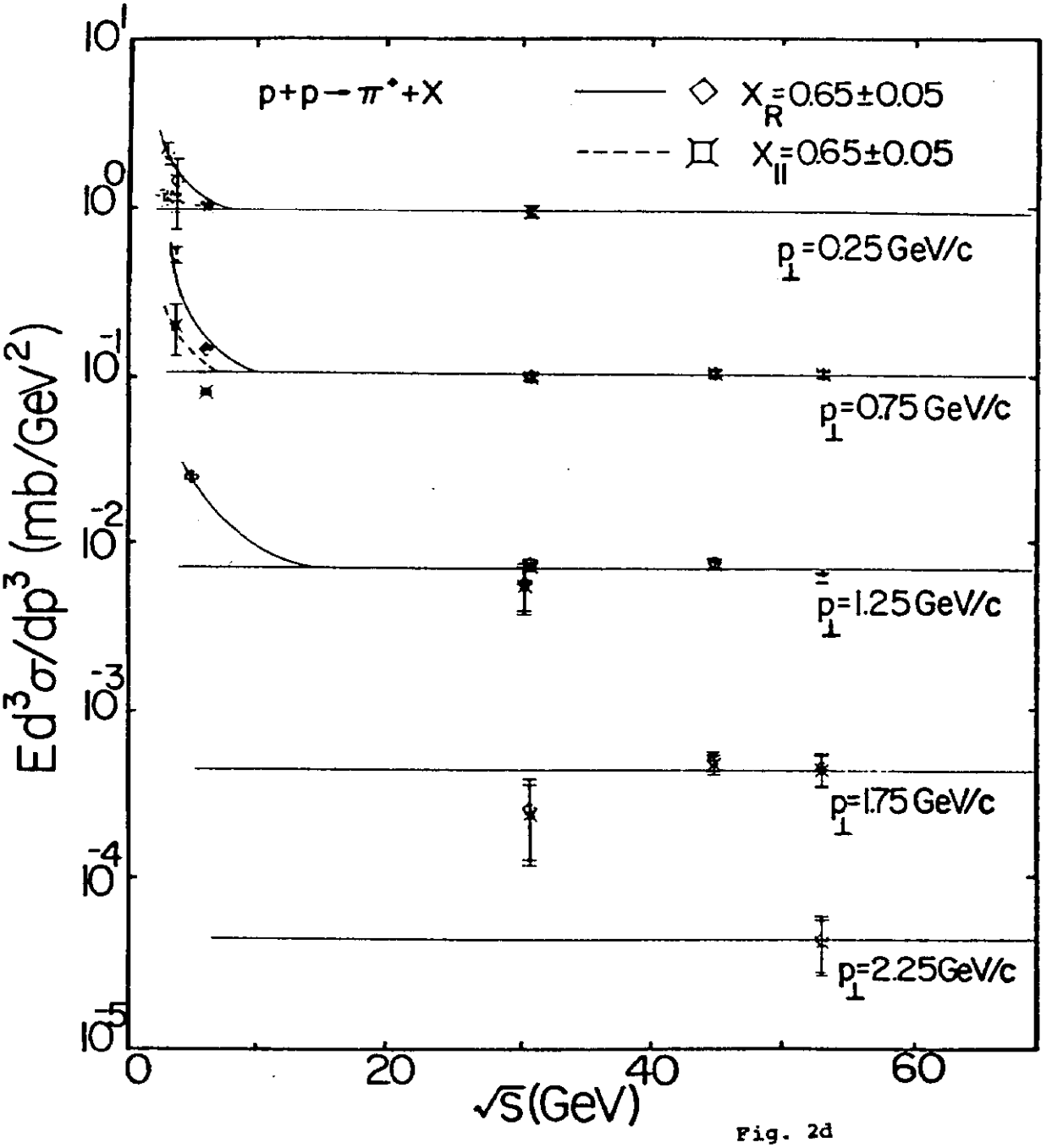
p+p→π°+X
X_R=0.65±0.05
X_II=0.65±0.05
p_⊥=0.25 GeV/c
p_⊥=0.75 GeV/c
p_⊥=1.25 GeV/c
p_⊥=1.75 GeV/c
p_⊥=2.25 GeV/c
Ed³σ/dp³ (mb/GeV²)
√s(GeV)
0
20
40
60

Fig. 2d

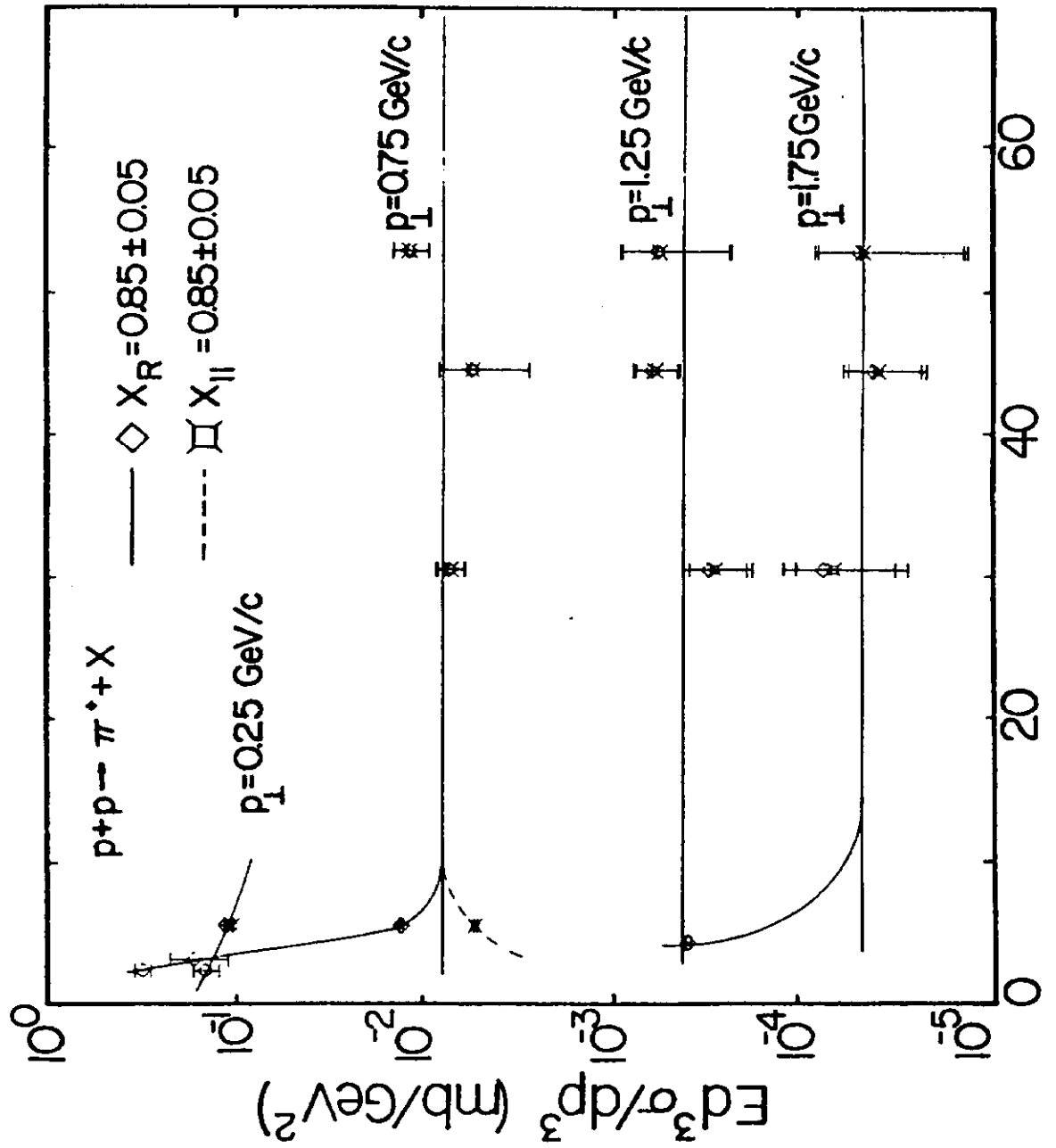
p+p → π°+X
p_T=0.25 GeV/c
p_T=0.75 GeV/c
p_T=1.25 GeV/c
p_T=1.75GeV/c
◇ X_R=0.85±0.05
□ X_∥ =0.85±0.05
Ed³σ/dp³ (mb/GeV²)
√s(GeV)

Fig. 2e

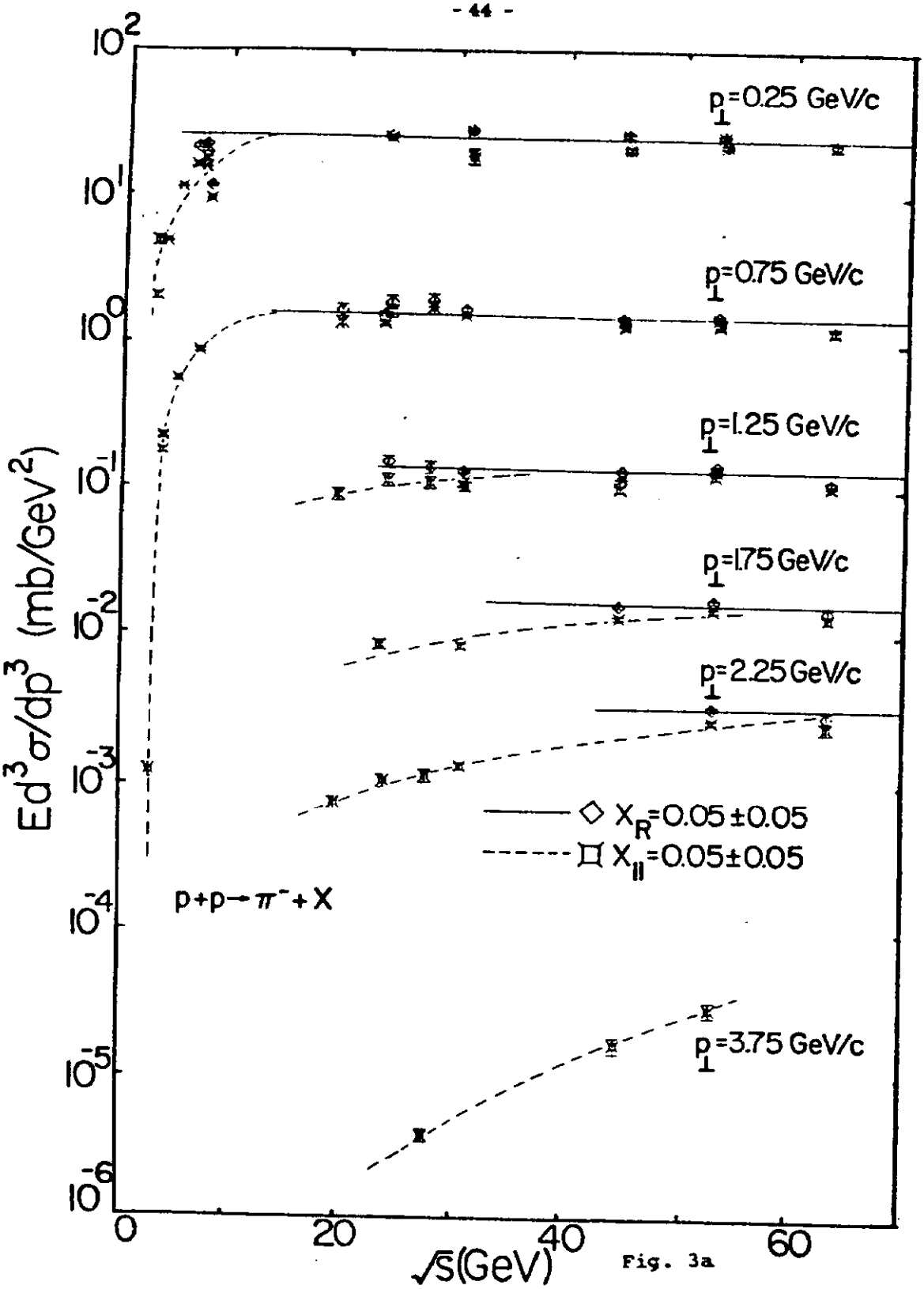
10^2
10^1
10^0
10^{-1}
10^{-2}
10^{-3}
10^{-4}
10^{-5}
10^{-6}
$Ed^3\sigma/dp^3$ (mb/GeV^2)
$p_\perp$=0.25 GeV/c
$p_\perp$=0.75 GeV/c
$p_\perp$=1.25 GeV/c
$p_\perp$=1.75 GeV/c
$p_\perp$=2.25 GeV/c
$p_\perp$=3.75 GeV/c
◇ X_R=0.05±0.05
□ $X_{||}$=0.05±0.05
p+p→π⁻+X
0
20
40
60
$\sqrt{s}$(GeV)

Fig. 3a

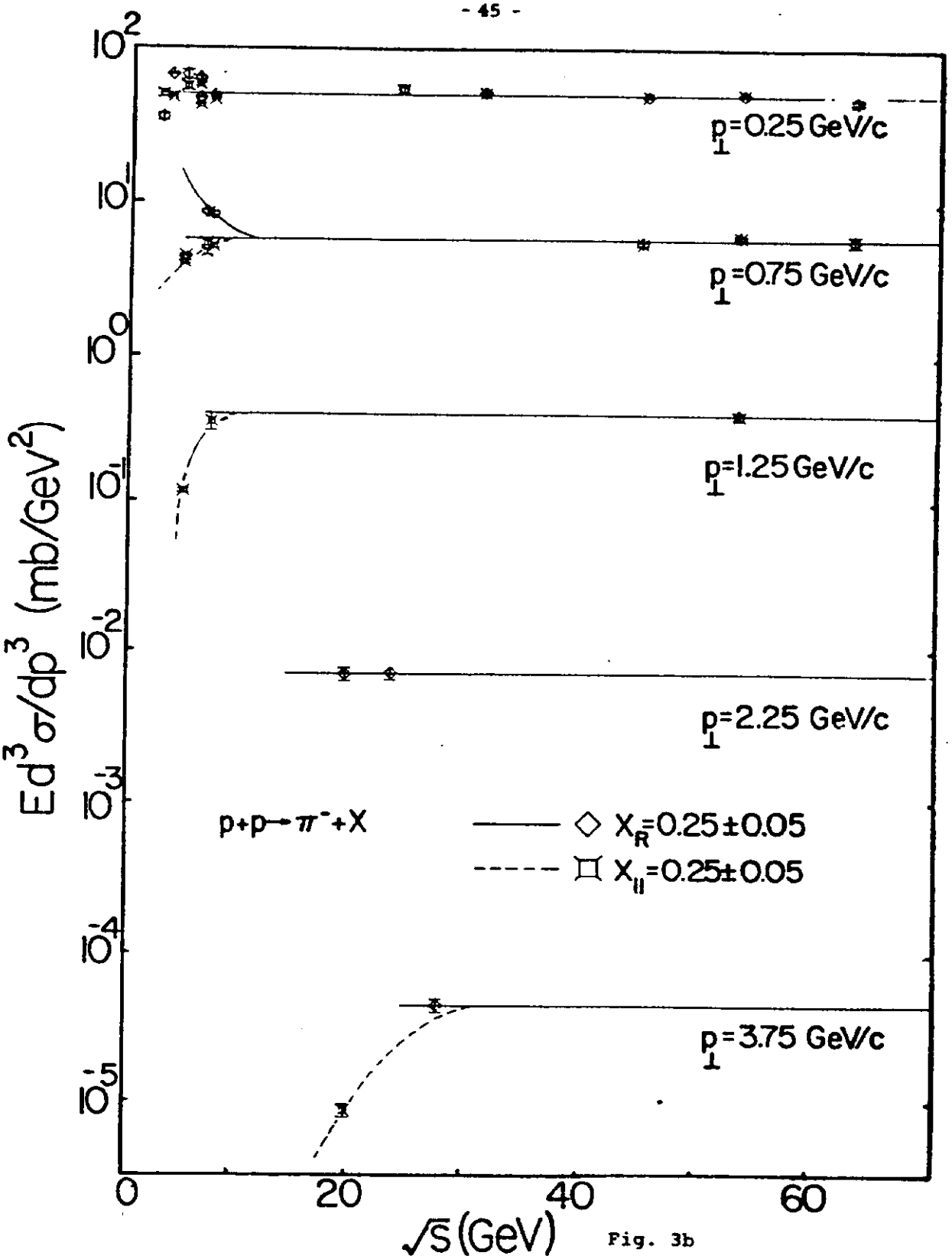
10^2
10
10^0
10^{-1}
10^{-2}
10^{-3}
10^{-4}
10^{-5}
$Ed^3\sigma/dp^3$ (mb/GeV^2)
$p_\perp$=0.25 GeV/c
$p_\perp$=0.75 GeV/c
$p_\perp$=1.25 GeV/c
$p_\perp$=2.25 GeV/c
$p_\perp$=3.75 GeV/c
$p+p\rightarrow\pi^-+X$
X_R=0.25±0.05
$X_{||}$=0.25±0.05
0
20
40
60
$\sqrt{s}$ (GeV)

Fig. 3b

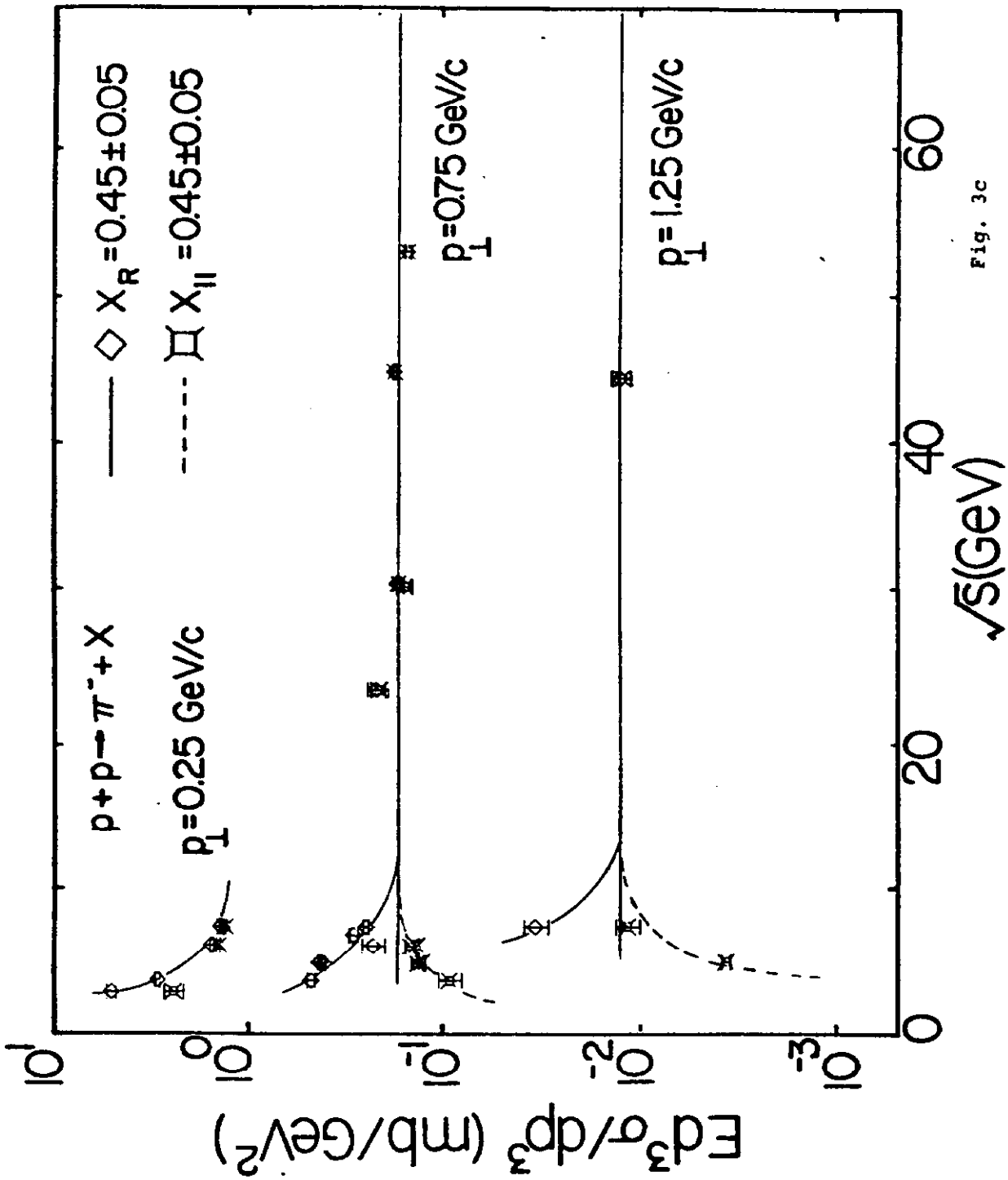
$Ed^3\sigma/dp^3$ (mb/GeV^2)
10^1
10^0
10^{-1}
10^{-2}
10^{-3}
0
20
40
60
$\sqrt{s}$(GeV)
p+p→π⁻+X
p_T=0.25 GeV/c
p_T=0.75 GeV/c
p_T= 1.25 GeV/c
—— ◇ X_R=0.45±0.05
----- ⌑ X_{II} =0.45±0.05

Fig. 3c

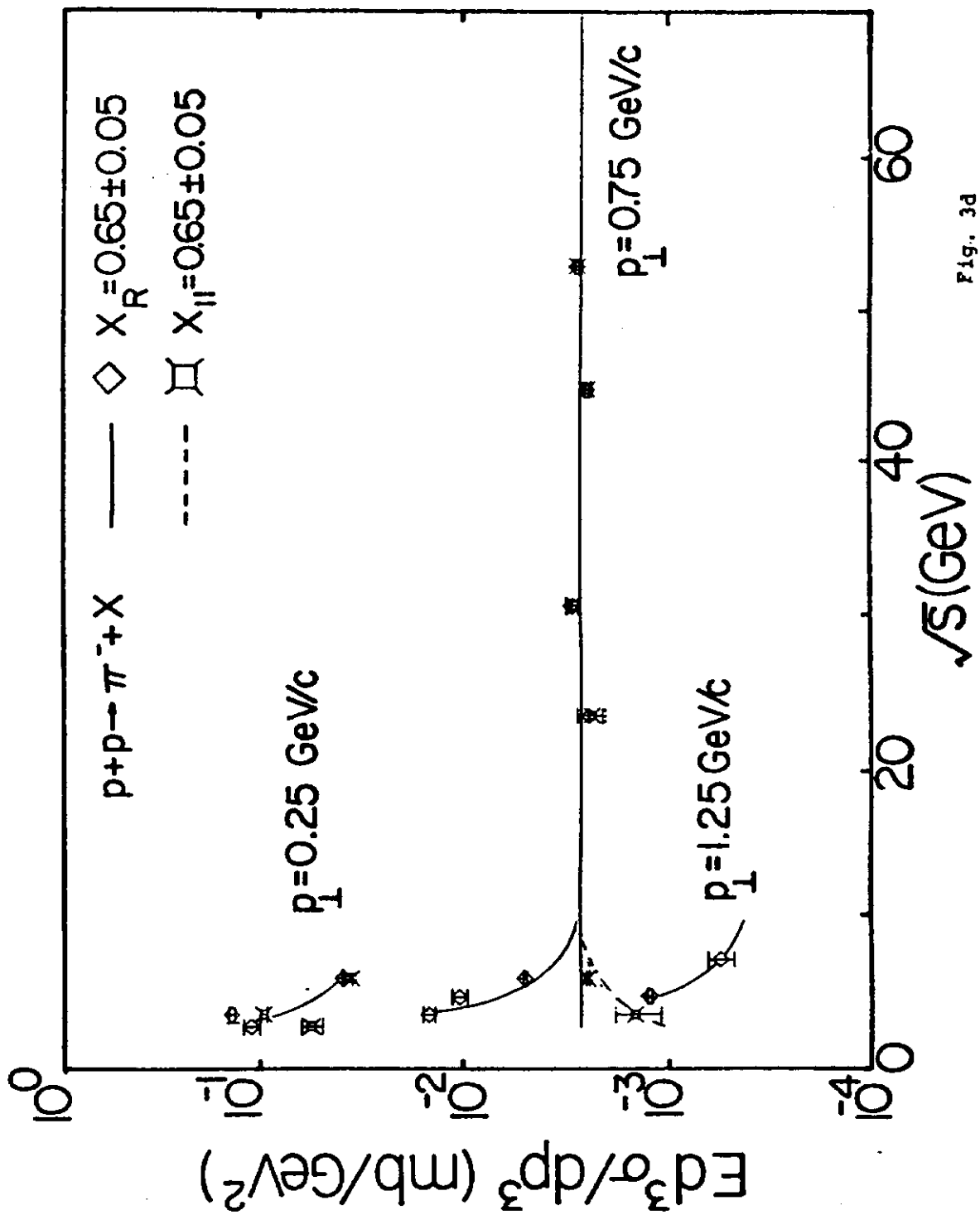
p+p→π⁻+X
X_R=0.65±0.05
X_II=0.65±0.05
p_T=0.25 GeV/c
p_T=0.75 GeV/c
p_T=1.25 GeV/c
Ed³σ/dp³ (mb/GeV²)
√S(GeV)
10⁰
10⁻¹
10⁻²
10⁻³
10⁻⁴
0
20
40
60

Fig. 3d

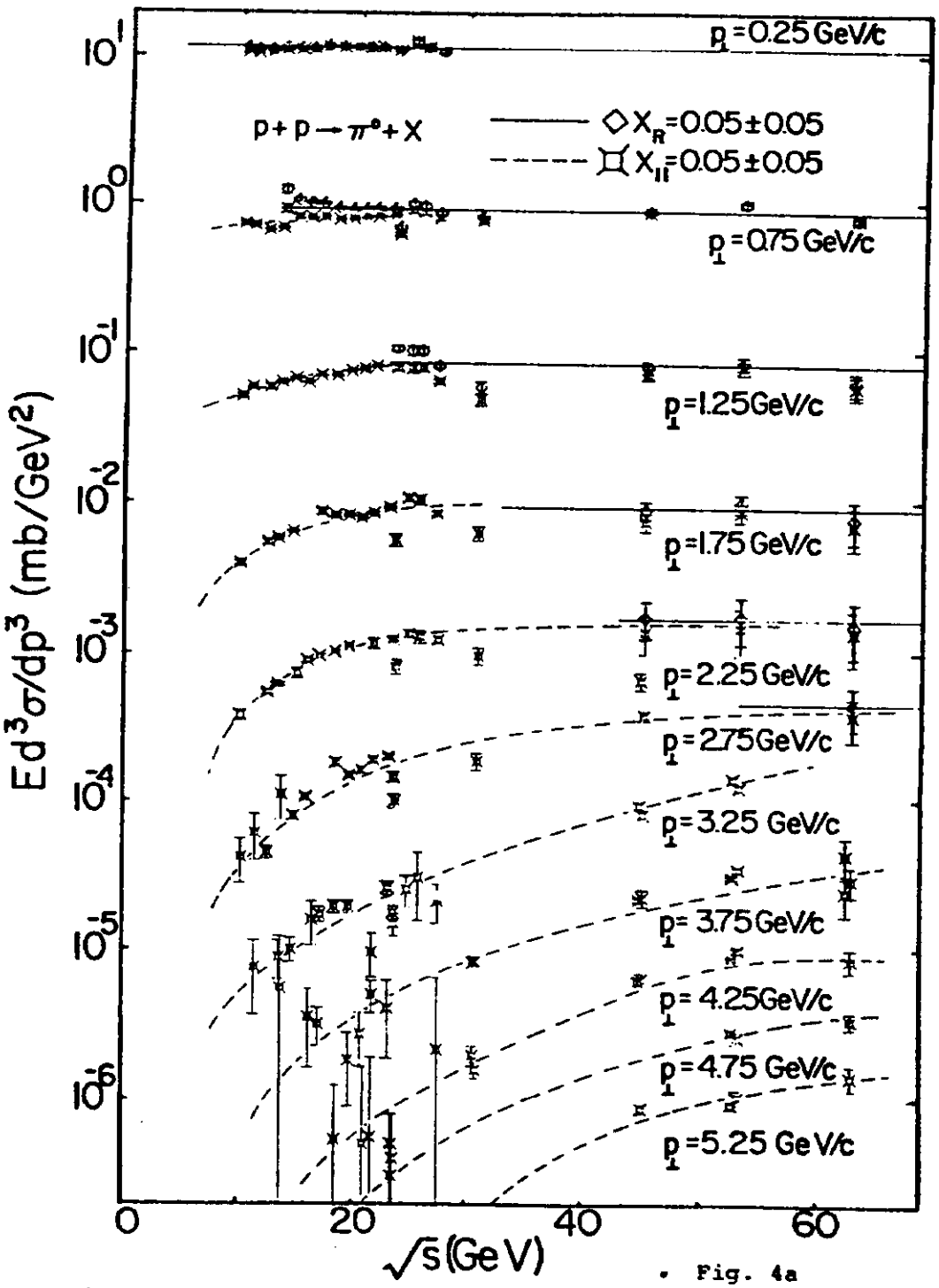
$p_\perp$=0.25 GeV/c
$p+p \to \pi^0+X$
$\diamond X_R$=0.05±0.05
$\square X_{II}$=0.05±0.05
$p_\perp$=0.75 GeV/c
$p_\perp$=1.25GeV/c
$p_\perp$=1.75 GeV/c
$p_\perp$=2.25 GeV/c
$p_\perp$=2.75GeV/c
$p_\perp$=3.25 GeV/c
$p_\perp$=3.75GeV/c
$p_\perp$=4.25GeV/c
$p_\perp$=4.75 GeV/c
$p_\perp$=5.25 GeV/c
$Ed^3\sigma/dp^3$ (mb/GeV^2)
$\sqrt{s}$(GeV)
0
20
40
60

Fig. 4a

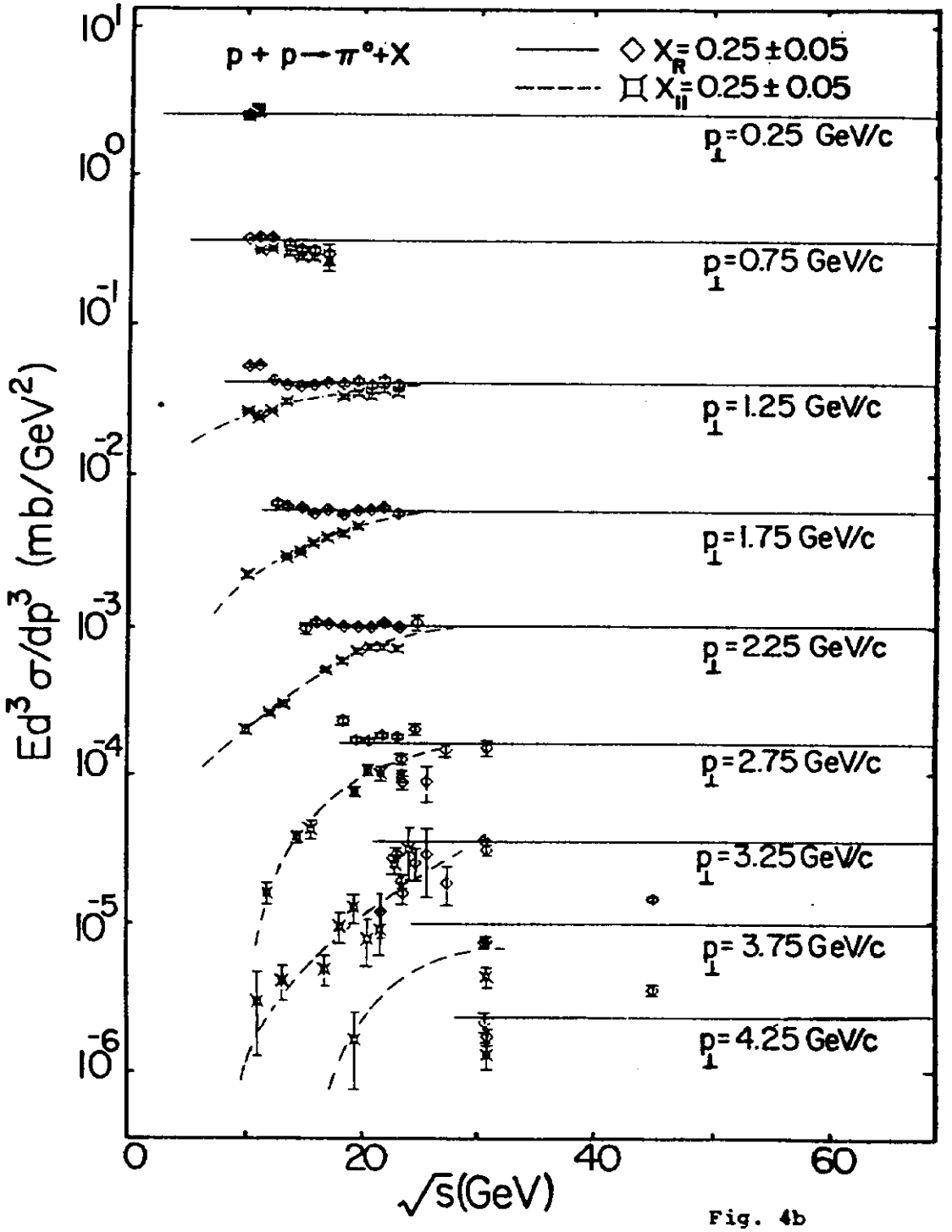
p + p → π° + X
◇ X_R = 0.25 ± 0.05
□ X_II = 0.25 ± 0.05
p_⊥ = 0.25 GeV/c
p_⊥ = 0.75 GeV/c
p_⊥ = 1.25 GeV/c
p_⊥ = 1.75 GeV/c
p_⊥ = 2.25 GeV/c
p_⊥ = 2.75 GeV/c
p_⊥ = 3.25 GeV/c
p_⊥ = 3.75 GeV/c
p_⊥ = 4.25 GeV/c
Ed³σ/dp³ (mb/GeV²)
√s(GeV)
0
20
40
60

Fig. 4b

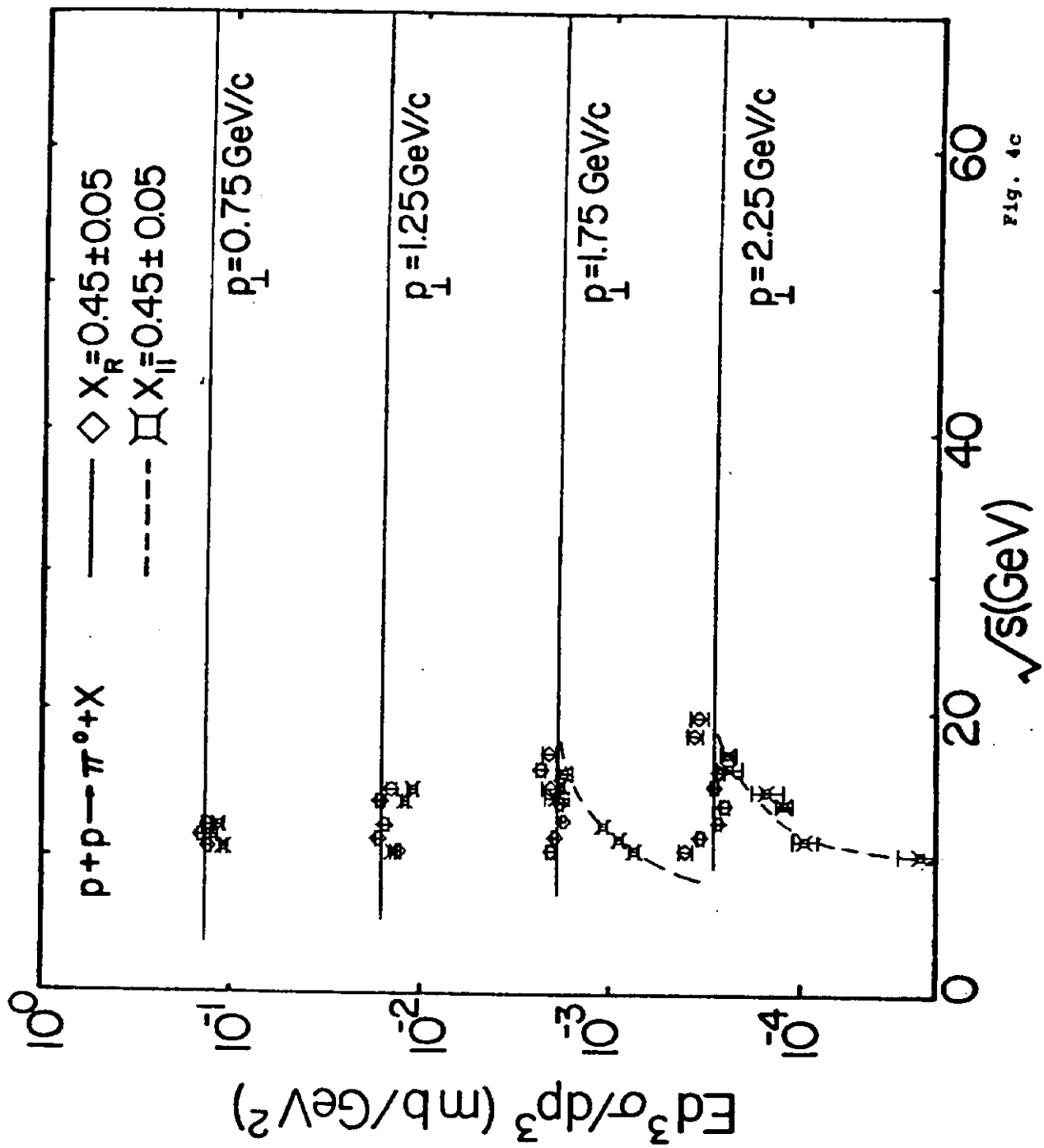
p+p→π°+X
◇ X_R=0.45±0.05
X_II=0.45±0.05
p_T=0.75 GeV/c
p_T=1.25 GeV/c
p_T=1.75 GeV/c
p_T=2.25 GeV/c
Ed³σ/dp³ (mb/GeV²)
√s(GeV)
10⁰
10⁻¹
10⁻²
10⁻³
10⁻⁴
0
20
40
60

Fig. 4c

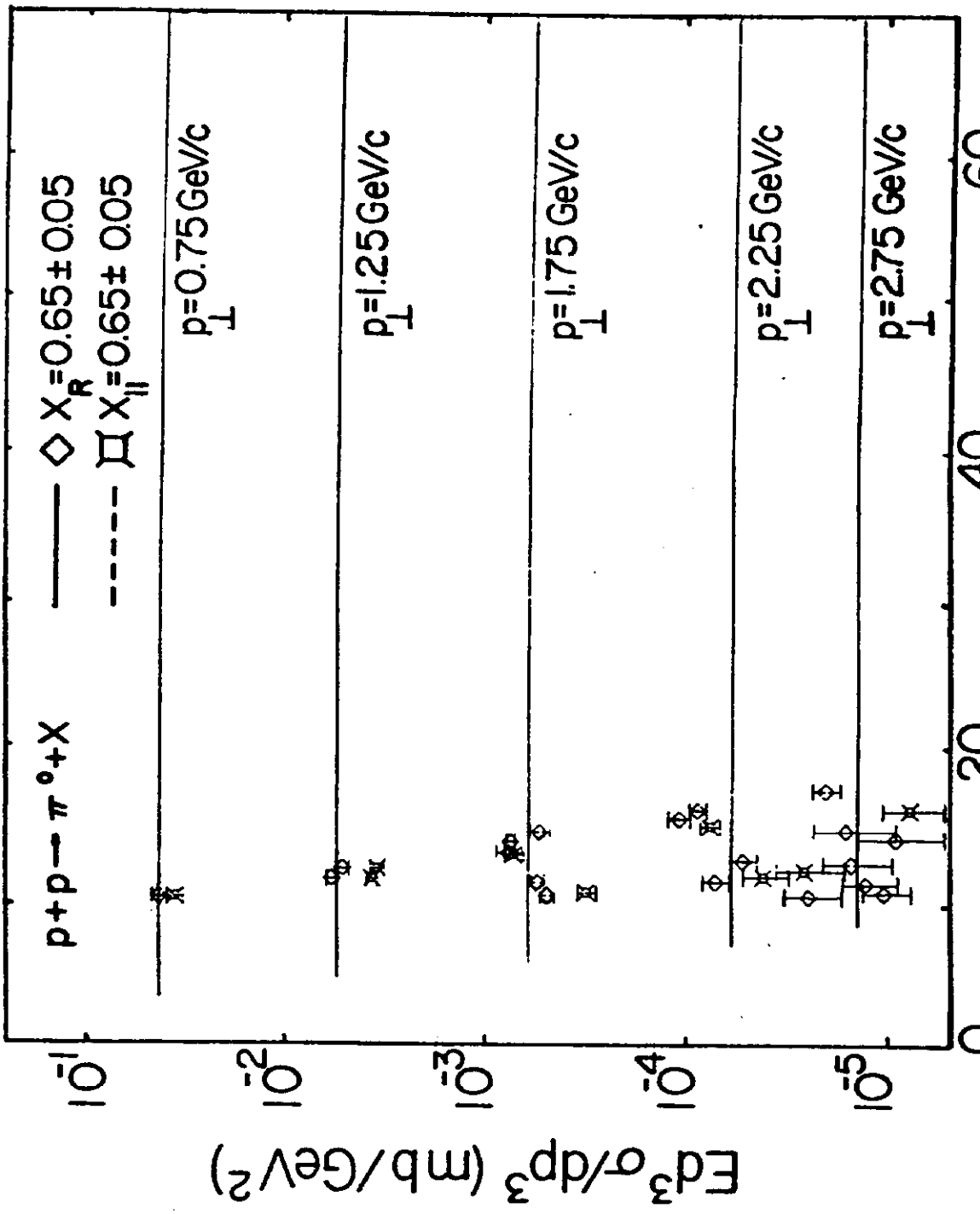
p+p→π°+X
◇ X_R=0.65±0.05
□ X_∥=0.65±0.05
p_T=0.75 GeV/c
p_T=1.25 GeV/c
p_T=1.75 GeV/c
p_T=2.25 GeV/c
p_T=2.75 GeV/c
Ed³σ/dp³ (mb/GeV²)
√s(GeV)
0
20
40
60
10⁻¹
10⁻²
10⁻³
10⁻⁴
10⁻⁵

Fig. 4d

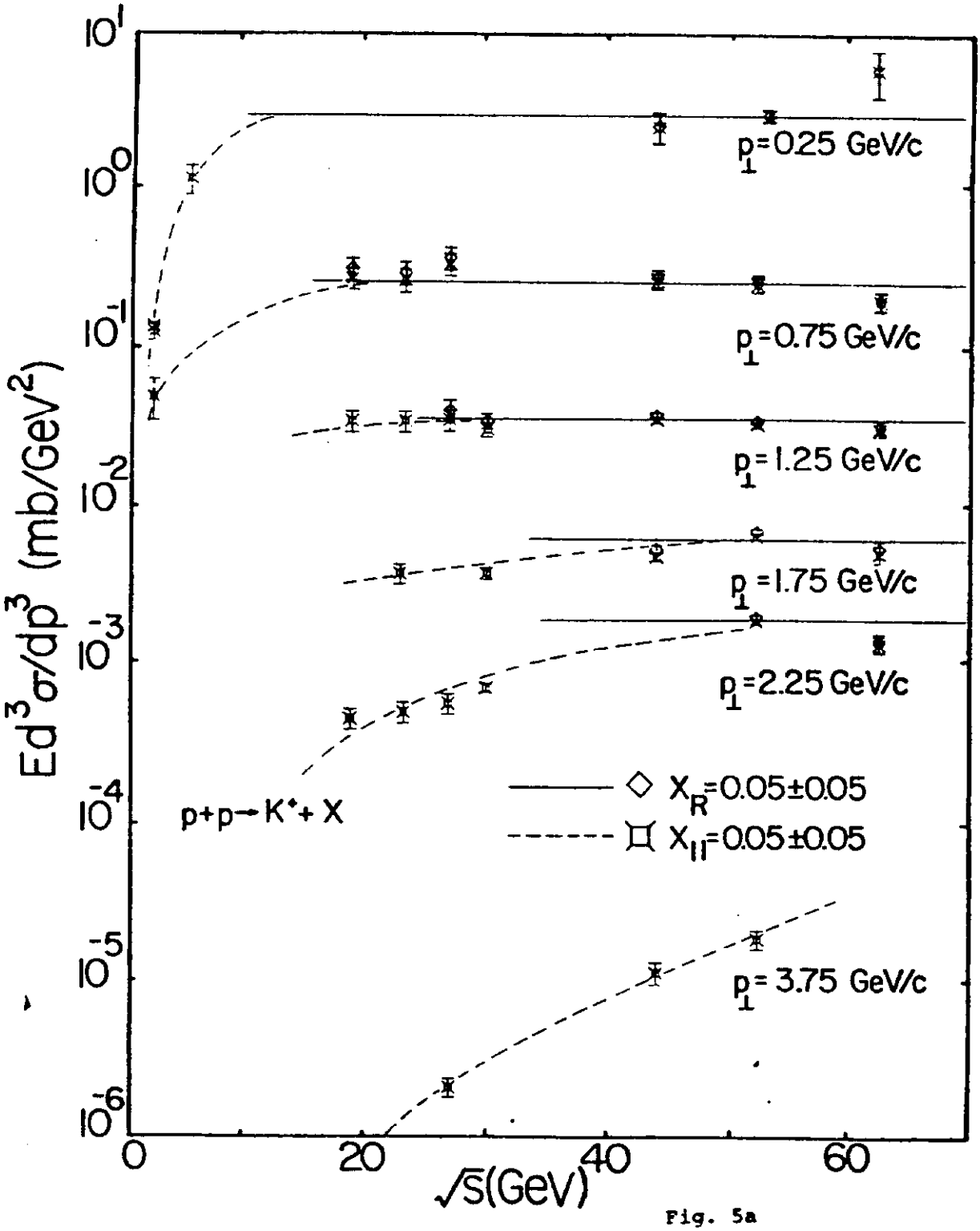
$Ed^3\sigma/dp^3$ (mb/GeV^2)
10^1
10^0
10^{-1}
10^{-2}
10^{-3}
10^{-4}
10^{-5}
10^{-6}
0
20
40
60
$\sqrt{s}$(GeV)
$p_\perp$=0.25 GeV/c
$p_\perp$=0.75 GeV/c
$p_\perp$=1.25 GeV/c
$p_\perp$=1.75 GeV/c
$p_\perp$=2.25 GeV/c
$p_\perp$= 3.75 GeV/c
$p+p \rightarrow K^* + X$
◇ X_R=0.05±0.05
□ X_{II}=0.05±0.05

Fig. 5a

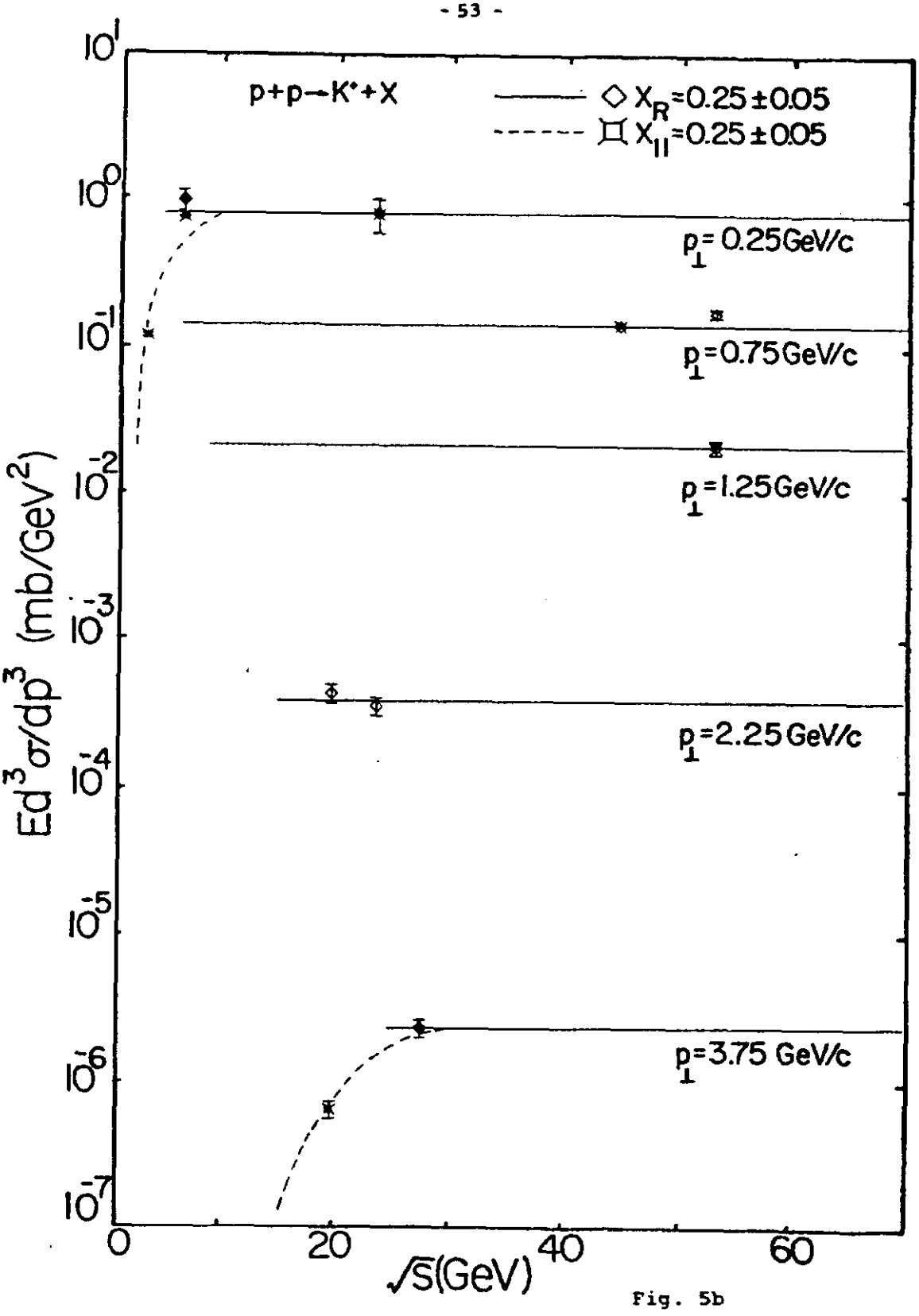
p+p→K°+X
◇ X_R=0.25±0.05
⌑ X_{II}=0.25±0.05
$p_\perp$= 0.25GeV/c
$p_\perp$=0.75GeV/c
$p_\perp$=1.25GeV/c
$p_\perp$=2.25GeV/c
$p_\perp$=3.75 GeV/c
$Ed^3\sigma/dp^3$ (mb/GeV^2)
$\sqrt{s}$(GeV)
10^1
10^0
10^{-1}
10^{-2}
10^{-3}
10^{-4}
10^{-5}
10^{-6}
10^{-7}
0
20
40
60

Fig. 5b

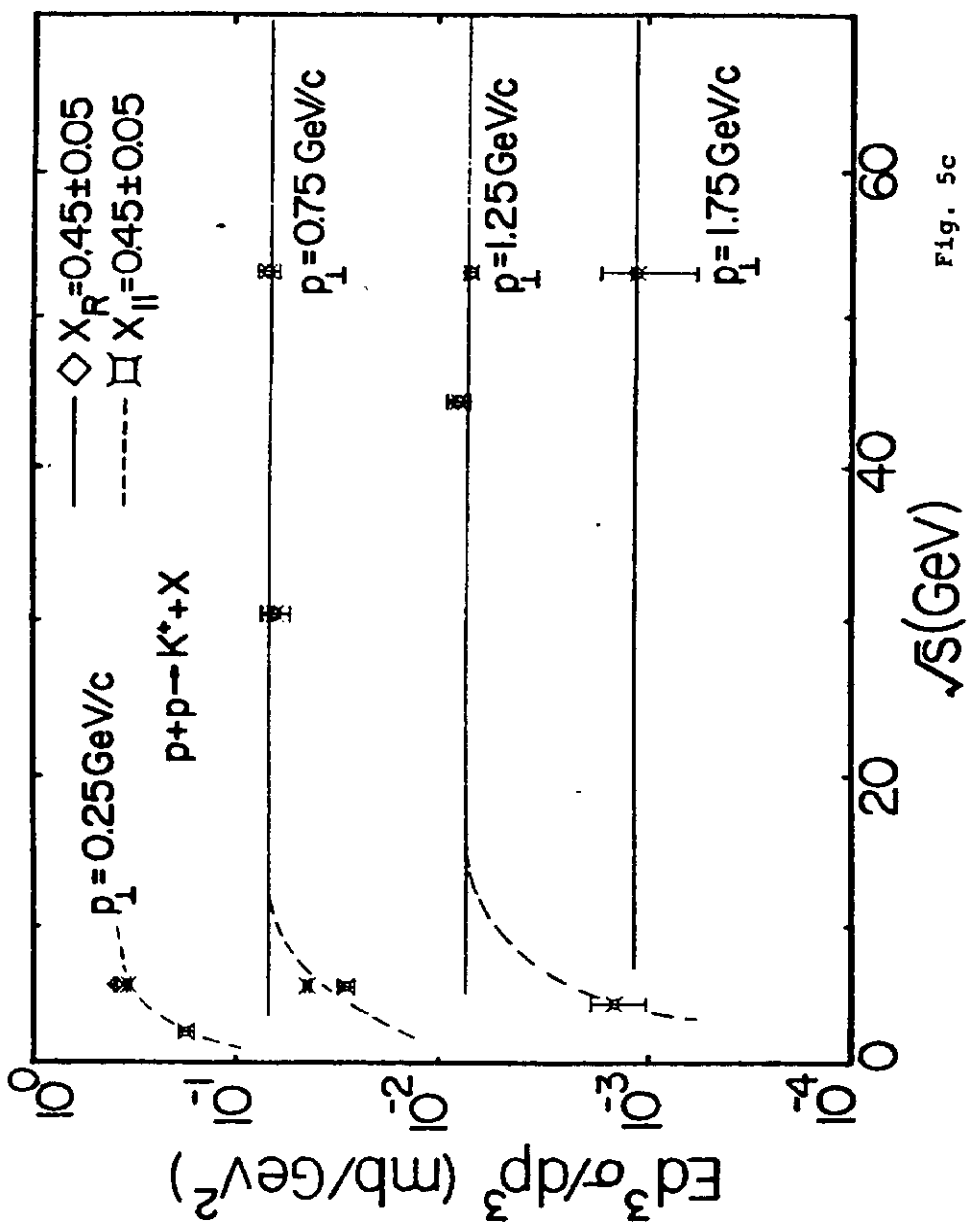
$Ed^3\sigma/dp^3$ (mb/GeV^2)
10^0
10^{-1}
10^{-2}
10^{-3}
10^{-4}
0
20
40
60
$\sqrt{s}$(GeV)
p+p→K$^+$+X
p_T=0.25GeV/c
p_T=0.75 GeV/c
p_T=1.25GeV/c
p_T=1.75GeV/c
◇ X_R=0.45±0.05
□ $X_{||}$=0.45±0.05

Fig. 5c

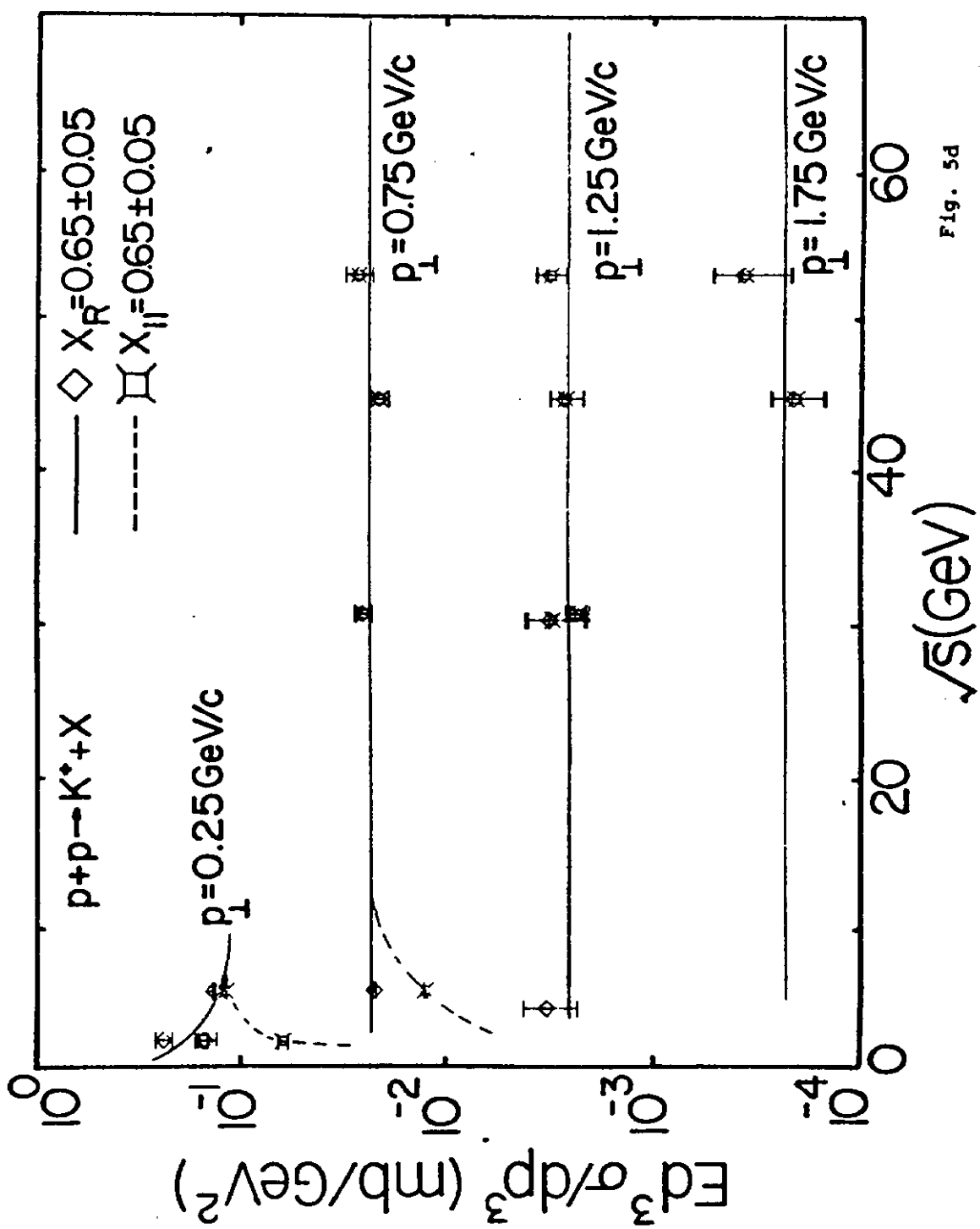
p+p→K°+X
◇ X_R=0.65±0.05
□ X_{II}=0.65±0.05
p_T=0.25GeV/c
p_T=0.75GeV/c
p_T=1.25GeV/c
p_T=1.75GeV/c
$Ed^3\sigma/dp^3$ (mb/GeV^2)
$\sqrt{s}$(GeV)
10^0
10^{-1}
10^{-2}
10^{-3}
10^{-4}
0
20
40
60

Fig. 5d

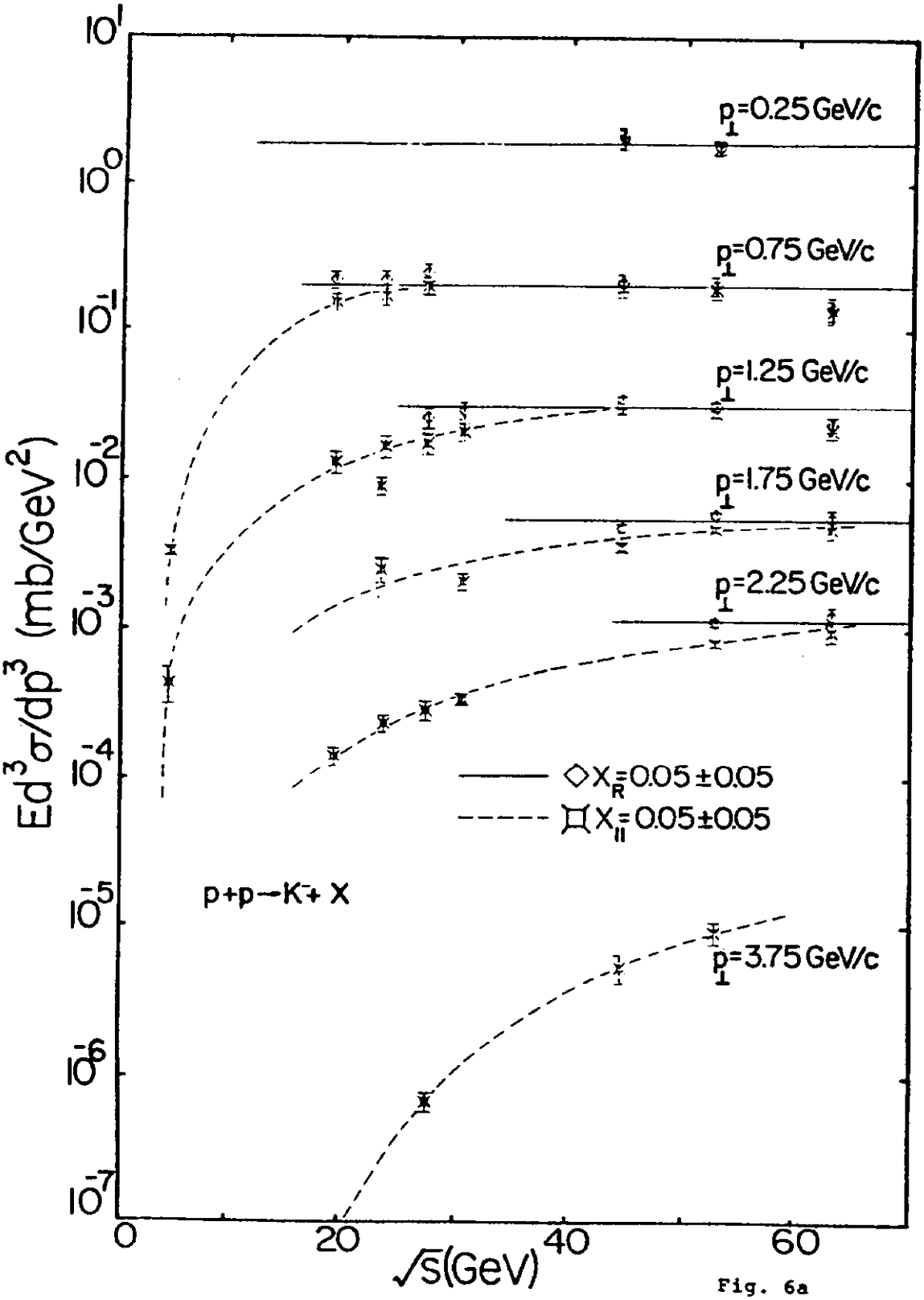
10^{1}
10^{0}
10^{-1}
10^{-2}
10^{-3}
10^{-4}
10^{-5}
10^{-6}
10^{-7}
$Ed^3\sigma/dp^3$ (mb/GeV^2)
$p_\perp$=0.25 GeV/c
$p_\perp$=0.75 GeV/c
$p_\perp$=1.25 GeV/c
$p_\perp$=1.75 GeV/c
$p_\perp$=2.25 GeV/c
$p_\perp$=3.75 GeV/c
◇ X_R=0.05±0.05
□ $X_{||}$=0.05±0.05
p+p→K$^-$+ X
0
20
40
60
$\sqrt{s}$(GeV)

Fig. 6a

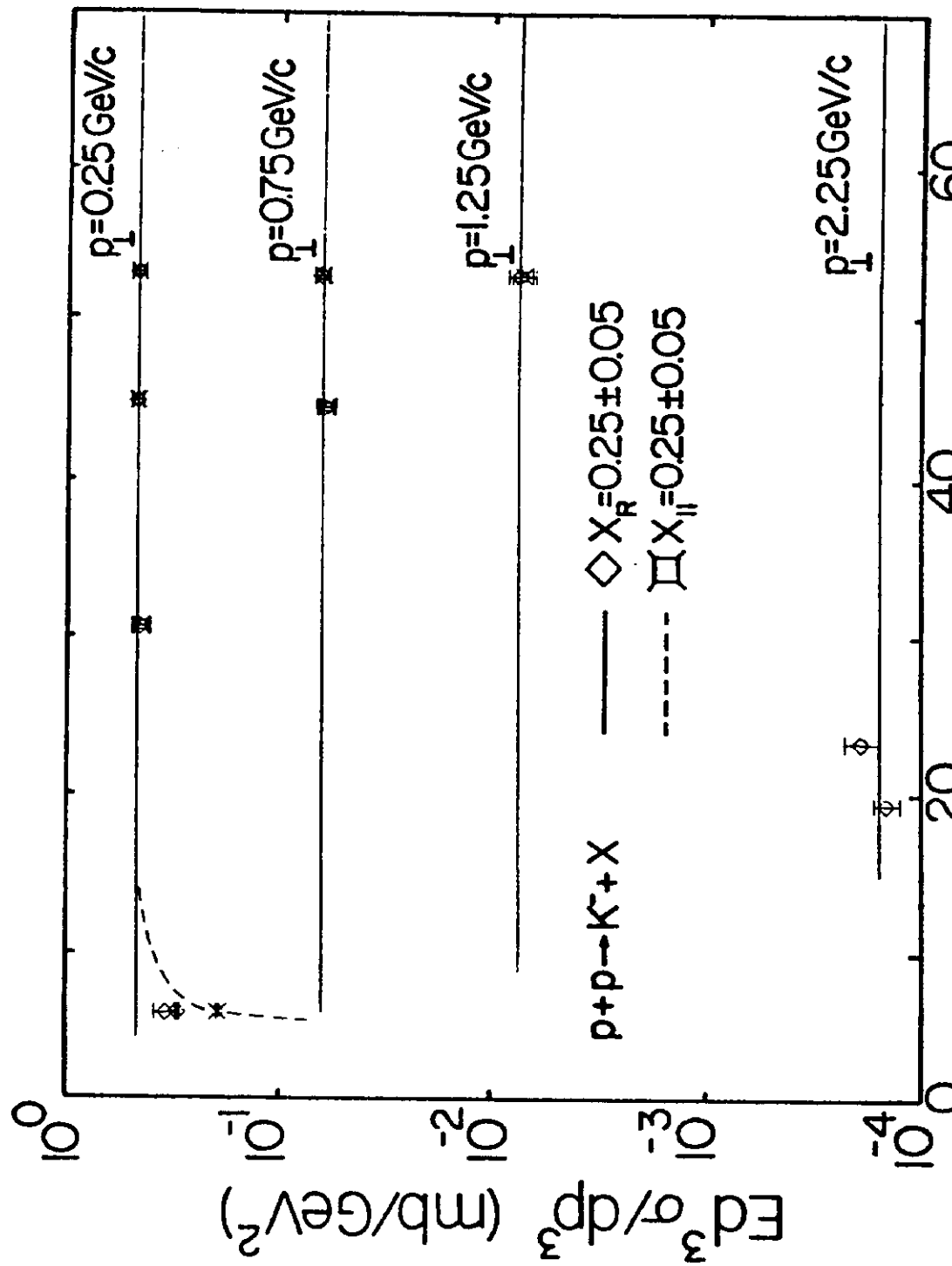
$Ed^3\sigma/dp^3$ (mb/GeV^2)
10^0
10^{-1}
10^{-2}
10^{-3}
10^{-4}
0
20
40
60
$\sqrt{s}$(GeV)
p_T=0.25GeV/c
p_T=0.75GeV/c
p_T=1.25GeV/c
p_T=2.25GeV/c
p+p→K$^+$+X
◇ X_R=0.25±0.05
□ $X_{||}$=0.25±0.05

Fig. 6b

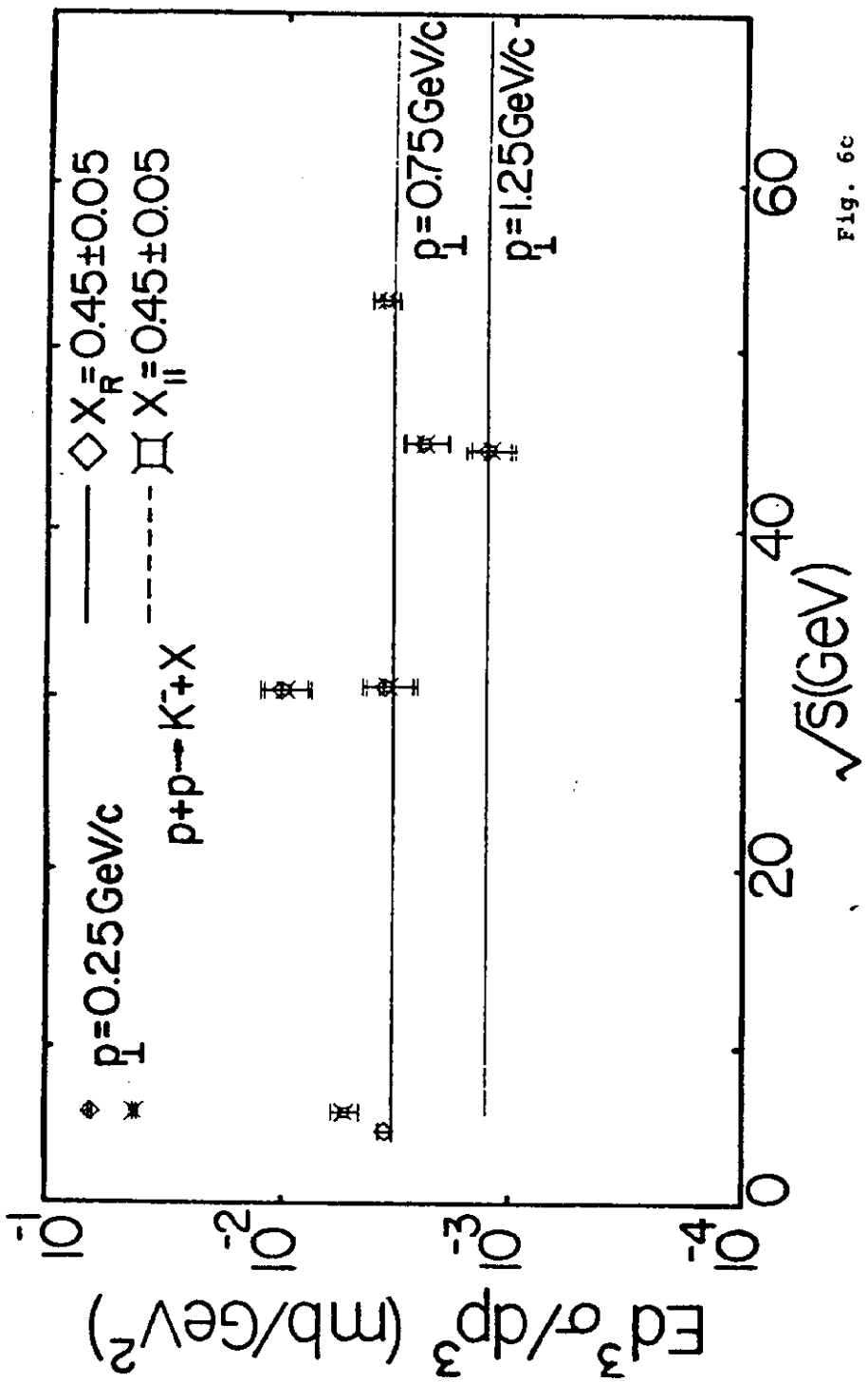
Ed³σ/dp³ (mb/GeV²)
10⁻¹
10⁻²
10⁻³
10⁻⁴
0
20
40
60
√s(GeV)
p+p→K⁻+X
p_T=0.25GeV/c
◇ X_R=0.45±0.05
□ X_∥=0.45±0.05
p_T=0.75GeV/c
p_T=1.25GeV/c

Fig. 6c

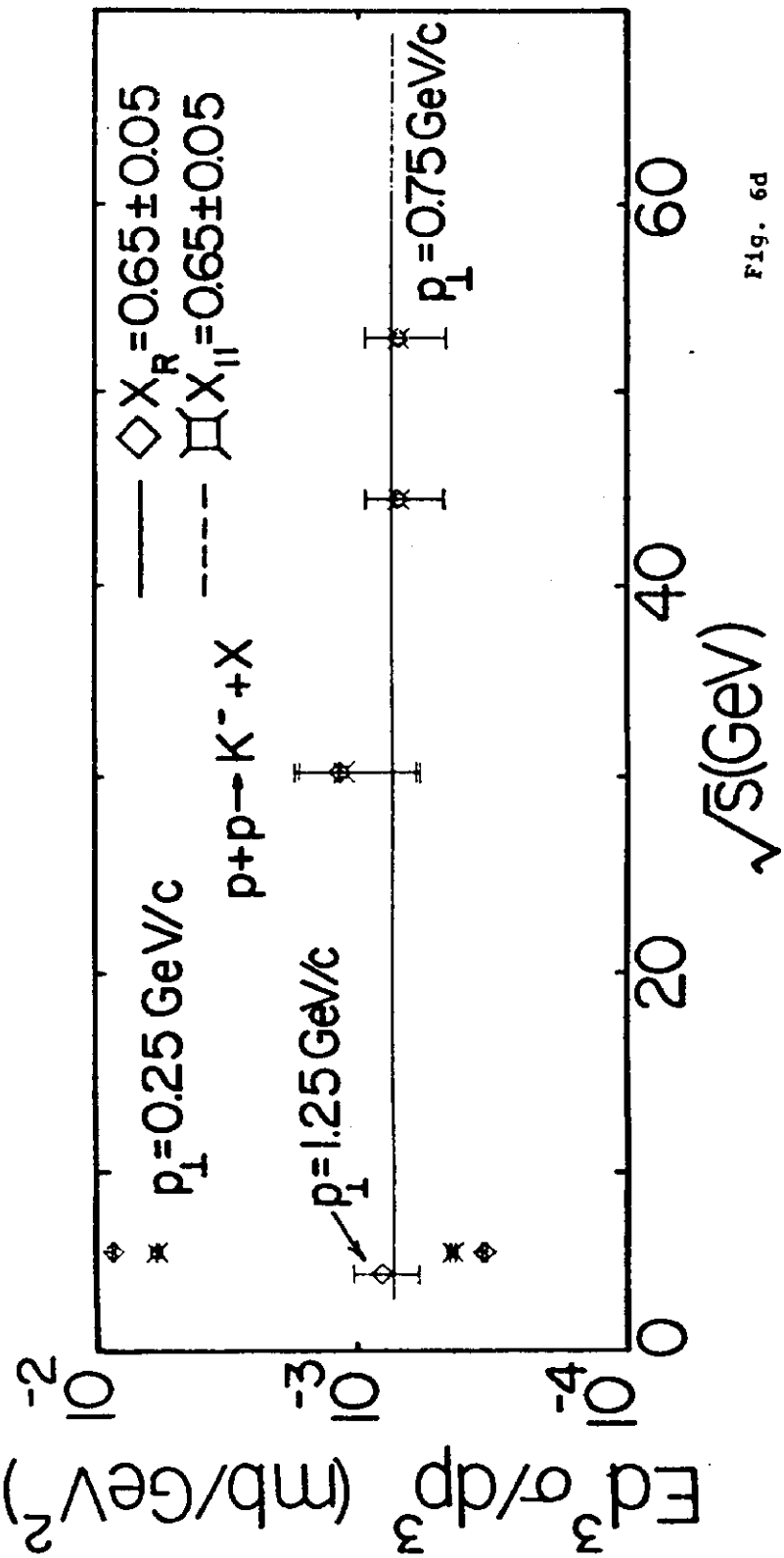
Ed³σ/dp³ (mb/GeV²)
10⁻²
10⁻³
10⁻⁴
0
20
40
60
√s(GeV)
p+p→K⁻+X
p_T=0.25 GeV/c
p_T=1.25 GeV/c
p_T=0.75 GeV/c
◇ X_R=0.65±0.05
□ X_II=0.65±0.05

Fig. 6d

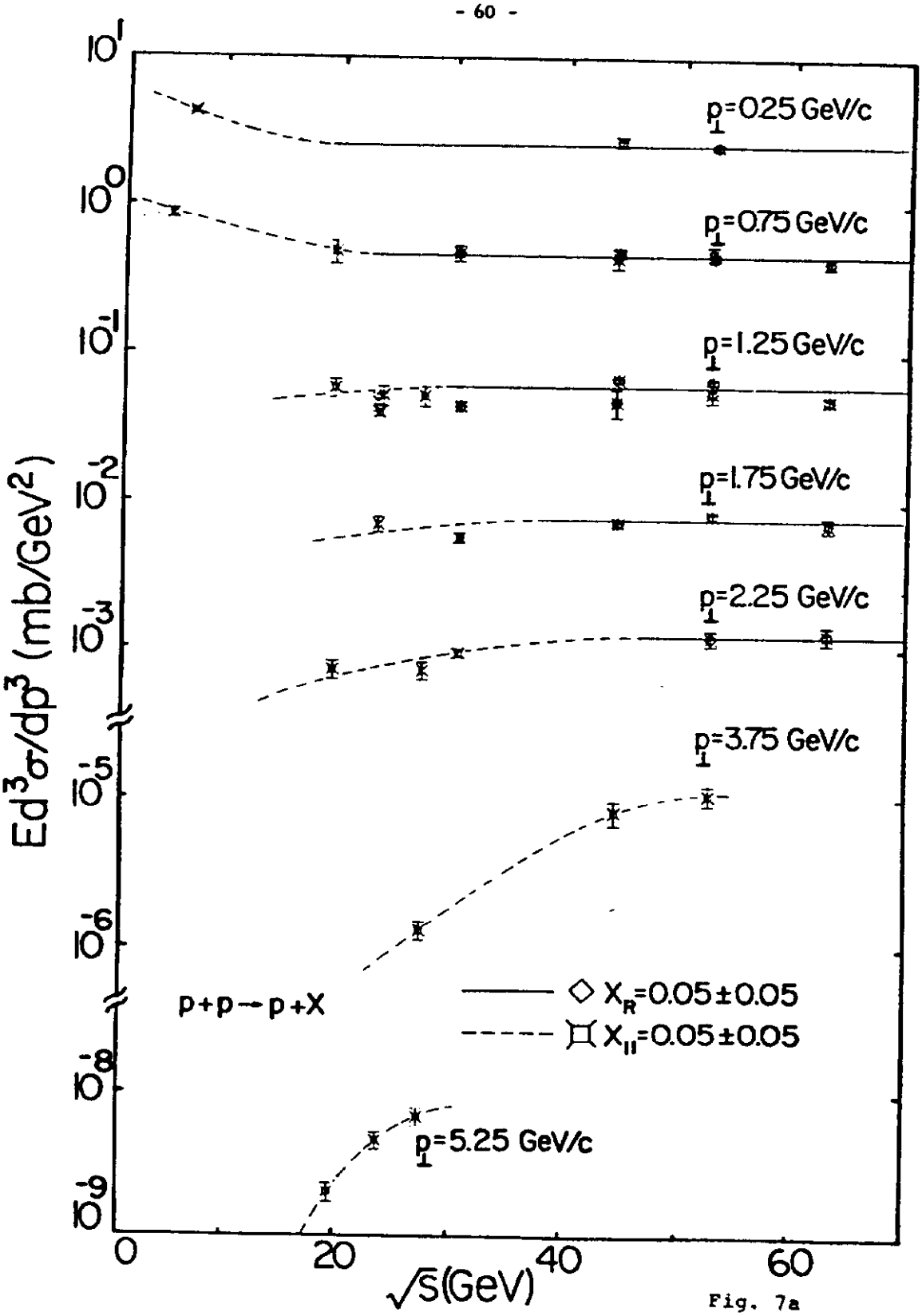
$Ed^3\sigma/dp^3$ (mb/GeV^2)
10^1
10^0
10^{-1}
10^{-2}
10^{-3}
10^{-5}
10^{-6}
10^{-8}
10^{-9}
$p_\perp$=0.25 GeV/c
$p_\perp$=0.75 GeV/c
$p_\perp$=1.25 GeV/c
$p_\perp$=1.75 GeV/c
$p_\perp$=2.25 GeV/c
$p_\perp$=3.75 GeV/c
$p_\perp$=5.25 GeV/c
p+p→p+X
◇ X_R=0.05±0.05
X_{II}=0.05±0.05
0
20
40
60
$\sqrt{s}$(GeV)

Fig. 7a

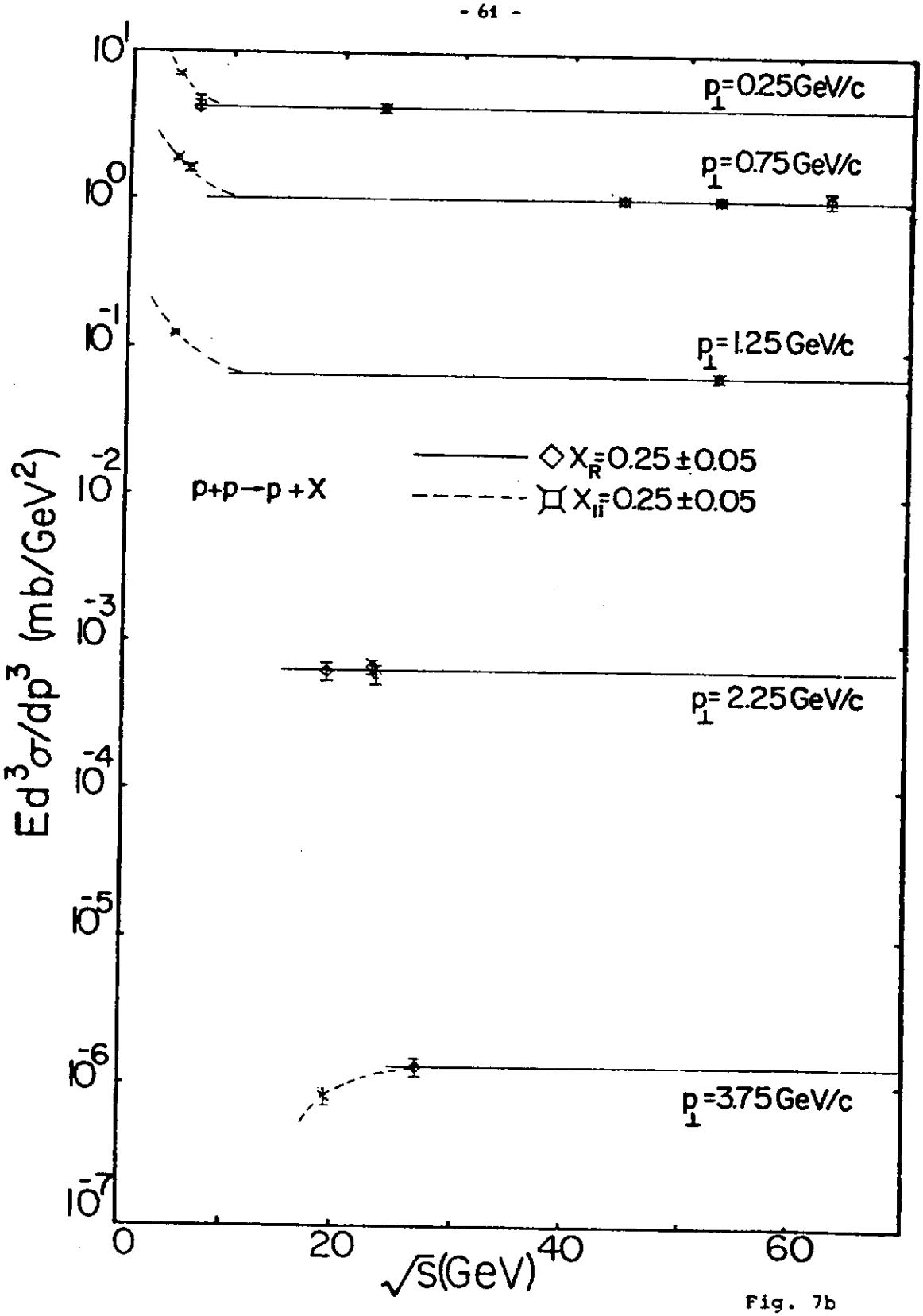
$p_\perp$=0.25GeV/c
$p_\perp$=0.75GeV/c
$p_\perp$=1.25GeV/c
$p_\perp$=2.25GeV/c
$p_\perp$=3.75GeV/c
◇ X_R=0.25±0.05
⌑ X_{II}=0.25±0.05
p+p→p+X
$Ed^3\sigma/dp^3$ (mb/GeV^2)
$\sqrt{s}$(GeV)
0
20
40
60

Fig. 7b

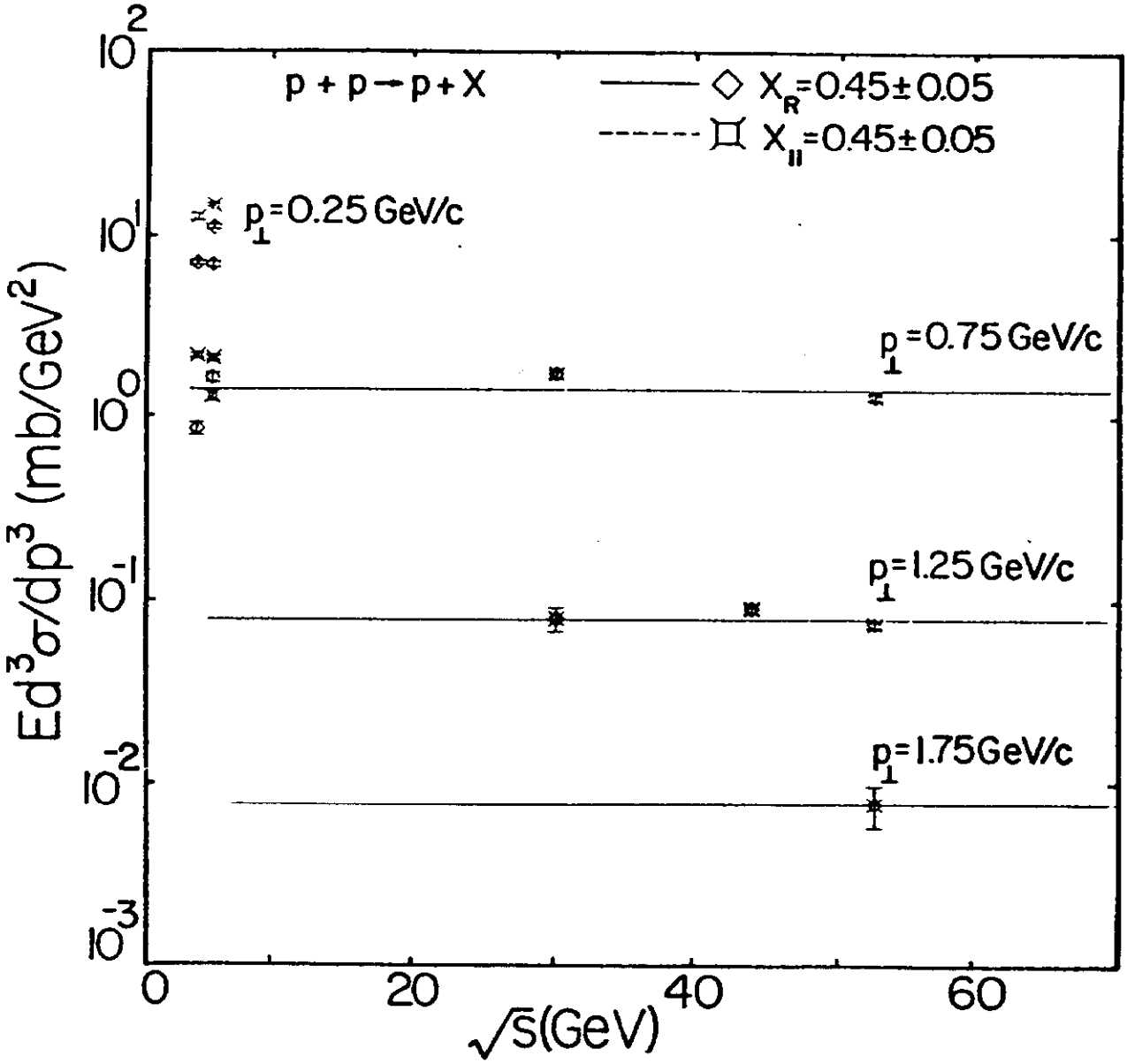
p + p → p + X
◇ X_R=0.45±0.05
□ X_{II}=0.45±0.05
$p_\perp$=0.25 GeV/c
$p_\perp$=0.75 GeV/c
$p_\perp$=1.25 GeV/c
$p_\perp$=1.75 GeV/c
$Ed^3\sigma/dp^3$ (mb/GeV^2)
10^2
10^1
10^0
10^{-1}
10^{-2}
10^{-3}
0
20
40
60
$\sqrt{s}$(GeV)

Fig. 7c

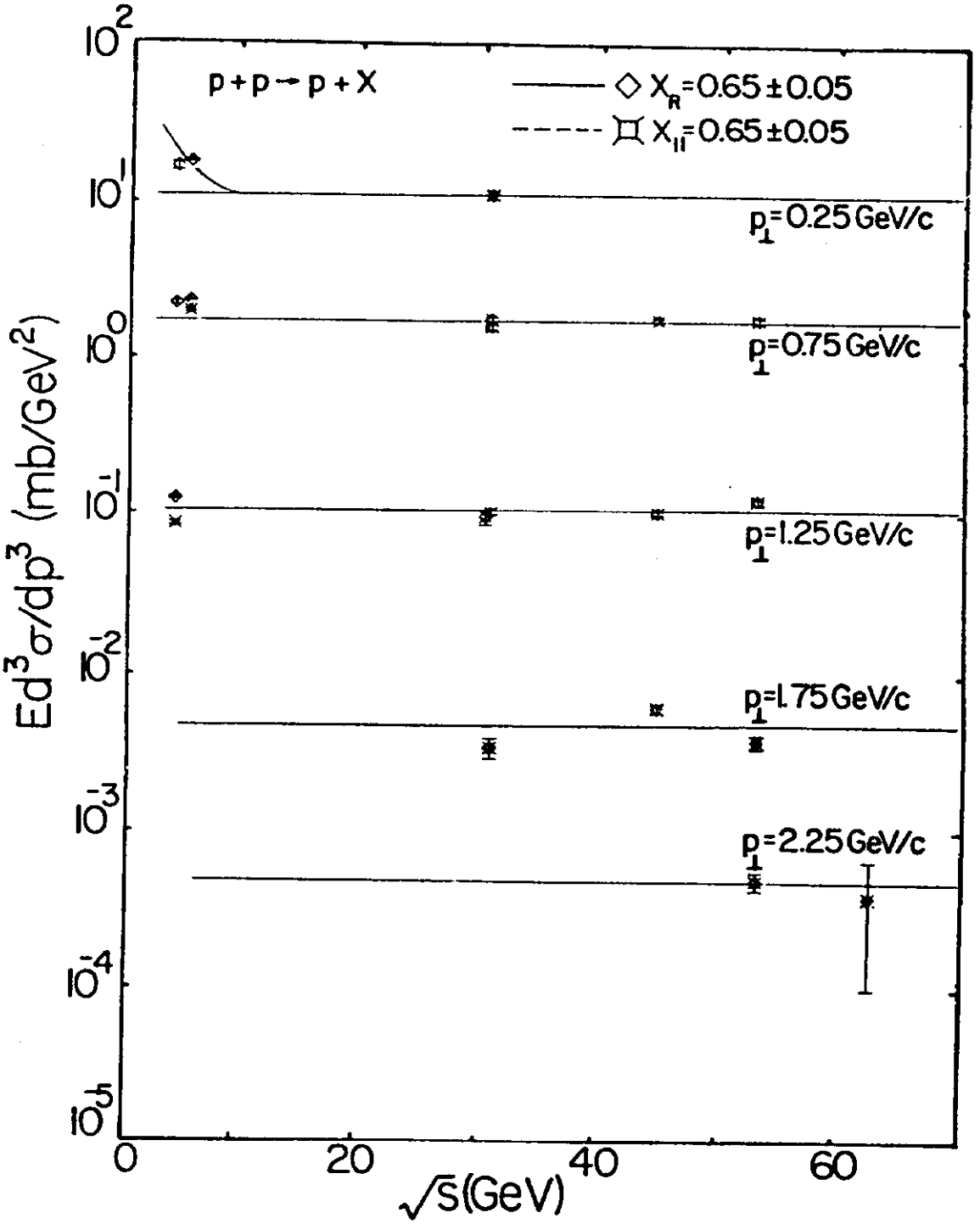
p+p→p+X
◇ X_R=0.65±0.05
⌑ X_II=0.65±0.05
p_⊥=0.25 GeV/c
p_⊥=0.75 GeV/c
p_⊥=1.25 GeV/c
p_⊥=1.75 GeV/c
p_⊥=2.25 GeV/c
Ed³σ/dp³ (mb/GeV²)
√s(GeV)
0
20
40
60

Fig. 7d

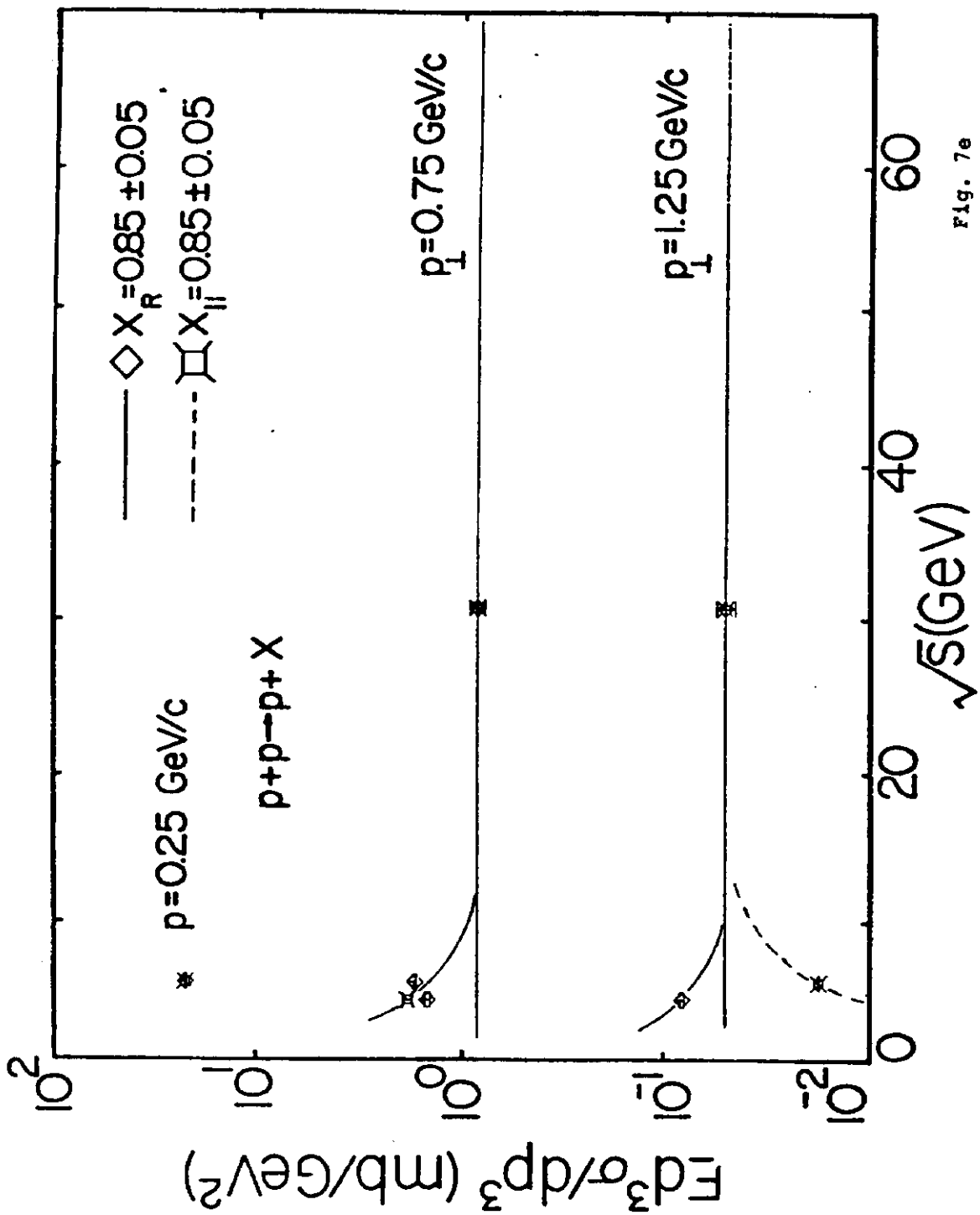
$Ed^3\sigma/dp^3$ (mb/GeV^2)
10^2
10^1
10^0
10^{-1}
10^{-2}
0
20
40
60
$\sqrt{s}$(GeV)
$\diamond X_R$=0.85 ±0.05
$\square X_{ll}$=0.85 ±0.05
p=0.25 GeV/c
p+p→p+X
p_T=0.75 GeV/c
p_T=1.25 GeV/c

Fig. 7a

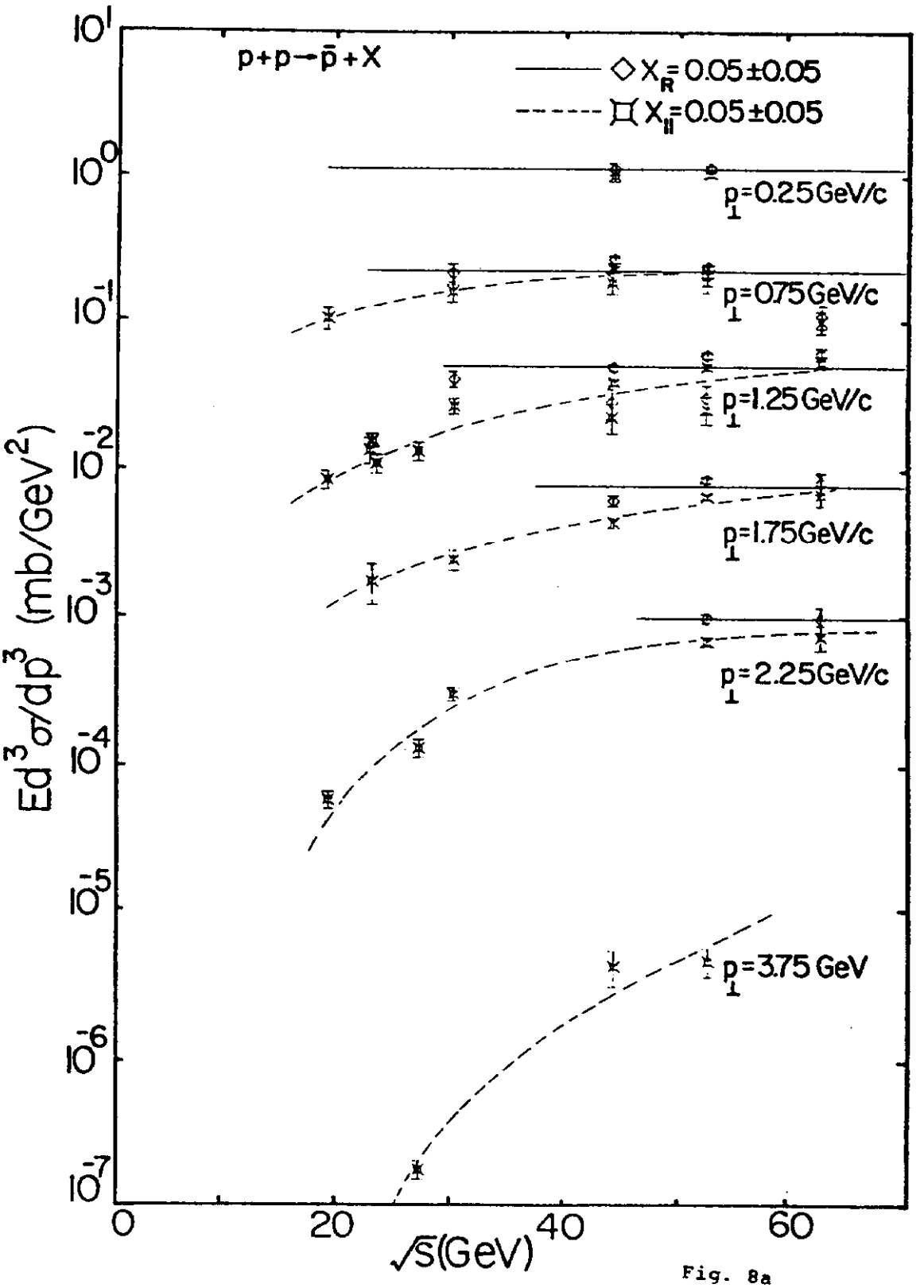
p+p→p̄+X
◇ X_R = 0.05±0.05
X_II = 0.05±0.05
p_⊥=0.25GeV/c
p_⊥=0.75GeV/c
p_⊥=1.25GeV/c
p_⊥=1.75GeV/c
p_⊥=2.25GeV/c
p_⊥=3.75 GeV
Ed³σ/dp³ (mb/GeV²)
√s(GeV)
10¹
10⁰
10⁻¹
10⁻²
10⁻³
10⁻⁴
10⁻⁵
10⁻⁶
10⁻⁷
0
20
40
60

Fig. 8a

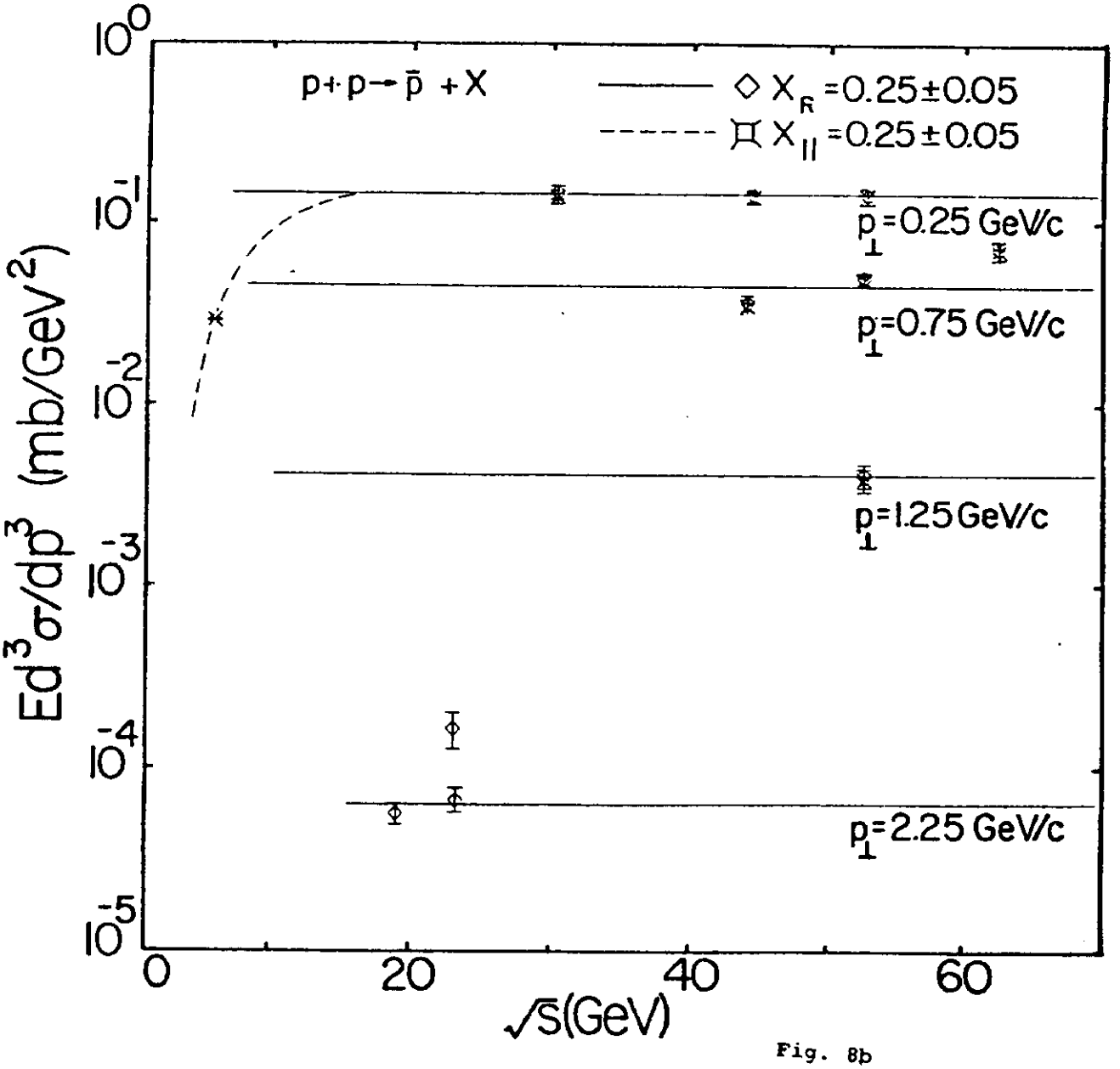
p+p→p̄ +X
◇ X_R =0.25±0.05
X_II =0.25±0.05
p_⊥=0.25 GeV/c
p_⊥=0.75 GeV/c
p_⊥=1.25 GeV/c
p_⊥=2.25 GeV/c
Ed³σ/dp³ (mb/GeV²)
√s(GeV)
10⁰
10⁻¹
10⁻²
10⁻³
10⁻⁴
10⁻⁵
0
20
40
60

Fig. 8b

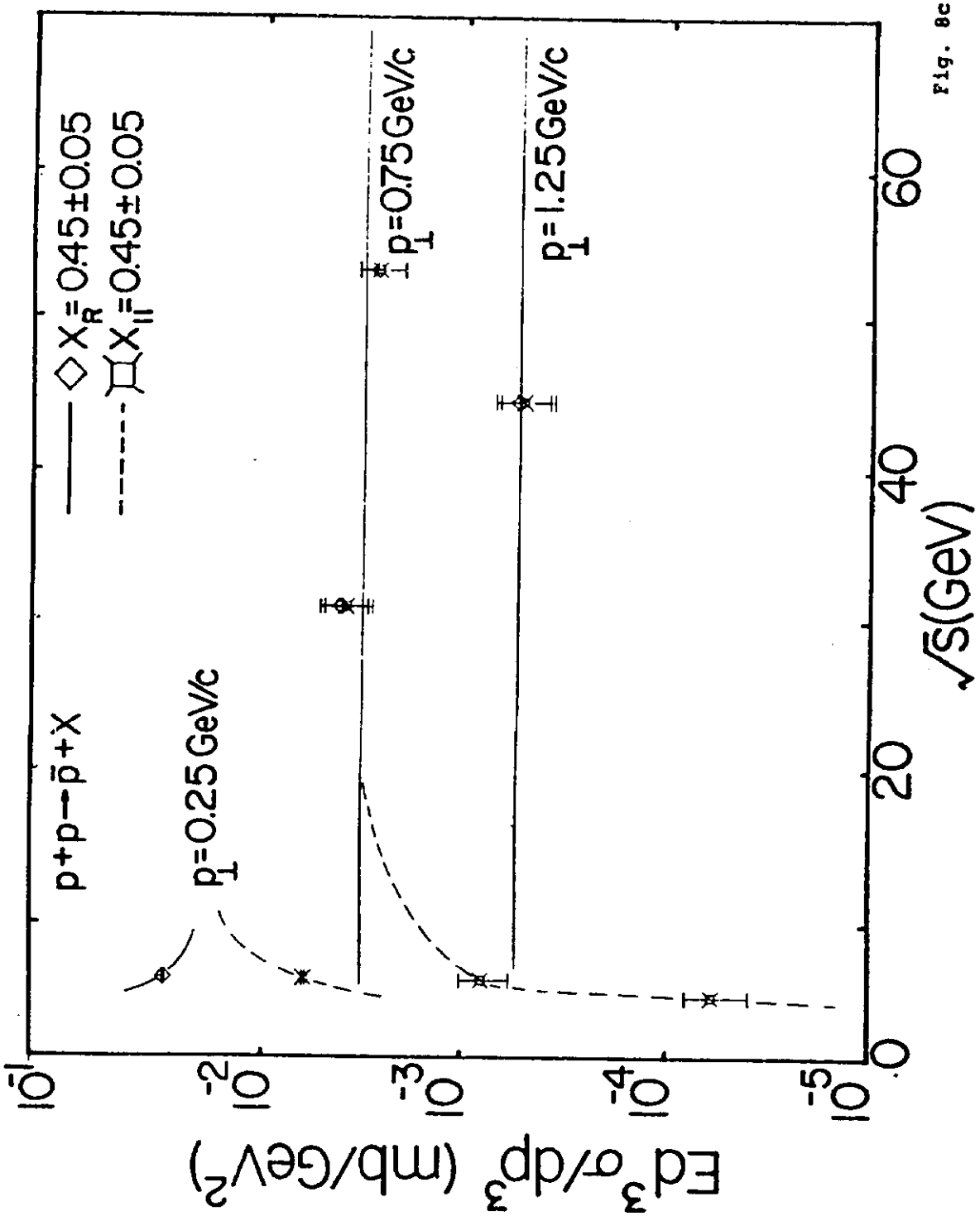
$Ed^3\sigma/dp^3$ (mb/GeV^2)
10^{-1}
10^{-2}
10^{-3}
10^{-4}
10^{-5}
0
20
40
60
$\sqrt{s}$(GeV)
$p+p\rightarrow\bar{p}+X$
p_T=0.25GeV/c
p_T=0.75GeV/c
p_T=1.25GeV/c
$\diamond$ X_R=0.45±0.05
$\square$ X_{II}=0.45±0.05

Fig. 8c

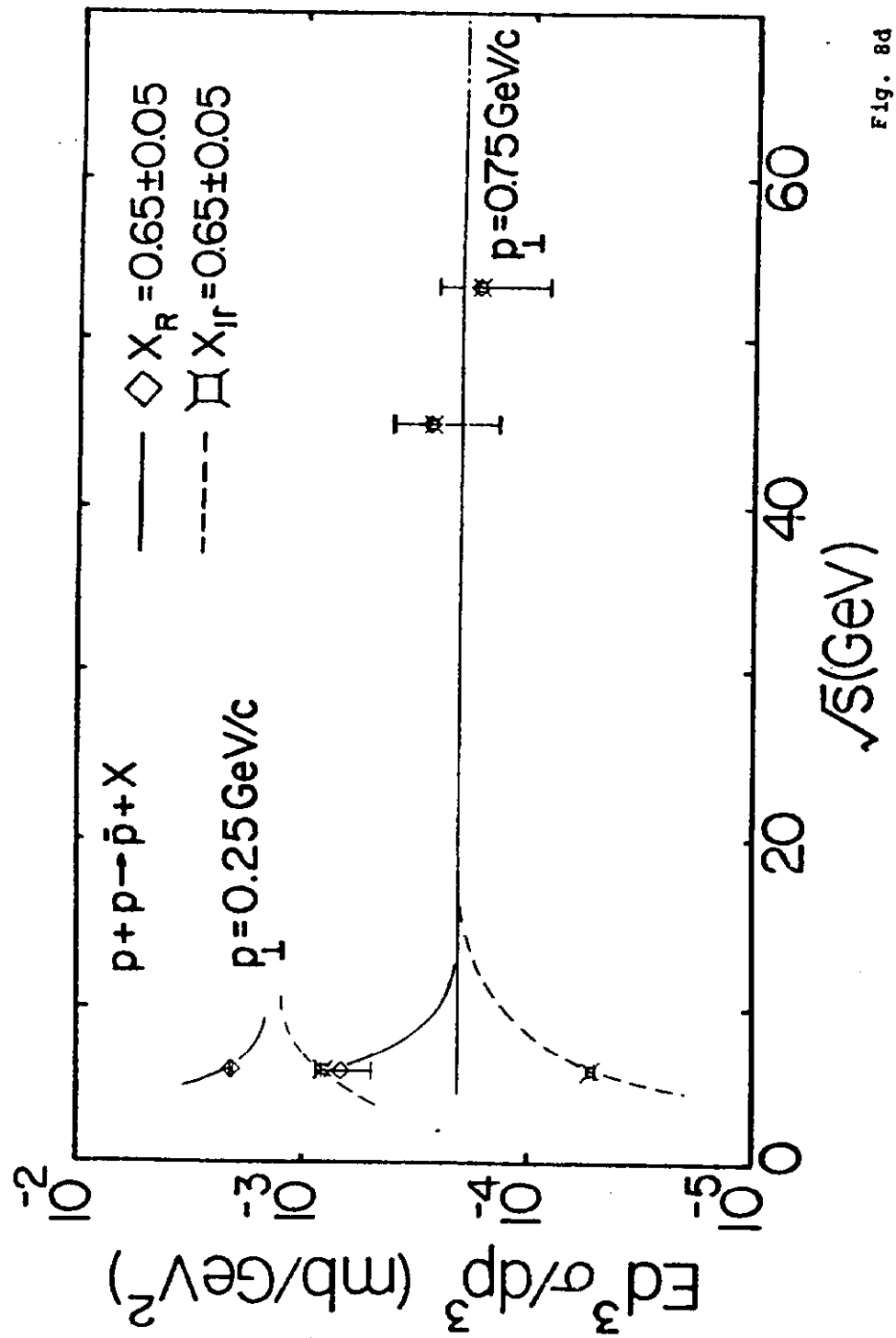
$Ed^3\sigma/dp^3$ (mb/GeV^2)
10^{-2}
10^{-3}
10^{-4}
10^{-5}
0
20
40
60
$\sqrt{s}$(GeV)
p+p→p̄+X
p_T=0.25GeV/c
p_T=0.75GeV/c
◇ X_R=0.65±0.05
□ X_{IR}=0.65±0.05

Fig. 8d

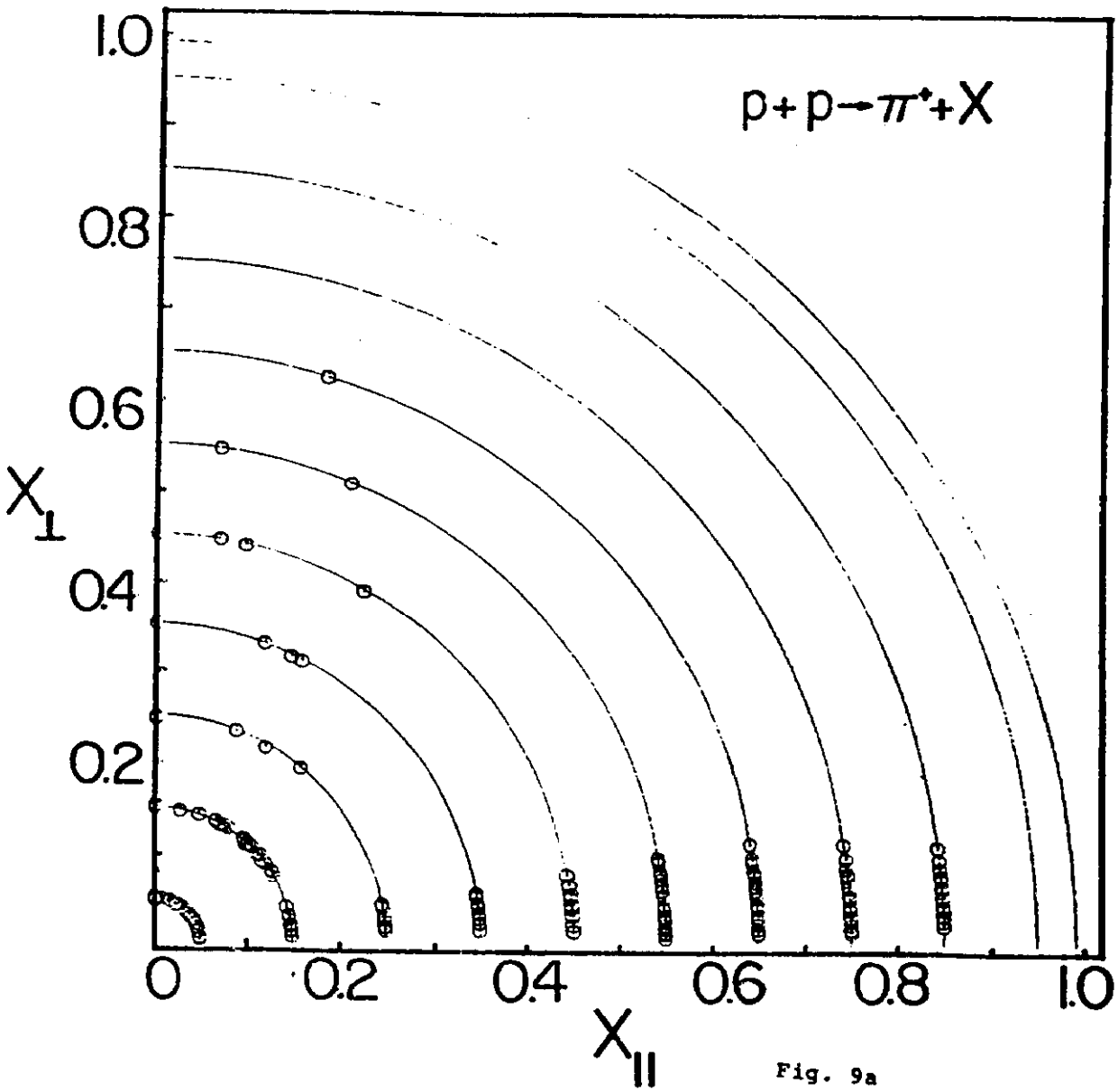

Fig. 9a

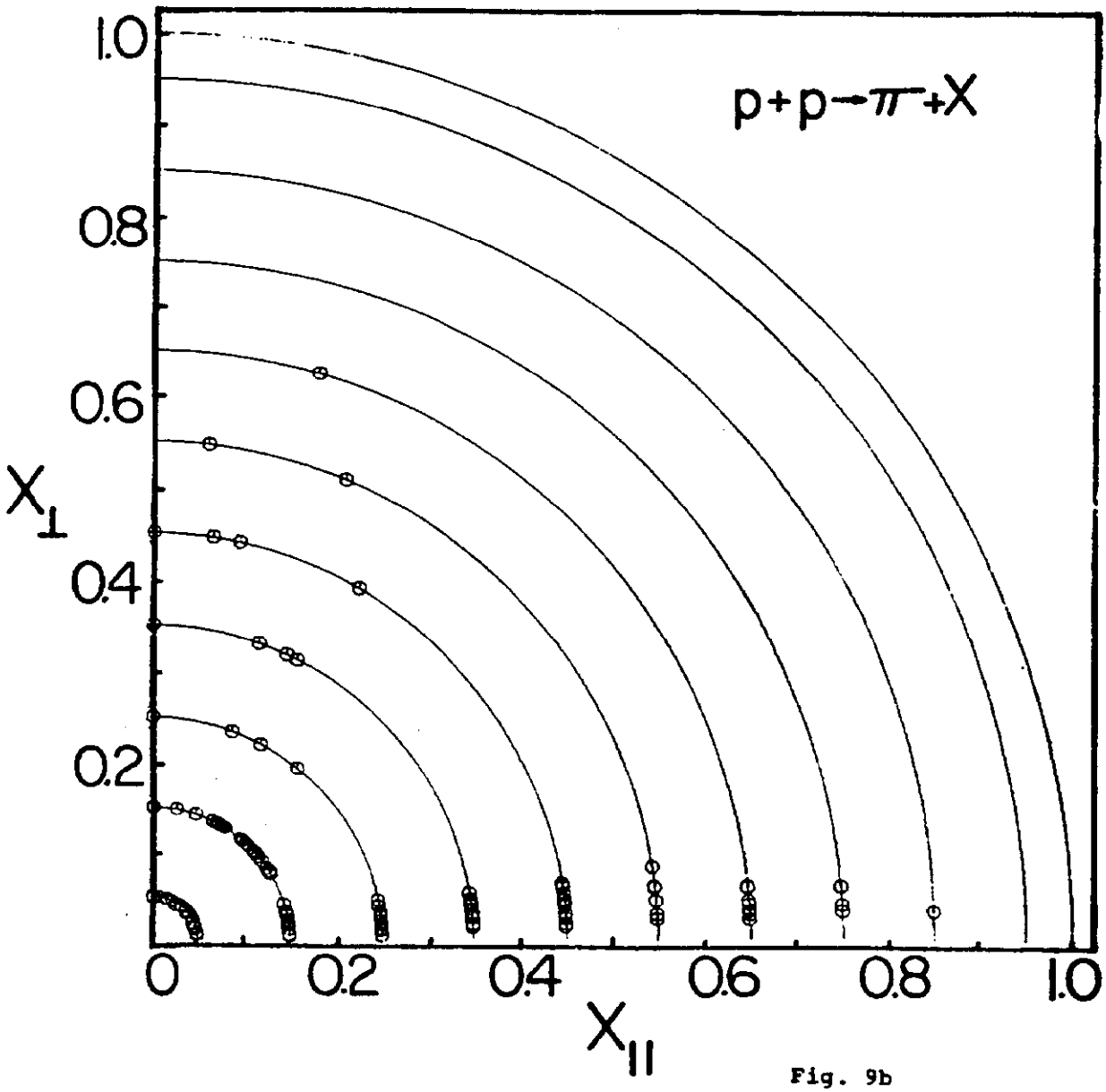

Fig. 9b

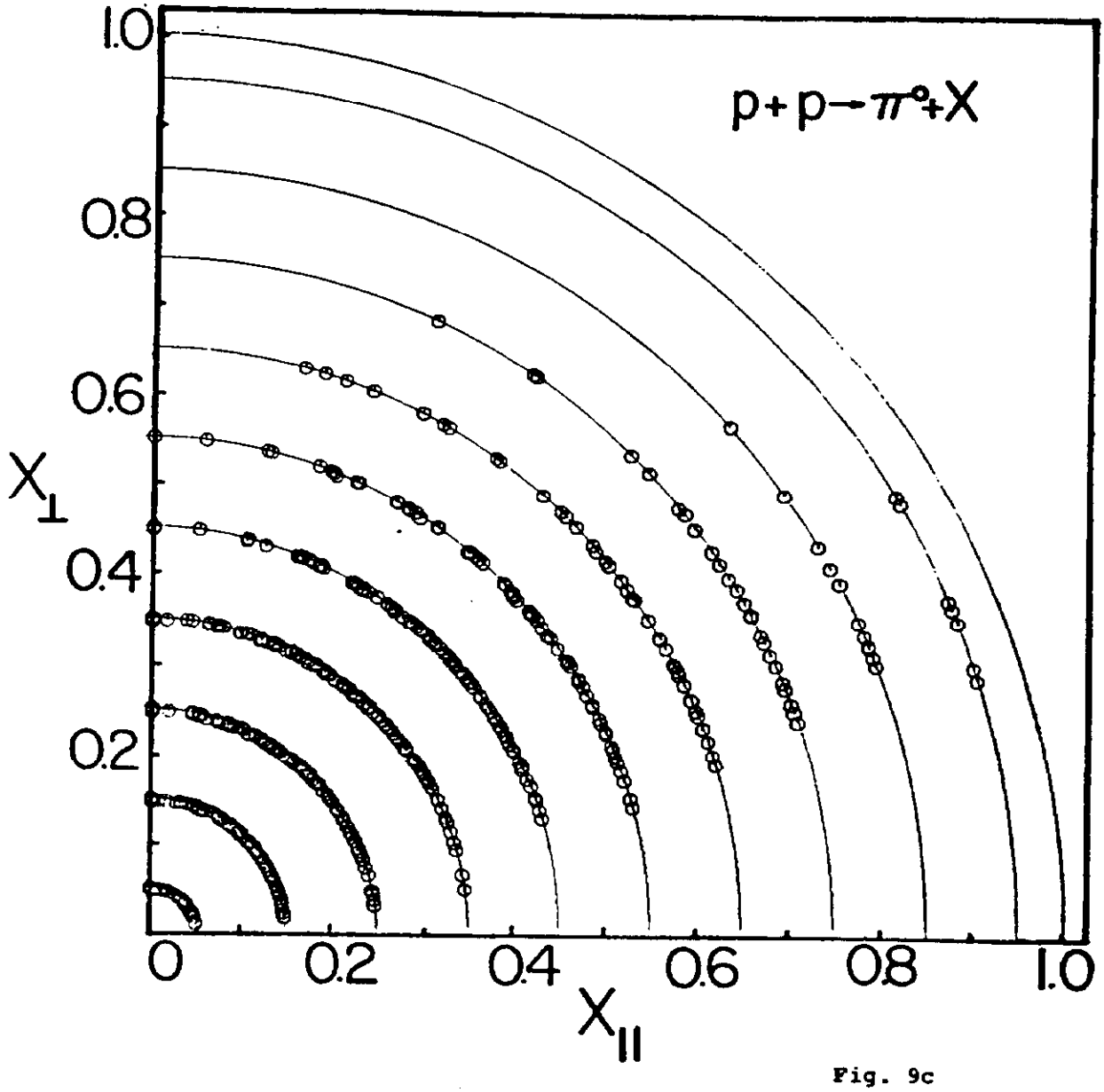

Fig. 9c

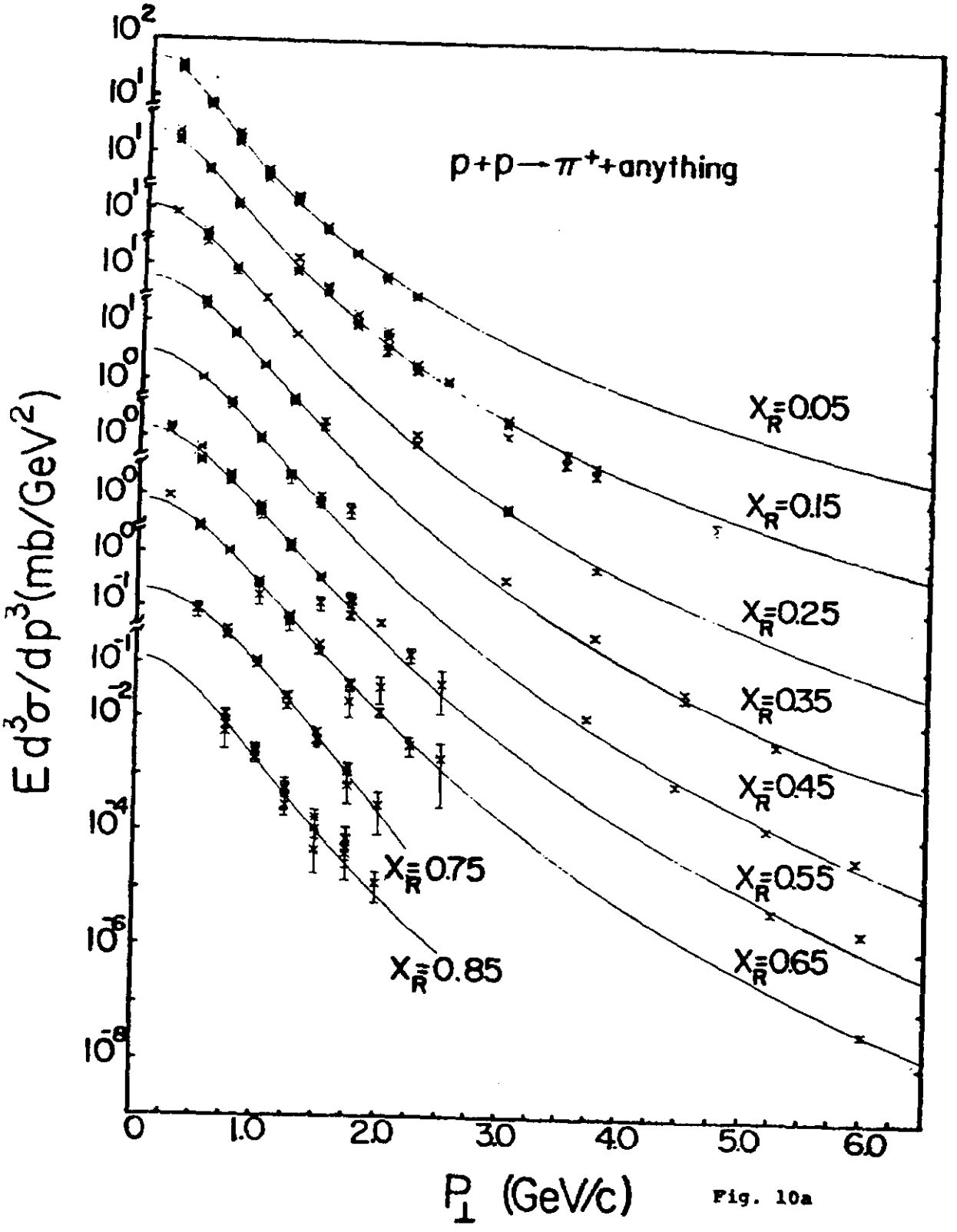
p+p→π⁺+anything
X_R=0.05
X_R=0.15
X_R=0.25
X_R=0.35
X_R=0.45
X_R=0.55
X_R=0.65
X_R=0.75
X_R=0.85
E d³σ/dp³(mb/GeV²)
P_⊥ (GeV/c)
0
1.0
2.0
3.0
4.0
5.0
6.0

Fig. 10a

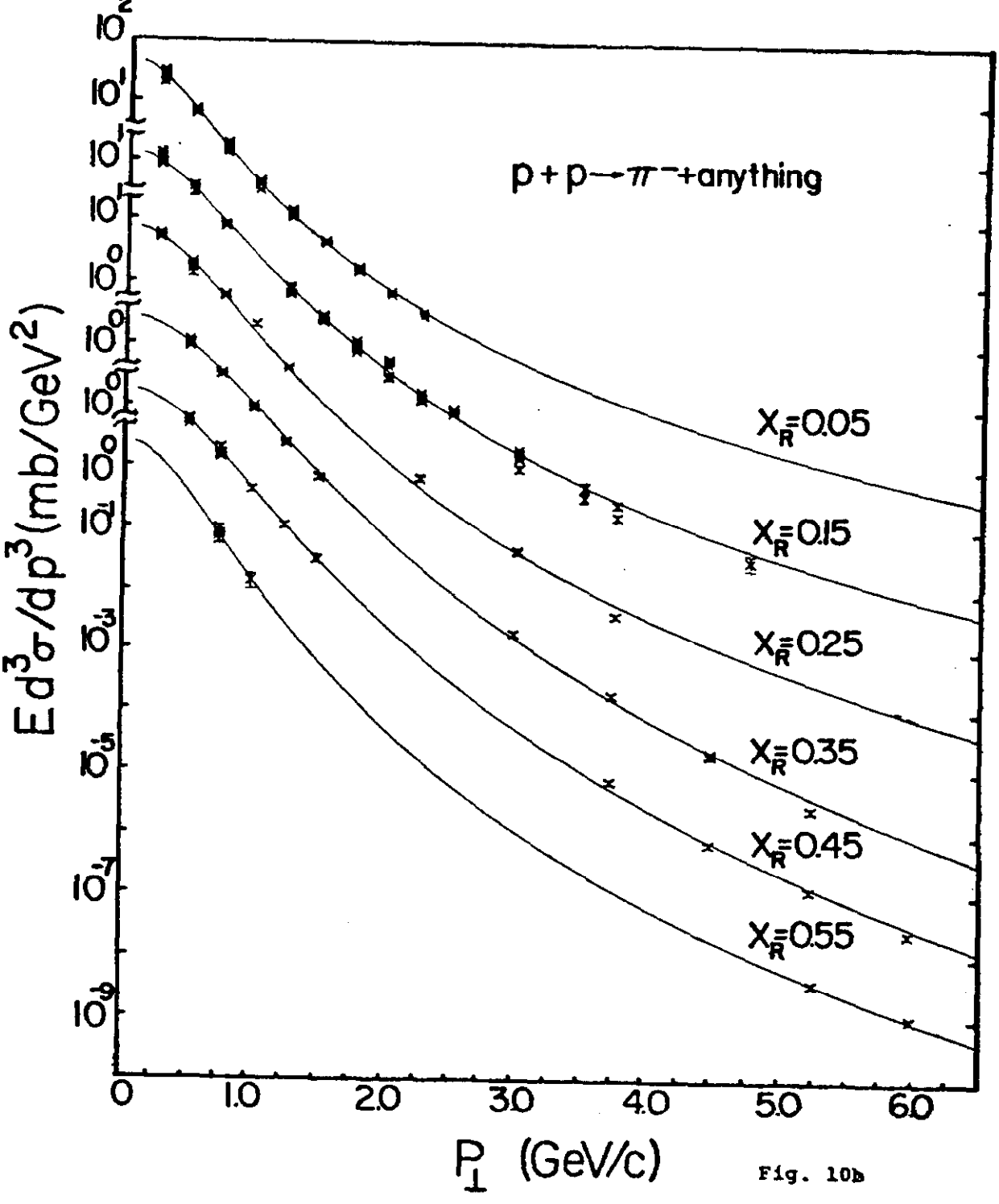
p + p → π⁻ + anything
X_R = 0.05
X_R = 0.15
X_R = 0.25
X_R = 0.35
X_R = 0.45
X_R = 0.55
E d³σ/dp³ (mb/GeV²)
P_⊥ (GeV/c)
0
1.0
2.0
3.0
4.0
5.0
6.0

Fig. 10b

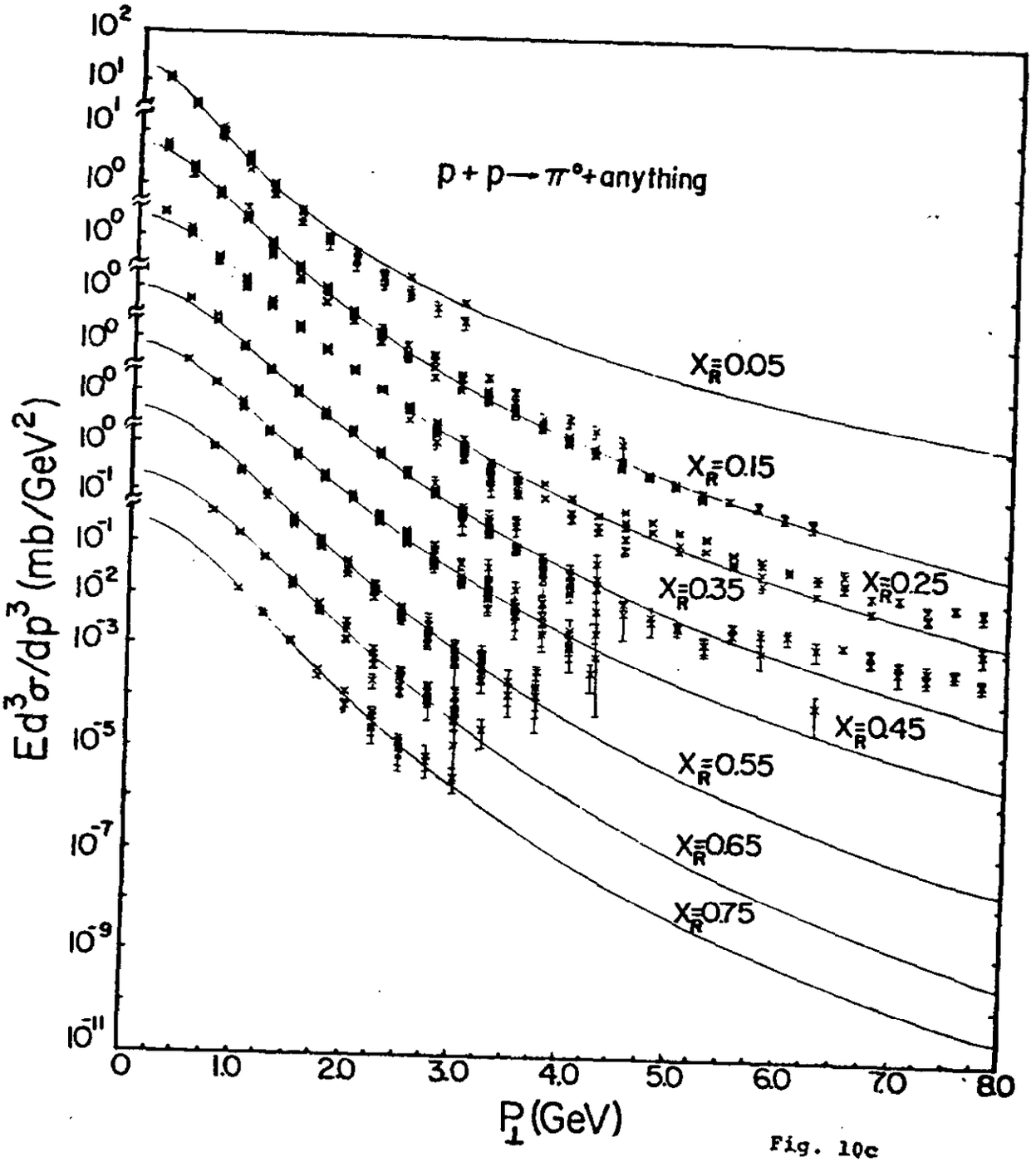
p + p → π° + anything
X_R=0.05
X_R=0.15
X_R=0.25
X_R=0.35
X_R=0.45
X_R=0.55
X_R=0.65
X_R=0.75
$Ed^3\sigma/dp^3$ (mb/GeV^2)
$P_\perp$ (GeV)
0
1.0
2.0
3.0
4.0
5.0
6.0
7.0
8.0

Fig. 10c

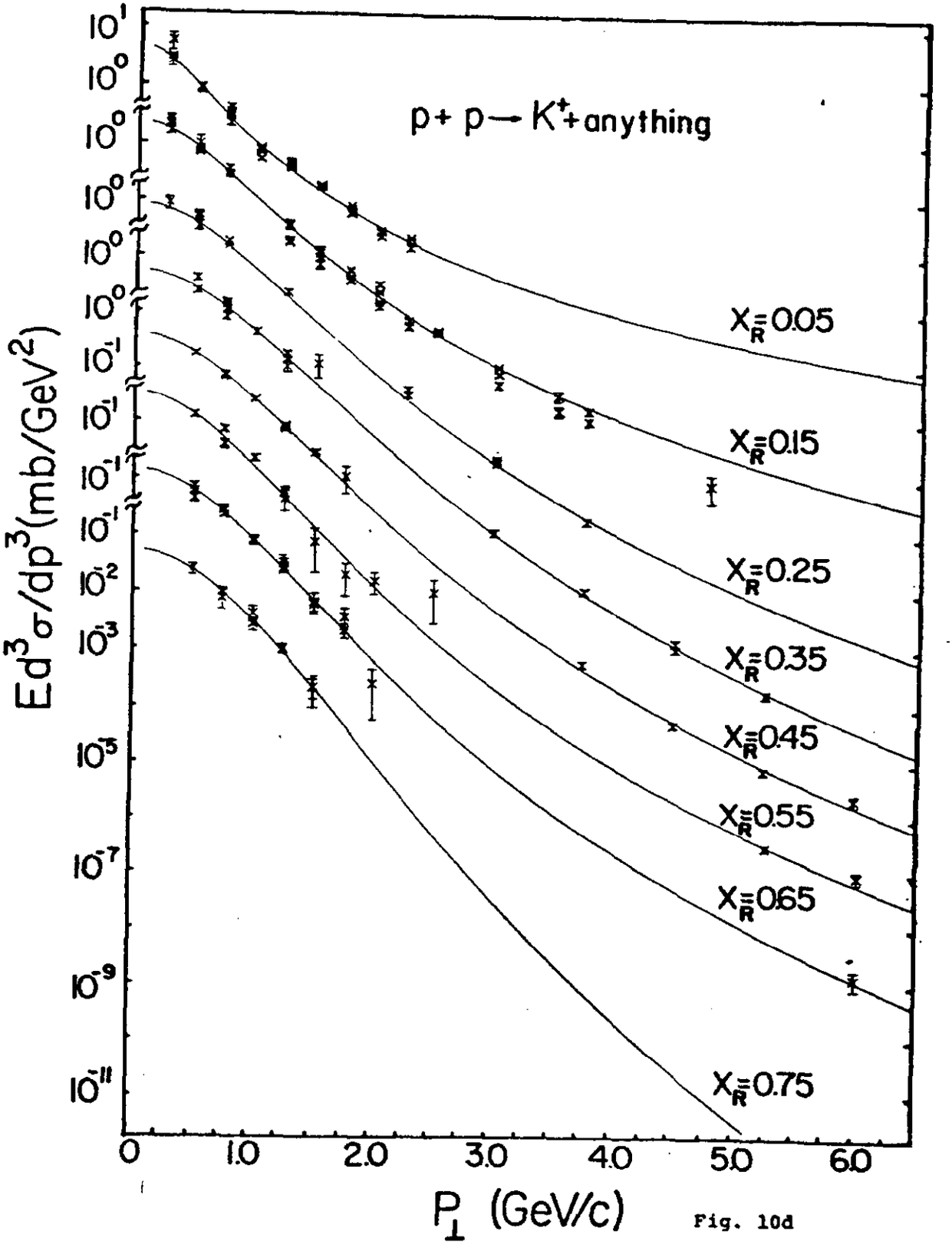
p+ p— K⁺+anything
X_R=0.05
X_R=0.15
X_R=0.25
X_R=0.35
X_R=0.45
X_R=0.55
X_R=0.65
X_R=0.75
$Ed^3\sigma/dp^3$(mb/GeV^2)
$P_\perp$ (GeV/c)
0
1.0
2.0
3.0
4.0
5.0
6.0

Fig. 10d

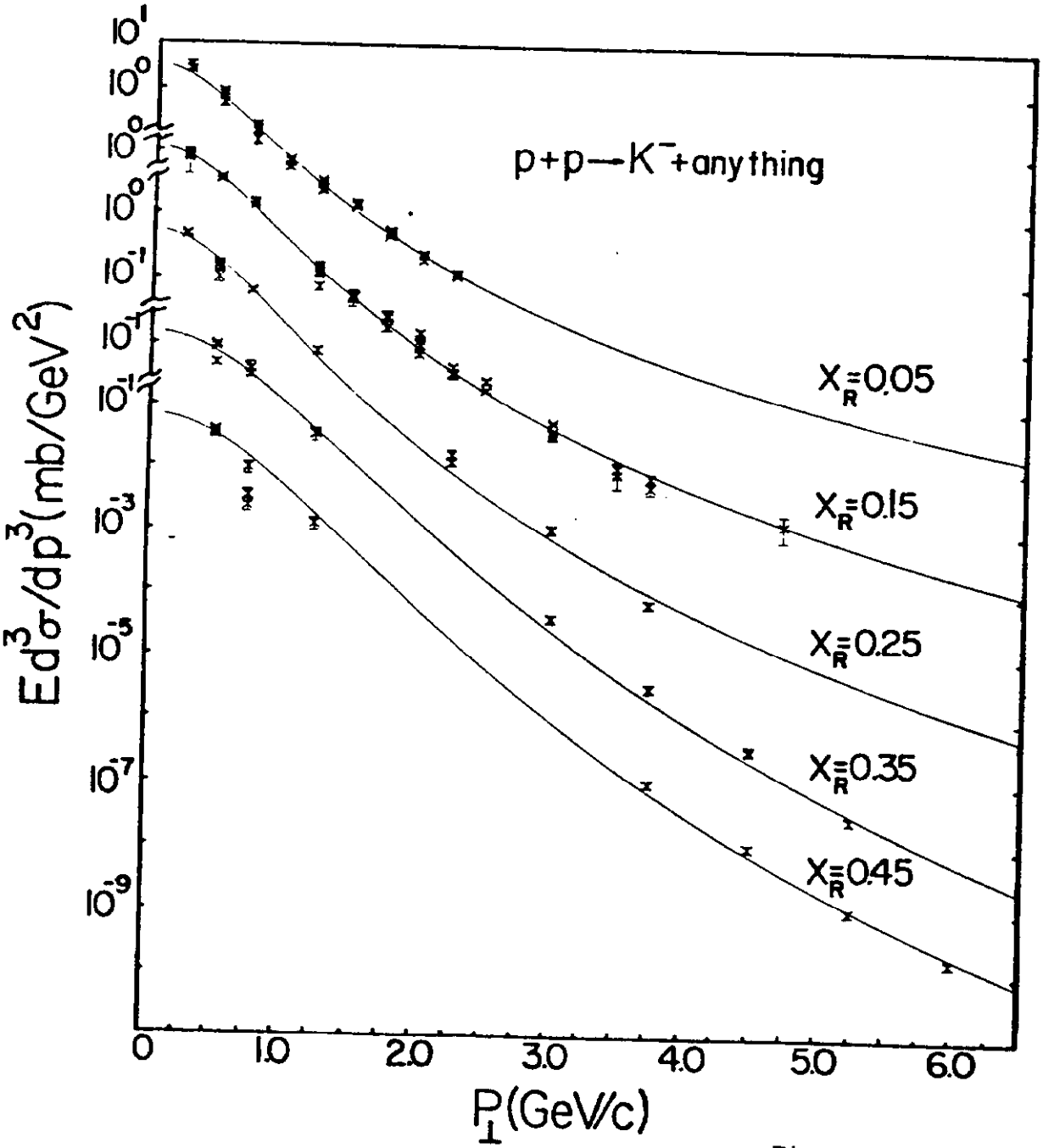
p+p→K⁻+anything
X_R=0.05
X_R=0.15
X_R=0.25
X_R=0.35
X_R=0.45
$Ed^3\sigma/dp^3$(mb/GeV^2)
$P_\perp$(GeV/c)
0
1.0
2.0
3.0
4.0
5.0
6.0

Fig. 10e

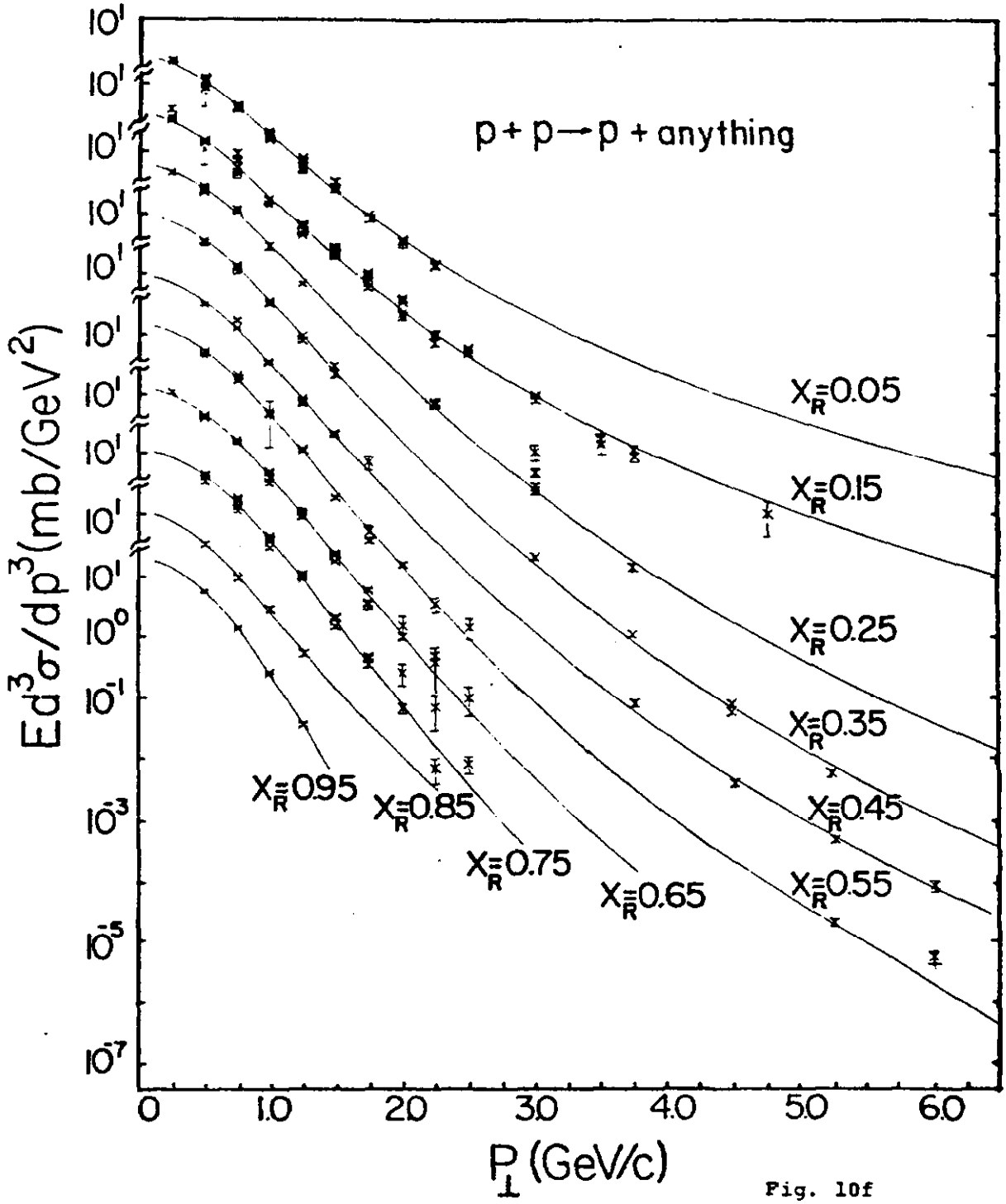
p + p → p + anything
$Ed^3\sigma/dp^3$(mb/GeV^2)
$P_\perp$ (GeV/c)
X_R=0.05
X_R=0.15
X_R=0.25
X_R=0.35
X_R=0.45
X_R=0.55
X_R=0.65
X_R=0.75
X_R=0.85
X_R=0.95
0
1.0
2.0
3.0
4.0
5.0
6.0

Fig. 10f

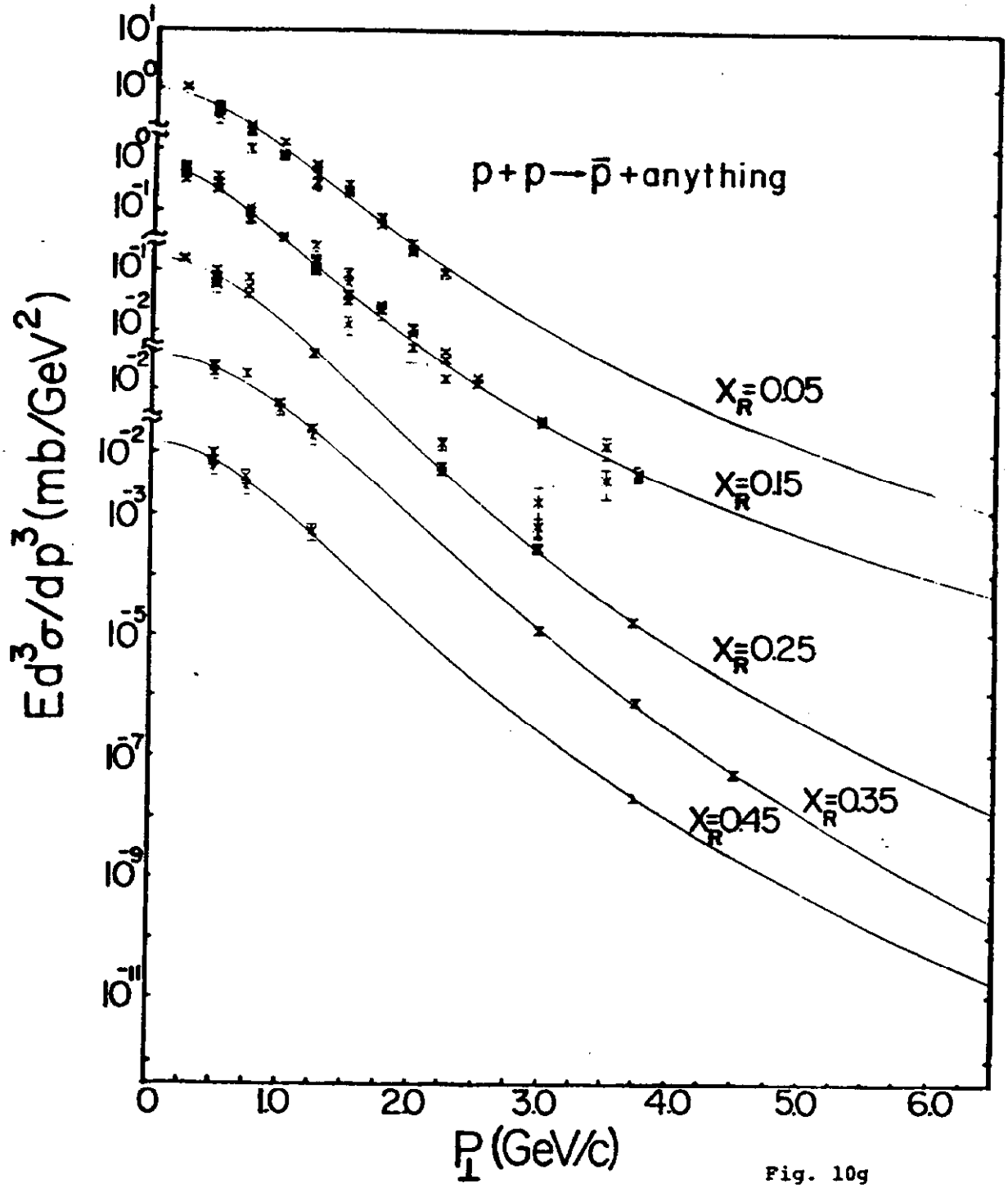
p+p→p̄+anything
X_R=0.05
X_R=0.15
X_R=0.25
X_R=0.35
X_R=0.45
Ed³σ/dp³(mb/GeV²)
P_T (GeV/c)
0
1.0
2.0
3.0
4.0
5.0
6.0

Fig. 10g

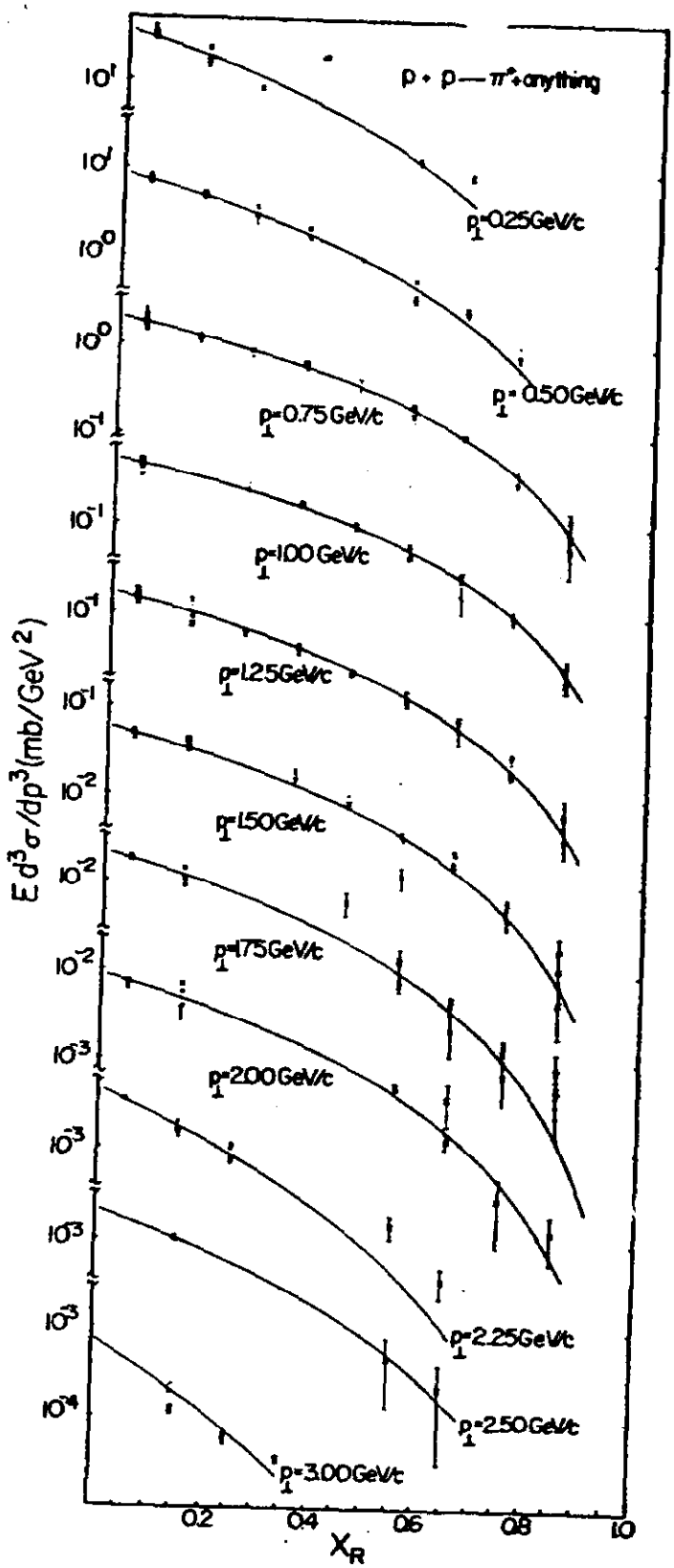
p + p — π° + anything
p_T=0.25GeV/c
p_T=0.50GeV/c
p_T=0.75GeV/c
p_T=1.00GeV/c
p_T=1.25GeV/c
p_T=1.50GeV/c
p_T=1.75GeV/c
p_T=2.00GeV/c
p_T=2.25GeV/c
p_T=2.50GeV/c
p_T=3.00GeV/c
E d³σ/dp³(mb/GeV²)
X_R
0.2
0.4
0.6
0.8
1.0

Fig. 11a

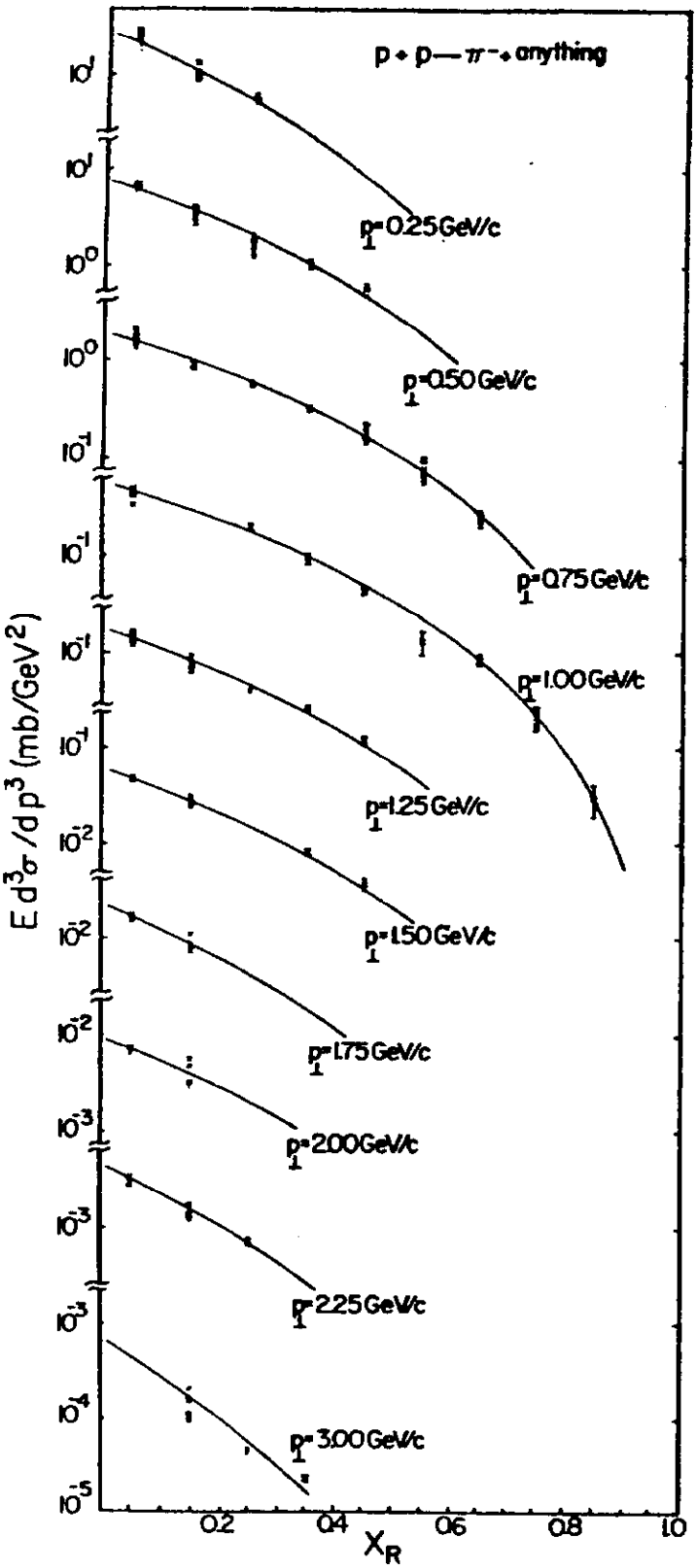
p + p — π⁻ + anything
p_T=0.25 GeV/c
p_T=0.50 GeV/c
p_T=0.75 GeV/c
p_T=1.00 GeV/c
p_T=1.25 GeV/c
p_T=1.50 GeV/c
p_T=1.75 GeV/c
p_T=2.00 GeV/c
p_T=2.25 GeV/c
p_T=3.00 GeV/c
E d³σ/dp³ (mb/GeV²)
X_R
0.2
0.4
0.6
0.8
1.0

Fig. 11b

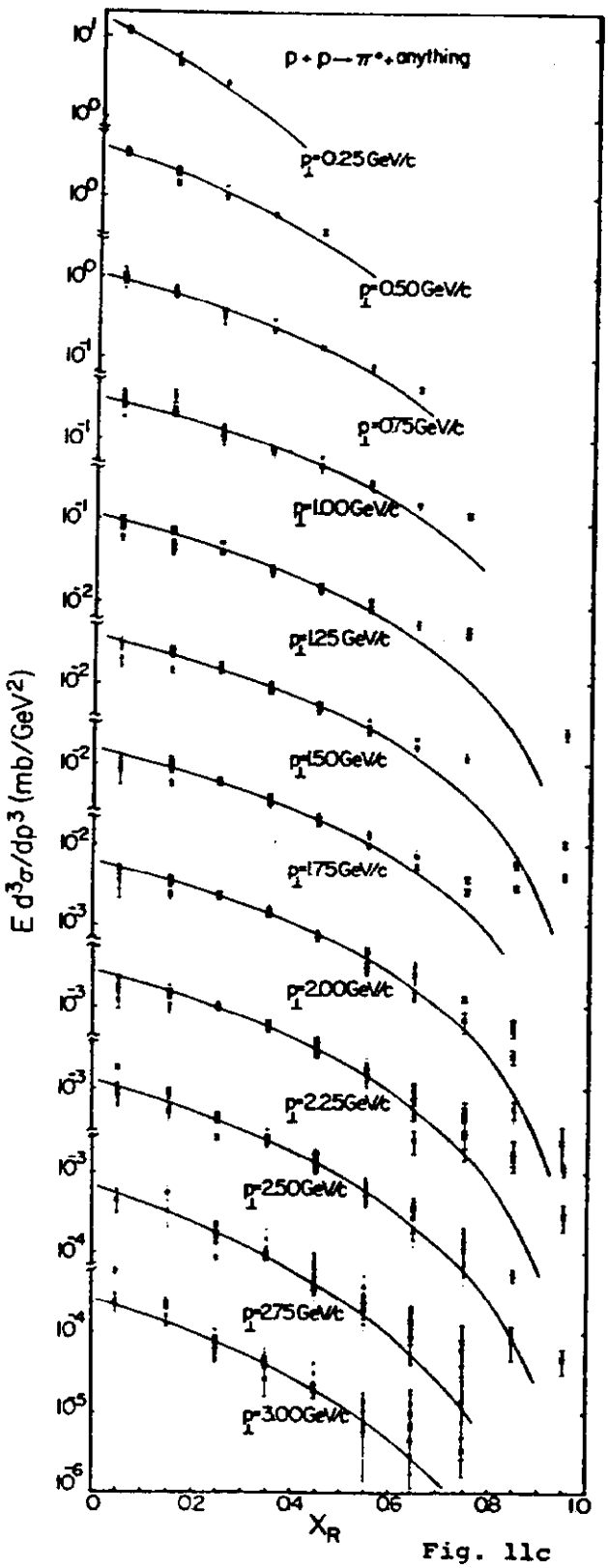
p + p — π⁺ + anything
p_T=0.25 GeV/c
p_T=0.50 GeV/c
p_T=0.75 GeV/c
p_T=1.00 GeV/c
p_T=1.25 GeV/c
p_T=1.50 GeV/c
p_T=1.75 GeV/c
p_T=2.00 GeV/c
p_T=2.25 GeV/c
p_T=2.50 GeV/c
p_T=2.75 GeV/c
p_T=3.00 GeV/c
E d³σ/dp³ (mb/GeV²)
X_R
0
02
04
06
08
10

Fig. 11c

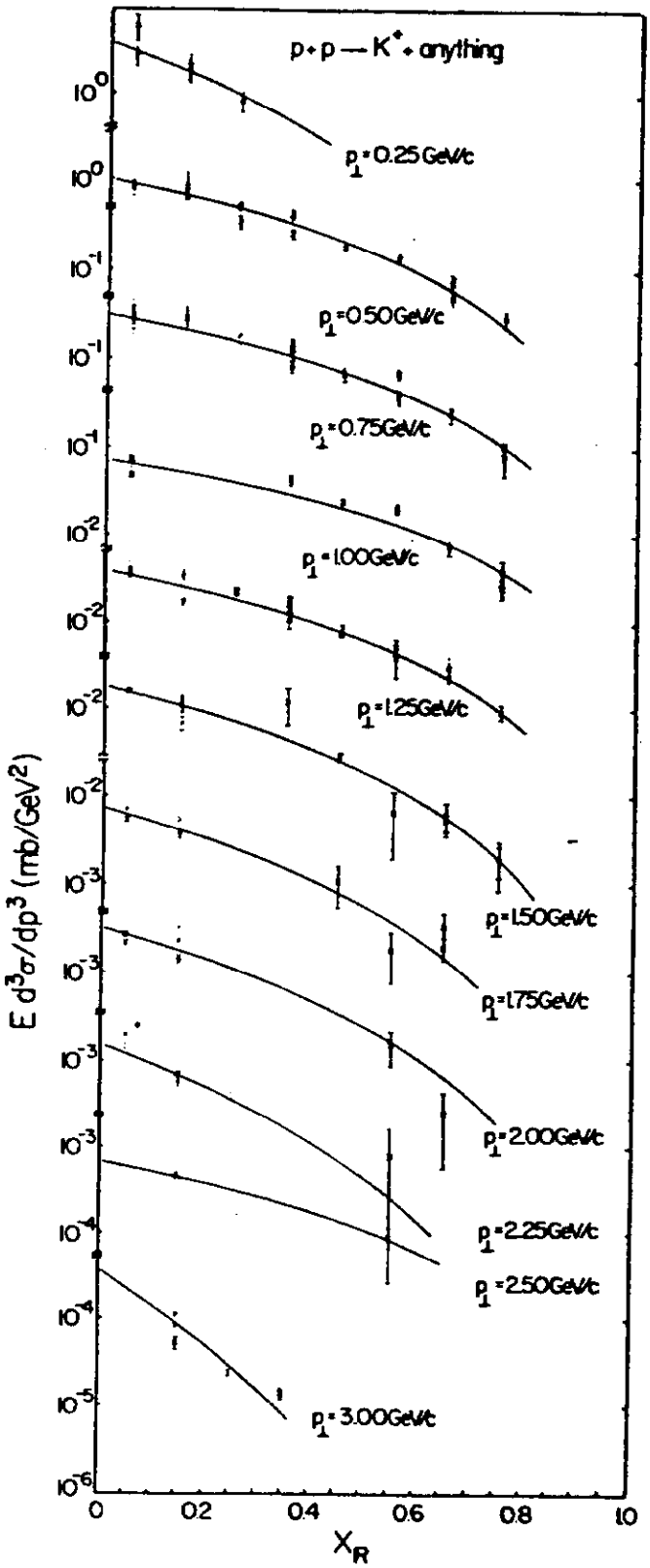
p+p — K⁺+ anything
p_1=0.25GeV/c
p_1=0.50GeV/c
p_1=0.75GeV/c
p_1=1.00GeV/c
p_1=1.25GeV/c
p_1=1.50GeV/c
p_1=1.75GeV/c
p_1=2.00GeV/c
p_1=2.25GeV/c
p_1=2.50GeV/c
p_1=3.00GeV/c
E d³σ/dp³ (mb/GeV²)
X_R
0
0.2
0.4
0.6
0.8
1.0

Fig. 11d

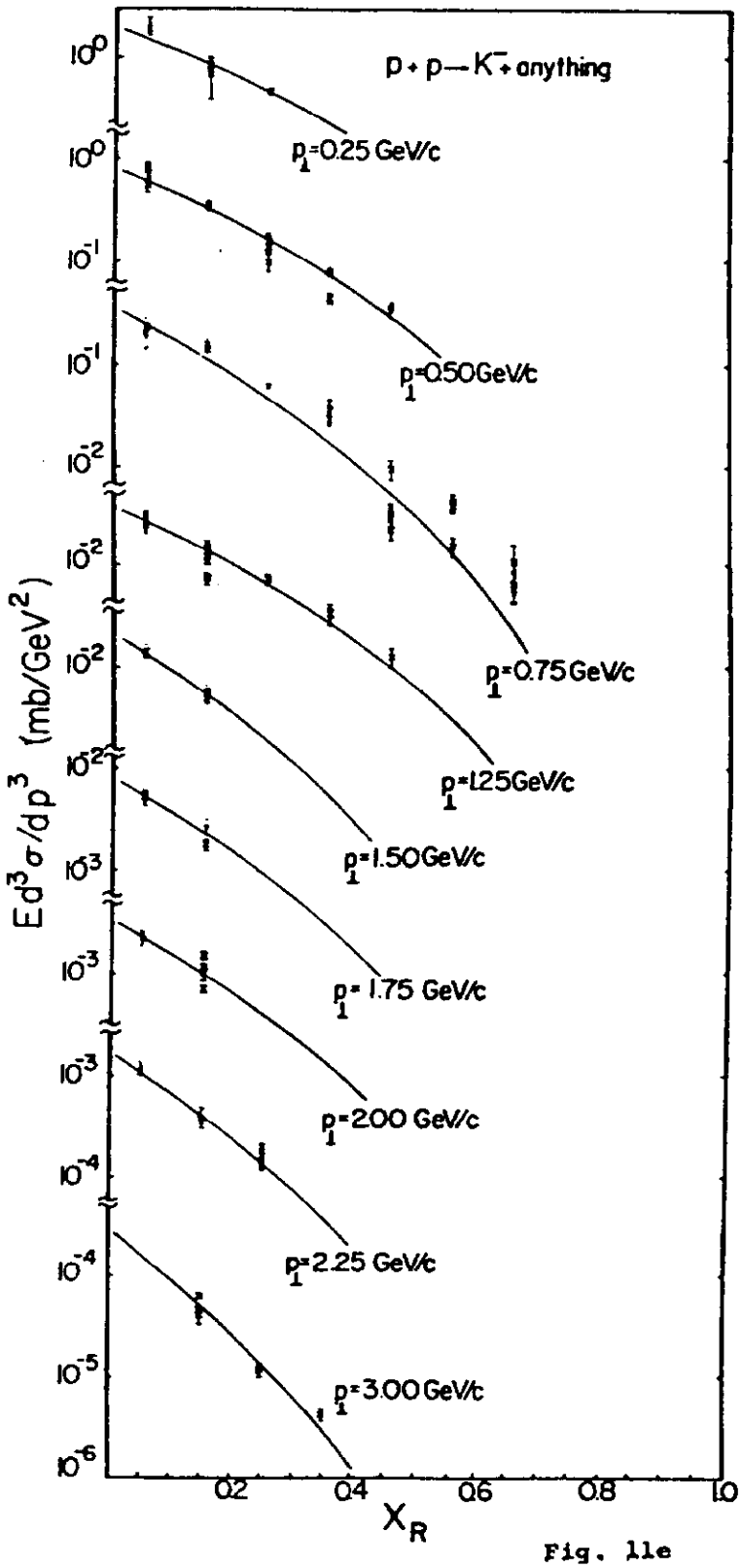
p + p — K⁻ + anything
p_1=0.25 GeV/c
p_1=0.50GeV/c
p_1=0.75GeV/c
p_1=1.25GeV/c
p_1=1.50GeV/c
p_1= 1.75 GeV/c
p_1=2.00 GeV/c
p_1=2.25 GeV/c
p_1=3.00GeV/c
Ed³σ/dp³ (mb/GeV²)
X_R
0.2
0.4
0.6
0.8
1.0

Fig. 11e

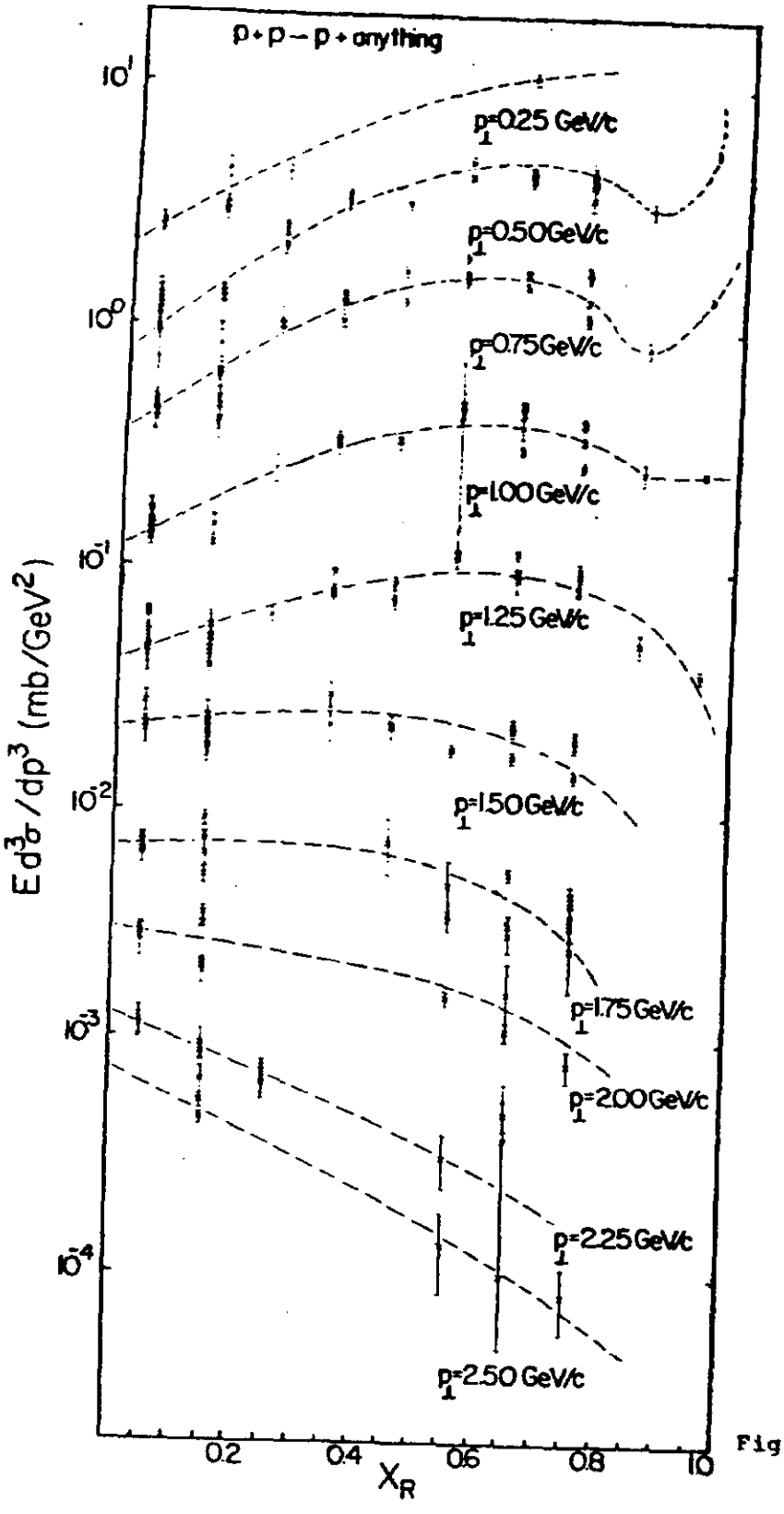
p + p → p + anything
$p_\perp$=0.25 GeV/c
$p_\perp$=0.50GeV/c
$p_\perp$=0.75GeV/c
$p_\perp$=1.00GeV/c
$p_\perp$=1.25 GeV/c
$p_\perp$=1.50GeV/c
$p_\perp$=1.75GeV/c
$p_\perp$=2.00GeV/c
$p_\perp$=2.25GeV/c
$p_\perp$=2.50 GeV/c
$E d^3\sigma/dp^3$ (mb/GeV^2)
10^1
10^0
10^{-1}
10^{-2}
10^{-3}
10^{-4}
0.2
0.4
0.6
0.8
1.0
X_R

Fig. 11f

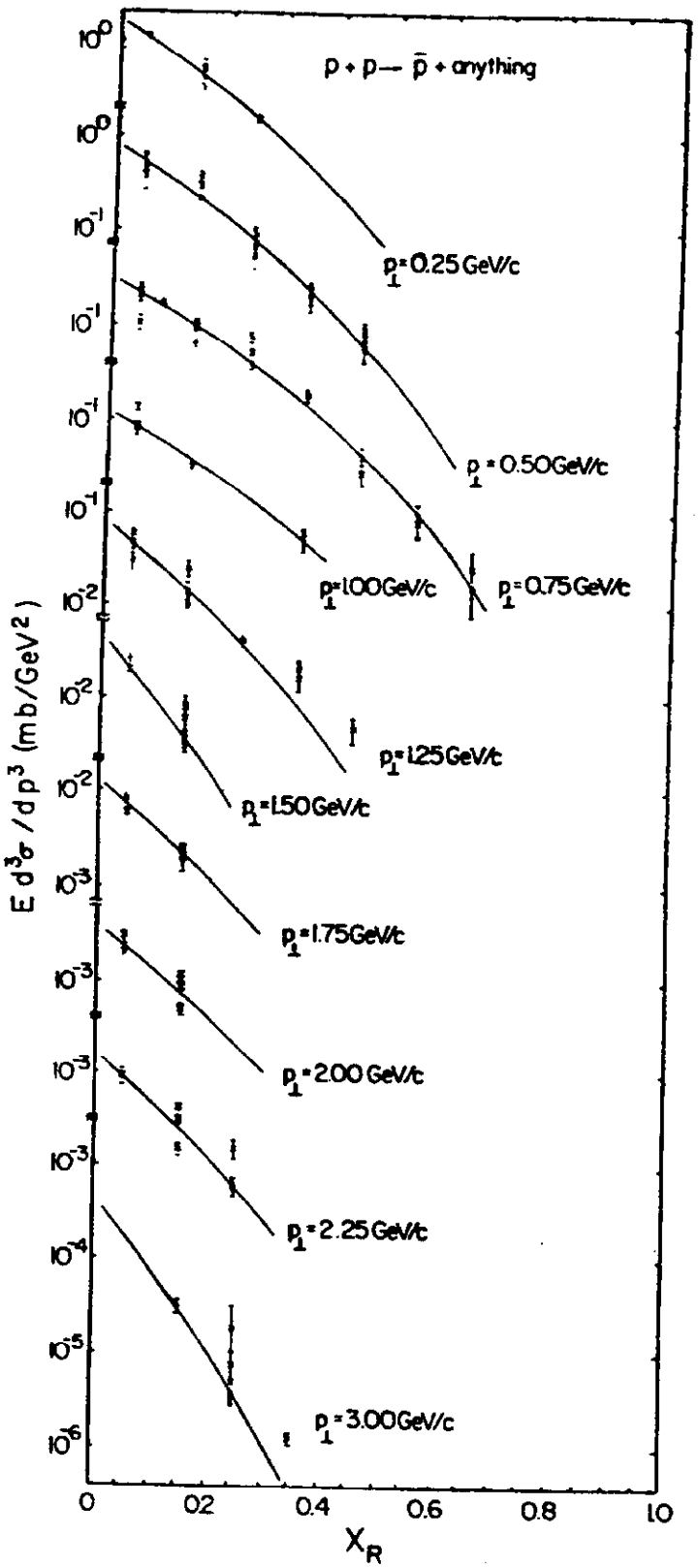
p + p— p̄ + anything
p_⊥=0.25 GeV/c
p_⊥=0.50GeV/c
p_⊥=0.75GeV/c
p_⊥=1.00GeV/c
p_⊥=1.25GeV/c
p_⊥=1.50GeV/c
p_⊥=1.75GeV/c
p_⊥=2.00 GeV/c
p_⊥=2.25GeV/c
p_⊥=3.00GeV/c
E d³σ/dp³ (mb/GeV²)
X_R
0
0.2
0.4
0.6
0.8
1.0

Fig. 11g